

A GEOLOGICAL AND GEOPHYSICAL INVESTIGATION OF THE
DIAMOND RUNS ON RUIGTELAAGTE AND VICINITY,
IN THE BAKERVILLE AREA, LICHTENBURG DISTRICT

by

EDGAR HEINZ STETTLER

Submitted in partial fulfilment of the requirements
for the degree of

MAGISTER SCIENTIAE

In the Faculty of Science of the University of Pretoria

PRETORIA

October 1979

A B S T R A C T

This geophysical and geological study was undertaken to determine the structural control and mode of deposition of the diamondiferous gravel runs north and east of Lichtenburg, especially on the farms Ruigtelaagte 353 JP, Welverdiend 361 JP and vicinity, which lie on the Welverdiend-Grasfontein run. This study formed part of a larger experimental geophysical investigation conducted by the Geological Survey to determine the present potential of the runs and whether gravel-filled sinkholes and channels could be found by means of geophysical techniques.

The geophysical investigation comprised detailed gravity, magnetic and electromagnetic surveys on parts of the above-mentioned farms. Geological mapping coupled with a sedimentological study and a heavy mineral analysis of the gravels were undertaken to reach a better understanding of the origin and mode of deposition of the gravels.

The gravel runs are situated on the Lyttelton and Monte Christo Formations of the Chuniespoort Group and the deposition and preservation of the gravels were controlled by karst areas which formed on or along dykes and quartz veins and in the immediate vicinity of the contact between the Lyttelton and Monte Christo Formations.

Possible post-Transvaal tension fractures and faults striking north-east and north-north-west, and along which sinkhole formation occurred are visible on the Bouguer and residual gravity maps as gravity lows. Filled palaeosinkholes also occur along three dolerite dykes that cross the study area. These dykes appear as gravity lows, indicating that they are deeply weathered.

Iterative, three-dimensional computer modelling of gravity data was undertaken to interpret parts of the residual gravity field over gravel-filled sinkholes ("potholes") and gravel runs.

From the geological and sedimentological information it is evident that no ordinary fluvial model can be proposed to explain the deposition of the gravels. It is concluded that the palaeoriver courses were governed by the exploitation of sinkholes and that flash floods and different stages of sinkhole collapse caused the palaeorivers to frequently change their course, resulting in the wide-spread gravel occurrences. The source of

the diamonds is believed to be locally present, yet undiscovered, kimberlites.

S A M E V A T T I N G

Hierdie geofisiese en geologiese studie van die diamanthoudende Welverdiend-Grasfontein-gruislope op die plase Ruigtelaagte 353 JP, Welverdiend 361 JP en omgewing is onderneem om die strukturele kontrole en afsettingsmeganisme van die gruislope noord en oos van Lichtenburg te bepaal. Hierdie studie het deel gevorm van 'n groter eksperimentele geofisiese ondersoek wat deur die Geologiese Opname uitgevoer is om die huidige potensiaal van die gruislope te bepaal en om vas te stel of gruisge vulde sinkgate en gruislope deur middel van geofisiese tegnieke opgespoor kan word.

Die geofisiese ondersoek het breedvoerige gravitasie- en magnetiese opnames van gedeeltes van die bogenoemde plase behels. Geologiese kartering, gekoppel aan 'n sedimentologiese ondersoek en swaarmineraalanalise van die gruis is onderneem om 'n beter begrip van die oorsprong en afsettingsmeganisme van die gruis te bekom.

Die gruislope kom voor op die Formasies Lyttelton en Monte Christo van die Groep Chuniespoort, en hulle afsetting en bewaring is beheer deur karstgebiede wat op en langs dolerietgange, kwartsare en op die kontak tussen die Formasies Lyttelton en Monte Christo ontstaan het.

Moontlike na-Transvaalse tensiebreuke en verskuiwings wat noordoos of noordnoordwes strek en waarlangs sinkgatontwikkeling plaasgevind het, is sigbaar as gravitasievallye op die Bouguer- en die residuele gravitasiekaarte. Sinkgate kom ook voor langs die drie dolerietgange wat die studiegebied deurkruis. Hierdie gange vertoon ook as gravitasie minima wat aantoon dat hulle diep verweer is.

Iteratiewe, drie-dimensionele rekenaarmodellering van gravitasiedata is onderneem om gedeeltes van die residuele gravitasieveld oor gruisge vulde sinkgate ("maalgate") en gruislope te interpreteer.

Van die geologiese en sedimentologiese gegewens is dit duidelik dat geen gewone rivierafsettingsmodel voorgestel kan word om die afsettings

van die gruisse te verklaar nie. Daar word tot die slotsom gekom dat die palaeorivierlope beheer is deur sinkgatuitbuiting en dat kitsoorstromings en verskillende stadia van sinkgatieenstortings veroorsaak het dat die palaeorivierlope gedurig van koers verander het sodat gruisafsettings oor 'n breë strook voorkom. Die mening word gehuldig dat die bron van die diamante, lokale, onbekende, kimberlietvoorkomste is.

C O N T E N T S

	<u>Page</u>
1. INTRODUCTION	1
2. PREVIOUS INVESTIGATIONS	3
3. GEOLOGY OF THE GRAVEL DEPOSITS NORTH OF LICHTENBURG	4
3.1 The Welverdiend-Grasfontein, Vlakplaats-Uitgevonden and Manana Runs	4
3.2 Sinkholes	12
4. SEDIMENTOLOGICAL INVESTIGATION OF THE GRAVELS	14
4.1 Classification of the gravels	14
4.2 Roundness of the pebbles	26
4.3 Analysis of heavy minerals	27
5. GRAVITY SURVEY	33
5.1 Fieldwork procedure and data reduction	34
5.1.1 Gravimeter base stations and drift corrections	36
5.1.2 Reduction of gravity data	39
5.2 Bouguer anomaly map	40
5.3 Residual gravity anomaly map	42
5.3.1 Qualitative discussion of the residual gravity anomaly map	47
(1) Dykes	47
(2) Gravity lows over leached, partly gravel-filled, zones	47
(3) Residual gravity anomalies not associated with the gravel runs	51
5.3.2 Three-dimensional gravity modelling by digital computer	52
5.3.3 The structure of the gravel runs based on residual gravity anomalies and borehole data	54
(1) Southern boundary of Ruigtelaagte 353 JP	55
(2) Pienaar's Pothole and sinkholes S ₁ and S ₂	64
(3) Welverdiend-Grasfontein run	73

	<u>Page</u>
6. MAGNETIC SURVEY	73
6.1 Qualitative discussion of the magnetic data	81
6.2 Quantitative discussion of the magnetic data	82
6.2.1 Method of Koulomzine, Nadau and Lamontagne	83
6.2.2 Methods of Reford and of Talwani and Heirtzler	86
6.2.3 Results	89
7. DEPOSITION OF THE DIAMONDIFEROUS GRAVELS	94
7.1 Karst formation in the dolomite	95
7.2 River capture	96
7.3 Mode of deposition	97
8. SUMMARY AND CONCLUSIONS	104
REFERENCES	106

A P P E N D I C E S

APPENDIX 1	THE DENSITIES OF ROCKS AND GRAVELS IN THE RUIGTELAAGTE AREA
APPENDIX 2	MATHEMATICAL BASIS FOR THE GRAVITY FORMULA OVER A RECTANGULAR PARALLELEPIPED
APPENDIX 3	APPLICATION, DISCUSSION AND PRINTOUT OF THE ITERATIVE THREE-DIMENSIONAL GRAVITY INTERPRETATION PROGRAM

	<u>Page</u>
ILLUSTRATIONS	
Figures	
1	Gravel runs and geology of the area surrounding Bakerville 2
2	Geology of the Ruigtelaagte area 6
3	Cross-section of a gravel run on Welverdiend 361 JP 8
4	Locations where gravel samples were collected for the sedimentological study 15
5	Histograms of mass per cent against "phi" values for gravels collected along the Pypklip and Welverdiend-Grasfontein runs 17
6(a)	Cummulative curves (mass per cent) 19
6(b)	Cummulative curves (mass per cent) 20
7	Plot of gravel composition 24
8	Histograms displaying the percentage of pebbles that fall into different roundness intervals for each sample 27
9	Relation between roundness or sphericity of pebbles and the distance of transport in a circular flume (km) 24
10	Composition of analysed garnet and ilmenite from Pienaar's Pothole 29
11	Composition of kimberlitic garnet from Pienaar's Pothole in terms of trivalent metals correlated with the composition of garnet from payable, provisionally payable and unpayable kimberlites 29
12	Common shapes of diamond from the Lichtenburg diamond fields 29
13	Bouguer anomaly map of the Ruigtelaagte area 41
14	Gravity and magnetic profiles across area where possible intrusion occurs 43

		<u>Page</u>
	ILLUSTRATIONS (continued)	
Figures		
15	Gravity stations and values (mgal) used in the calculation of the regional gravity field	44
16	Calculated regional gravity field (in mgal) over the Ruigtelaagte area	45
17	Residual gravity map of the Ruigtelaagte area	46
18	Geological map with residual gravity field overlay appears in map holder at the back of thesis	47
19	Residual gravity field (mgal) in the vicinity of sinkhole S_3 , near the southern boundary of Ruigtelaagte 353 JP	56
20	The dolomitic bedrock configuration in the vicinity of sinkhole S_3 , as calculated from the residual gravity field	60
21	Distribution of gravel as determined by the gravity method and drilling	61
22	Sections A, B and C based on the drilling results in the vicinity of sinkhole S_3	62
23	Interpretation of the drilling results near the southern boundary of Ruigtelaagte	63
24	The residual gravity field (in mgal) over Pienaar's Pothole and sinkholes S_1 and S_2	65
25	Dolomitic bedrock configuration at Pienaar's Pothole and vicinity as calculated from the residual gravity values	69
26	Gravel occurrences and borehole positions in the vicinity of Pienaar's Pothole and sinkholes S_1 and S_2	70
27	An interpretation of the drilling results of sinkhole S_1	71
28	Section H based on the drilling results of sinkhole S_1 compared with a cross-section of Pienaar's Pothole	72
29	Interpretation of the drilling results of sinkhole S_2	74
30	The residual gravity field over two parts of the Welverdiend-Grasfontein run	75

		<u>Page</u>
ILLUSTRATIONS (continued)		
Figures		
31	Dolomitic bedrock configuration beneath portions of the Welverdiend-Grasfontein run	79
32	Determination of the midpoint position of a dyke and the datum level from a total field magnetic profile by construction	85
33	Decomposition of the field curve into a symmetrical and asymmetrical component	85
34(a)	Polygonal body showing signs of faces	79
34(b)	Semi-infinite horizontal slab	
35(a)	Total field magnetic anomaly obtained over dyke d_1	90
35(b)	Total field magnetic anomaly obtained over dyke d_2	91
35(c)	Total field magnetic anomaly obtained over dyke d_2	92
35(d)	Total field magnetic anomaly obtained over dyke d_3	93
36	Proposed development of the diamondiferous gravel runs	99
37	Proposed development of the Harts River (after Mayer, 1973)	102
TABLES		
1	Screen analysis : Udden-Wentworth scale (percentage by mass)	16
2	Grain size parameters of gravels (after Folk, 1968)	23
3	Chemical analysis of garnet (a-w) from Pienaar's Pothole compared with kimberlitic garnet (A-F)	30
4	Composition of a typical kimberlite ilmenite (A) compared with that of ilmenite from Pienaar's Pothole	31
5	Structural formulas of garnet grains from the Pienaar's Pothole	32
6	Residual gravity field (in mgal) near the Ruigte-laagte-Zamenkomst boundary used for the calculation of the depth to the dolomitic bedrock	57
7	Interpreted thickness (in metres) to the dolomitic bedrock near the boundary between Ruigtelaagte and Zamenkomst	58

		<u>Page</u>
	TABLES (continued)	
8	Difference between observed and calculated residual gravity values after two iterations (in mgal)	59
9	Residual gravity values (in mgal) over Pienaar's Pothole and vicinity used for the calculation of the depth to the dolomitic bedrock	66
10	Calculated depth (in metres) to the solid dolomite bedrock over Pienaar's Pothole area and vicinity	67
11	Difference between the calculated and observed gravity values (in mgal) over Pienaar's Pothole area after two iterations	68
12	Residual gravity values (in mgal) obtained over a portion of the Welverdiend-Grasfontein run and used for the calculation of depth to the dolomitic bedrock	76
13	Calculated depth (in metres) to dolomitic bedrock over a portion of the Welverdiend-Grasfontein gravel run	77
14	Difference between observed and calculated gravity values (mgal) over a portion of the Welverdiend-Grasfontein gravel run after two iterations	78

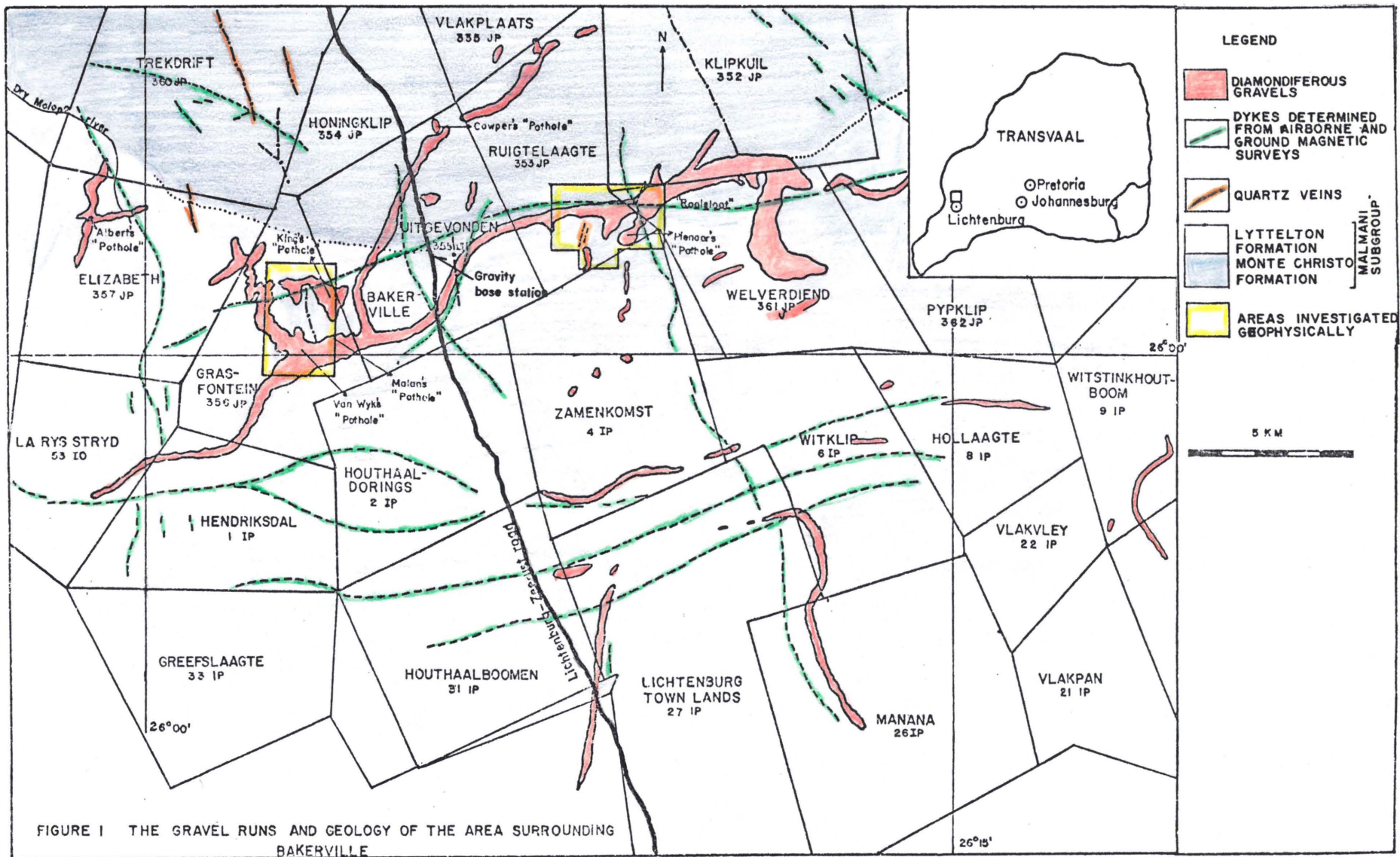
1. INTRODUCTION

The Lichtenburg diamondiferous gravel runs used to be one of the richest alluvial diamond fields in South Africa and the total diamond output of 7 220 846 carats between 1922 and 1947 (Du Toit 1951, p.38) certainly left a considerable impression on the mining history of South Africa. The area of prime importance at that time was the famous Welverdiend-Grasfontein diamondiferous gravel run which starts on the boundary of Klipkuil 352 JP and Welverdiend 361 JP in the east and extends westwards through Ruigte=laagte 353 JP, Uitgevonden 355 JP and Grasfontein 356 JP to end on the farm La Rys Stryd 53 IO (Figure 1). Until 1947 the diamond production on Ruigtelaagte 353 JP was 527 961 carats of which the bulk came from the famous Pienaar's Pothole (Du Toit, 1951, p.16). The richness of the Ruigtelaagte runs was surpassed only by those on Grasfontein 356 JP.

Due to the unusually low diamond price during the depression of the early 1930's, the rough terrain and shortage of water, many diamondiferous gravel layers were not economically viable. Combined with these problems Du Toit (1951, p.34) notes that small claims, claim laws prohibiting the removal of refuse and the unco-ordinated way in which the gravels were mined resulted in the situation where diamondiferous gravels still occur in sinkholes under worked material or a red soil cover.

Thus in 1977 a project was instigated by the Geological Survey to determine if gravel-filled sinkholes and runs could be located by the application of geophysics, to assess the present potential of the Lichtenburg gravel deposits and to acquire more information about the structural control and mode of deposition of the gravels, inter alia by the application of geophysics and sedimentology.

For the geophysical fieldwork two experimental areas were laid out for investigation, namely an area of 7 km² on the farms Grasfontein 356 JP and



Uitgevonden 355 JP as well as an area of 7,5 km² partly situated on the farms Ruigtelaagte 353 JP, Zamenkomst 4 IP and Welverdiend 361 JP. The latter of these was investigated by the author. The former area comprises the well-known King's and Malan's Potholes and the latter the well-known Pienaar's Pothole (Figure 1).

The Ruigtelaagte and Grasfontein experimental areas were laid out on a grid with stations spaced at 50 m intervals and on Ruigtelaagte alone 7 000 gravity readings, 4 000 precise levelling points, 15 000 magnetic readings and a total distance of 140 km of electromagnetic profiles were undertaken. The fieldwork of the project took one year to complete and was followed by a drilling program of considerable extent.

I wish to express my gratitude to the Director of the Geological Survey for his permission to use part of the results of this survey as a thesis.

The investigation was completed under the guidance of Prof. C.P. Snyman, Mr L.N.J. Engelbrecht and Dr R.J. Kleywegt and their valuable comments and stimulating discussions are much appreciated.

I also wish to thank Mr P.J. Hattingh of the University of Pretoria and the following members of the Geological Survey for their assistance:
Dr C. Frick, Messrs J.H.T. Beukes, G.F. Filmalter, J.F. Gordon-Welsh and D. Stigter.

2. PREVIOUS INVESTIGATIONS

In the heyday of the Lichtenburg diggings Draper (1927) and Harger (1928) were the first to comment on the possible mode of deposition of the Lichtenburg alluvial diamondiferous gravels. Harger proposed that the chert from the dolomite (Chuniespoort Group) or the Bevets conglomerate at the base of the Pretoria Group was the source of the diamonds.

Beetz (1930) explained the lack of sedimentary structures in the gravels by seasonal flash floods whereas Du Toit (1935 and 1951) emphasised the role of sinkholes in the deposition of the gravels. Retief (1961) also concluded that sinkhole formation played a major role in the trapping and preservation of the Lichtenburg diamondiferous gravel deposits and Mayer (1973) proposed that the gravel had been laid down by palaeotributaries of the Hartz River. Similarly Stratten (1977) attributed the gravel occurrences to palaeoriver systems that flowed towards the west and south-west.

3. THE GEOLOGY OF THE GRAVEL DEPOSITS NORTH OF LICHTENBURG

3.1 The Welverdiend-Grasfontein, Vlakplaats-Uitgevonden and Manana Runs

The gravel runs north of Lichtenburg are situated on the Lyttelton and/or the Monte Christo Formations of the Malmani Subgroup, Chuniespoort Group. The Lyttelton Formation consists of a dark-grey chert-poor dolomite. On outcrops "Rillen karren" and joint patterns are frequently seen and these joints facilitate the leaching of the Lyttelton Formation so that it weathers relatively quickly. The Lyttelton Formation is underlain by the Monte Christo Formation which consists of a basal oolitic chert and dolomite zone, followed by banded chert and dolomite-, and an upper chert-rich dolomitic zone on which most of the diamondiferous gravel runs are present (Davis and Prevost, 1978).

As on the Far West Rand the leaching of the dolomite along faults, joints and tension fractures of limited extent is an ongoing process in the Western Transvaal. It causes the presence of subterranean solution caves which subsequently develop into open sinkholes, gorges and channels (called karst areas) into which superficial sediments are deposited (Kleywegt and

Enslin, 1973). In the late Tertiary period (Du Toit, 1951) such open karst structures existed in the Bakerville area along dykes, quartz veins and along the contact of the Lyttelton and Monte Christo Formations and were exploited and filled with diamondiferous gravel by the palaeorives (Du Toit, 1951; Retief, 1961; Mayer, 1973; Stratten, 1974) (Figures 1 and 2). Three cycles of gravel deposition are visually identified by Retief (1961, p.62) and the gravels rest on a formerly exposed dolomitic floor, filling channels, small sinkholes and leached zones in the dolomite. Although the term "sinkhole" points to collapsed solution caverns (cavities) the palaeosinkholes filled with gravel or superficial sediments will for the sake of convenience be referred to as sinkholes.

According to Du Toit (1951, p.5), after the final deposition of the gravels, the surrounding dolomite was removed faster than the gravels which resulted in the runs forming mounds or chains of high ground situated above the general present-day dolomite terrain. The runs vary in width between 20 and 100 m. Gravel thicknesses of more than 40 m occur in sinkholes on the runs. Notwithstanding the fact that braided and meandering river patterns can be recognised on aerial photographs these gravel deposits cannot be fully identified with the classical braided or meandering river models as described by Blatt et al (1972) or Williams and Rust (1969) since:

- (1) they are almost devoid of the characteristic sedimentary structures and
- (2) the individual runs are too narrow and too deep to be typical of a meandering or a braided river model. The occasional presence of huge longitudinal gravel-layers or bars, e.g. on Welverdiend 361 JP, and of pebbles that are on occasion orientated with their long axes at right angles to the transport direction points to a

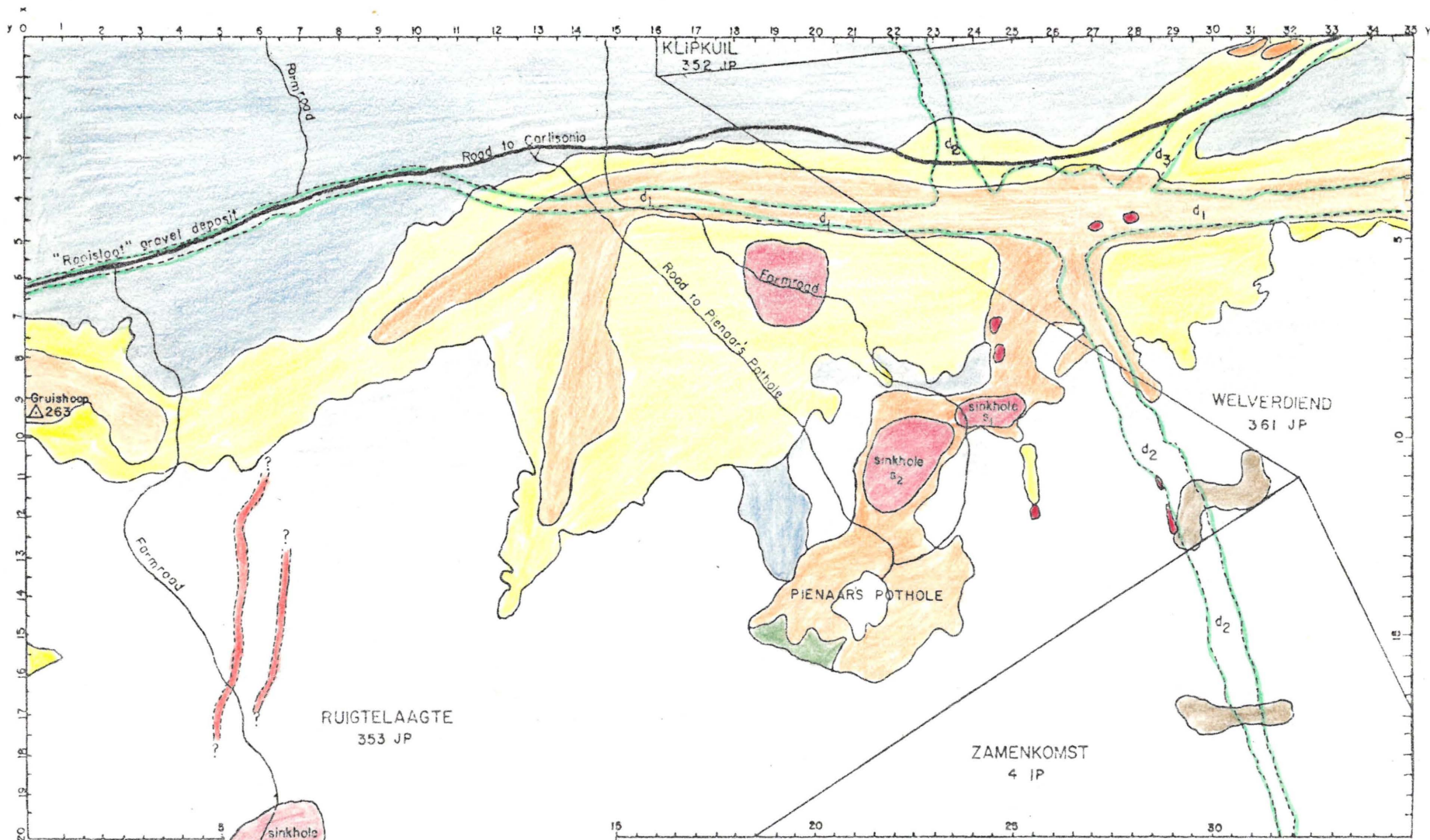









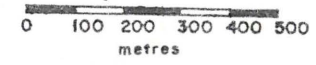


FIGURE 2 GEOLOGY OF THE RUIGTELAAGTE AREA

LEGEND

- | | | | |
|---|--|---|--|
|  | RED BROWN SOIL LAYER |  | KAOLINTIC CLAY } DWYKA FORMATION ? |
|  | DIAMONDIFEROUS GRAVELS (0<thickness<2m) |  | DYKES DETERMINED FROM GROUND MAGNETIC'S |
|  | DIAMONDIFEROUS GRAVELS (2m< thickness) |  | QUARTZ VEINS |
|  | NEWLY DISCOVERED VIRGIN GRAVEL DEPOSITS OCCURRING UNDER A RED SOIL COVER |  | LYTTELTON FORMATION } MALMANI SUBGROUP |
| | |  | MONTE CHRISTO FORMATION } MALMANI SUBGROUP |



deposition mechanism similar to that of rivers in non-migrating channels as described by Martini (1977).

A gravel run basically comprises a central part or channel of massive, well-packed gravel with a soil or clay matrix, bounded on both sides by loose rubble consisting of angular chert fragments, red-brown soil and sporadic rounded pebbles. The contact between the central gravel and the marginal rubble is sharp, but not erosional (Figure 3). The gravels in the central part of a run can be subdivided into (1) the upper and (2) the lower gravels.

- (1) The weathered and bleached upper gravels (called potato gravels by the diggers) consist of rounded chert pebbles in a red soil (terra rossa) matrix, containing pockets or layers of manganese nodules (small concretions of manganese oxide which are about 5 mm in diameter) in which diamonds of very good quality were often found.
- (2) The lower gravels consists mainly of blue, grey or red chert pebbles and manganese nodules in a pink, white, brown or grey soil-clay or clay matrix. In places only clay is present in the lower layer which can reach a thickness of 20 m or more. Beneath the lower gravel layer a basal layer of chert detritus, clay and wad was observed in borehole samples.

The lack of well-defined horizontal layering, bedding or sorting in both the upper and lower gravels is striking although it is reported by the diggers that in places the diamonds occur on a vaguely discernable horizon. The long axes of elongated pebbles in the central channel are very often orientated vertically so that a very crude vertical zonation is present. This is considered to be due to the collapse of pebble beds into narrow sinkholes. In general the gravels are very coarse and material of pebble

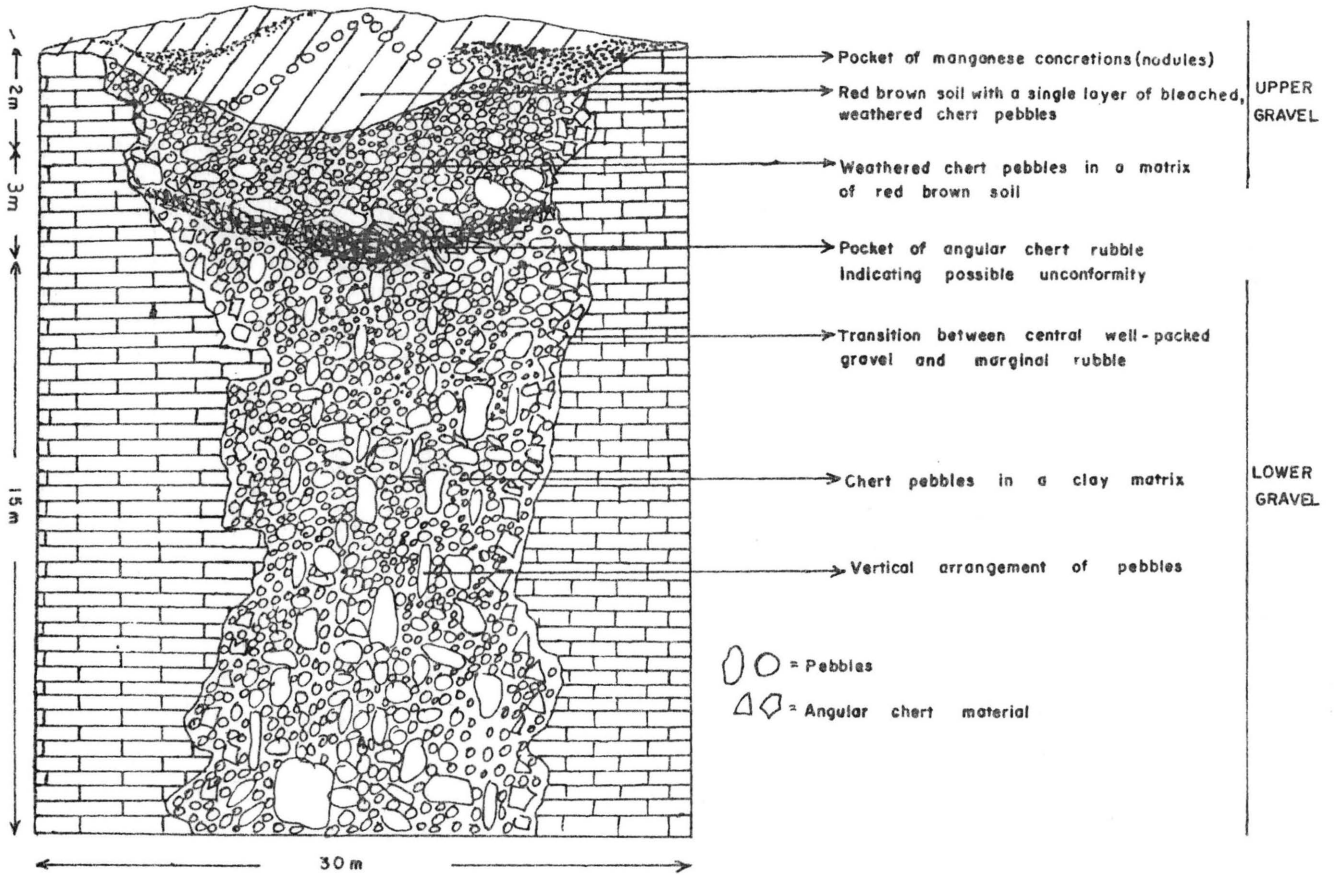


FIGURE 3 CROSS SECTION OF A GRAVEL RUN ON WELVERDIEND 361 JP

to boulder size is common. All gradations exist from extremely well-rounded pebbles to angular chert fragments.

The marginal rubble consisting of predominantly angular fragments probably represents collapsed roof material that incorporated some rounded pebbles during the collapse. Small chert blades (called boxwork) that only develop in subterranean water-filled chambers in dolomitic rocks (De Wit 1978) were observed on angular chert material especially in the Manana run. This indicates that abrasion during gravel deposition was minimal on the walls of open leached karst areas. It is thus concluded that the gravel was probably dumped into leached structures and not deposited by subterranean streams. Examples where gravel beds collapsed into subterranean caves (sinkholes) due to the combined effects of weakening of cave roofs by water infiltration and mass of the overlying gravel layers, can be seen on Pypklip 362 JP, Welverdiend 361 JP, Ruigtelaagte 353 JP and Grasfontein 356. These gravel beds dip towards the centre of the run although trough cross-bedding could show the same effect (McKee and Weir, 1953). At these localities the very crude vertical zonation of pebbles is thought to have been caused by their rearrangement in a vertical position during the collapse of the gravel layers into sinkholes which are normally funnel-shaped when seen in profile.

The gravel consists almost entirely of chert pebbles but the allochthonous constituents vary from one run to another. On the Manana and Vlakplaats-Uitgevonden runs occasional quartzite pebbles have been noted whereas on the Welverdiend-Grasfontein run agate, sandstone, quartzite, petrified wood and granite pebbles and cobbles are found. Due to the presence of these allochthonous gravel constituents, Retief (1961, p.62) considers the Welverdiend-Grasfontein run as the oldest.

Roundness measurements after Van Genderen, (1977) on quartzite pebbles and

examples of clustering similar to those described by Dal Chin (1968, p.233-241) show an increase in roundness to the west along the Welverdiend-Grasfontein run and point to the fact that these gravels were deposited by palaeostreams flowing from the north-east. The fact that the Vlakplaats-Uitgevonden run joins the Welverdiend-Grasfontein run perpendicularly, suggests that the Vlakplaats-Uitgevonden run presents a tributary to the Welverdiend-Grasfontein run and deposition took place from the north. A poor example of planar cross-bedding (Van Vuuren, et al, 1979) in the Manana run (Figure 1) suggests transport of material from the south to the north which is in agreement with the observations by Du Toit (1951, p.91) and Retief (1961, p.120).

On the Ruigtelaagte 353 JP - Welverdiend 361 JP boundary three basic dykes, namely d_1 , d_2 and d_3 intersect one another (Figure 2) and here the Welverdiend-Grasfontein run is characterised by isolated sinkholes and secondary runs branching off from the main channel. Except for the Welverdiend-Grasfontein run, diamondiferous gravels also occur along the strike of dyke d_1 and these are referred to as the "Rooisloot" gravel deposits. Diamonds of excellent quality were recovered from the "Rooisloot" and since it transgresses the Welverdiend-Grasfontein run on Welverdiend 361 JP and Ruigtelaagte 353 JP and consists of bleached chert pebbles in a red soil matrix, typical of areas underlain by dolomite in the Western Transvaal, Retief (1961, p.62) considers it to be the youngest of all the runs.

Diamondiferous gravels (about 2 m thick) underlain by gravel-bearing kaolinitic clay layers that can reach a thickness of 30 m are also present near the southern boundary of Ruigtelaagte 353 JP and on Zamenkomst 4 IP. Agate is abundant in these gravels and petrified wood, amethyst and large blocks of Karoo(?) sandstone were observed. Only a small portion of these

gravels was worked in the past and a large soil-covered area underlain by diamondiferous gravel was found here through the application of geophysics. The thick gravelly clay layers that occur here are very similar to a diamictite reported by Von Gottberg (1970, p.101) south of Lichtenburg. Due to dolerite intrusions into the diamictite south of Lichtenburg Von Gottberg considers it to be of Dwyka age. The author considers the gravel-bearing kaolinitic clay layers present near the southern boundary of Ruigtelaagte as fluvial sediments transported from a diamictite source, since the pebble shapes are not characteristic of a tillite. Due to fluvo-glacial activity however, the pebbles could also have become rounded.

Near the intersection of dykes d_1 , d_2 and d_3 , agate-bearing gravel was also noted along the strike of dyke d_3 (Figure 2).

It is very difficult to ascertain if there is a correlation between diamond-content and gravel types. More important indicators of the presence of diamond are structures in the dolomitic rock which acted as traps e.g. small or large palaeosinkholes or depressions and chert bars protruding from channel walls. Changes in the pattern of gravel deposition are also significant, especially where an increase in pebble size or heavy minerals is observed e.g. layers of cobbles or manganese nodule pockets and layers (Figure 3). It is also interesting to note that the diamond-bearing properties of the different runs vary widely. In contrast with the Manana run which produced diamonds of good quality at a steady rate, mainly low quality stones were found on the Welverdiend-Grasfontein run (Du Toit, 1951). The quality of the diamonds from the Vlakplaats-Uitgevonden run were also much better than those of the Welverdiend-Grasfontein run (Du Toit, 1951).

3.2 Sinkholes

All the famous potholes in the Lichtenburg diamond-fields are sinkholes that coincided with the palaeorivers and thus acted as gravel-traps. Most of them produced fabulous quantities of diamonds.

With a few exceptions all palaeosinkholes (whether filled with gravel or dolomitic debris) situated outside the gravel runs are covered with a red brown soil layer. They thus went undetected in the past since the diggers mostly concentrated on the runs that are visible since they form elevated areas. This fact makes the discovery of gravel filled sinkholes very difficult so that geophysical methods were employed with success to locate sinkholes. Boreholes were sunk into the sinkholes to establish if they contain gravel deposits.

Two types of gravel-filled sinkholes were noted, namely

- (1) narrow gorge-like sinkholes, e.g. King's and Malan's Potholes that are situated along the eastern side of Grasfontein 356 JP (Figure 1);
- (2) broad, roundish sinkholes, e.g. Pienaar's (Figure 2) and Cowper's Potholes (Figure 1) situated on the south-eastern portion of Ruigte=laagte 353 JP and the extreme north of Uitgevonden 355 JP, respectively.

Most of the larger, well-known potholes occur outside the present main gravel runs. For a detailed description of all the potholes the reader is referred to the publication of Du Toit (1951).

Du Toit (1951, p.26) recognised the following vertical zoning in the larger potholes.

- (1) Basal white layer

- (2) Diamondiferous lower red zone
- (3) Poor intermediate zone
- (4) Diamondiferous upper pale gravel layer

This zoning seems to indicate that they were filled up or developed in stages.

A dolomite pinnacle that cropped out in the north-west of Pienaar's Pothole and projected as a rib into the south-eastern layers of the pothole probably had an influence on the concentration of diamonds (Du Toit 1951, p.17). On the northern side of the pothole thick layers of shale were recently exposed that could be of Karoo age. Since they dip at an angle of about 60° towards the centre it seems that they collapsed into the sinkhole.

Agates and very well rounded chert and quartzite cobbles are in abundance in Pienaar's Pothole. Ilmenite and garnet of kimberlitic and non-kimberlitic origin are present in the heavy mineral fraction and it is the only gravel filled sinkhole where the amount of these minerals varies sympathetically with the diamond content (Du Toit 1951, p.19; Mr D. Roux, Roux Diamonds (Pty) Ltd, pers. comm.). Garnet and abundant agate were found in most of the large potholes but of the runs, only the Welverdiend-Grasfontein one is agate-bearing (Du Toit 1951, p.30).

The drill-hole samples from two newly discovered gravel filled sinkholes (S_1 and S_2 , Figure 2) north-east of Pienaar's Pothole also exhibit the alternation of gravels as described by Du Toit. These two sinkholes as well as S_3 found near the southern border of Ruigtelaagte are similar in shape to Pienaar's Pothole (Figures 22, 27 and 28, pp. 61, 70 and 71 respectively. All four these sinkholes were covered by a 2 to 3 m thick red soil cover.

Boxwork structures that are inter alia present on the walls of King's Pot-hole indicate that no continued gravel movement took place through this sinkhole. Only a very narrow vertical zone in the centre of King's Pot-hole was diamondiferous and Du Toit (1951, p.20) reports the presence of a yellow diamondiferous sand at its bottom.

4. SEDIMENTOLOGICAL INVESTIGATION OF THE GRAVELS

Although most investigations stressed the importance of a palaeoriver system in the formation of the gravel runs, the already mentioned absence of stratification casts doubt on the fluvial models previously proposed. A sedimentological investigation was therefore embarked on to prove or disprove the validity of the fluvial models.

4.1 Classification of the gravels

Gravel samples collected from the upper and lower layers of the Pypklip and Welverdiend-Grasfontein runs (Figure 4) were screened for 10 minutes and classified according to the Udden-Wentworth sieve scale (Blatt et al, 1972, p.46) (Table 1). The Udden-Wentworth scale was converted to Krumbein's 'phi'-values as revised by McManus (1963), namely

$$\phi = -\log_2 d/d_0$$

where d_0 = standard grain size (i.e. 1 mm)

d = Udden-Wentworth scale so that

ϕ is dimensionless.

Histograms of mass per cent against 'phi' values (Folk, 1968)(Figure 5) indicate that the greatest contribution comes from the cobbles and pebbles, and the gravels can thus be considered as coarse. The erratic orientation

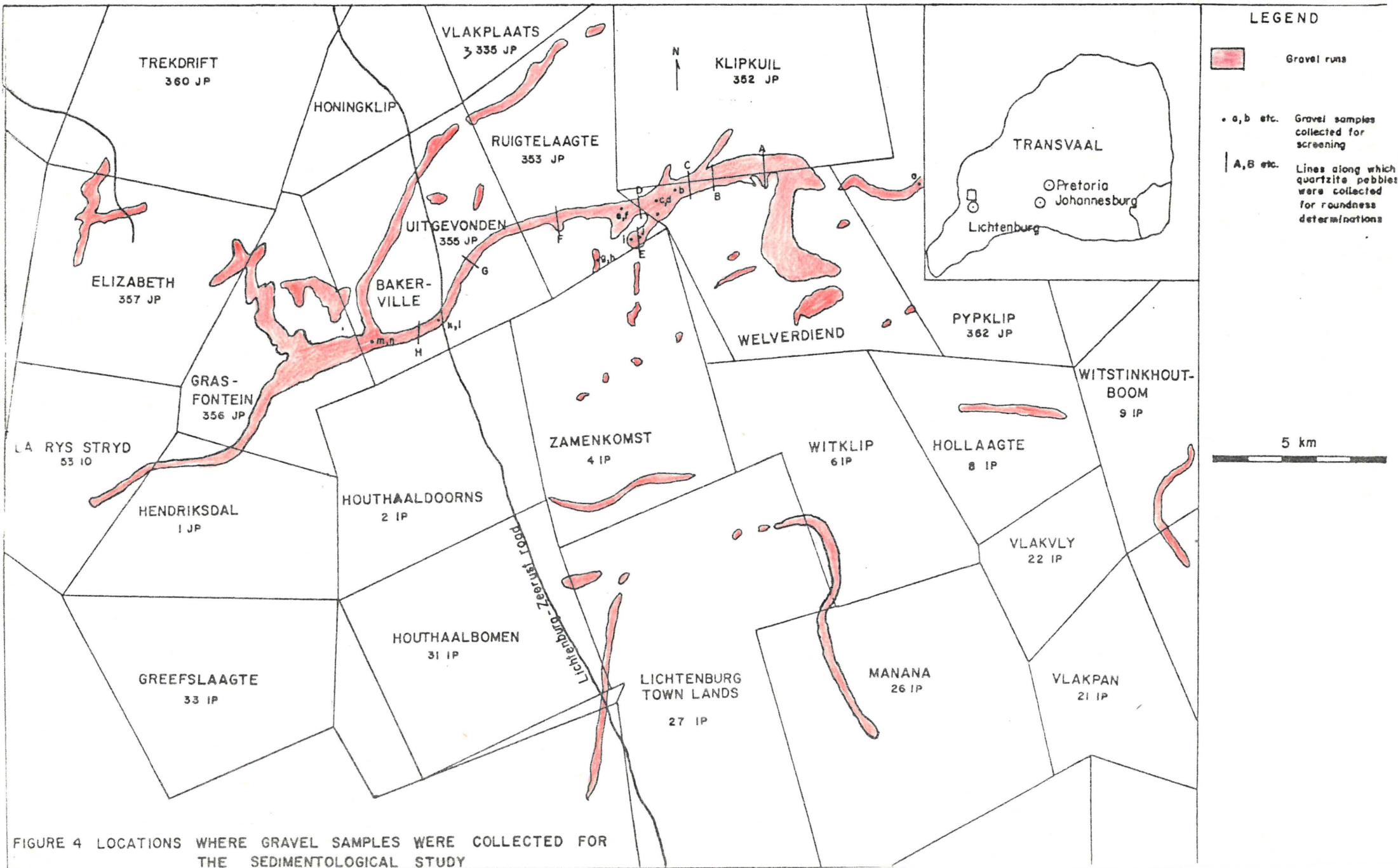


FIGURE 4 LOCATIONS WHERE GRAVEL SAMPLES WERE COLLECTED FOR THE SEDIMENTOLOGICAL STUDY

TABLE 1 : Screen analysis : Udden Wentworth scale (percentage by mass)

Size	a	b	c	d	e	f	g	h	i	j	k	l	m	n	o	phi
< 64mm	44,2	23,4	20,83	27,44	25,82	37,04	31,5	34,9	7,10	-	18,92	32,10	34,0	27,5	6,12	-6
64-4mm	38,52	56,36	46,7	54,33	45,23	45,27	47,2	48,1	66,0	71,09	57,84	52,2	48,5	51,0	67,35	-2
4-2mm	4,2	3,55	15,05	7,94	7,4	5,56	3,7	3,3	8,5	7,37	9,32	5,0	4,5	5,0	8,45	-1
2-1mm	2,96	1,06	5,56	2,71	1,97	2,26	1,3	1,6	3,0	2,65	3,38	2,6	2,0	2,0	3,35	0
1-0,5mm	4,44	1,06	4,86	2,53	1,48	3,09	1,7	4,4	4,2	2,65	3,51	5,3	2,0	0,5	3,50	1
0,5-0,25mm	1,98	1,06	3,94	2,17	1,81	3,29	4,3	2,5	5,9	3,54	1,62	1,5	4,1	5,7	5,98	2
0,25-0,05mm*	2,12	8,54	1,71	1,64	9,05	1,87	4,8	3,6	4,0	4,96	3,03	0,5	2,8	4	2,04	4
0,05-0,005mm	1,01	3,79	0,81	0,87	3,45	0,95	2,6	1,3	1,0	3,86	1,24	0,2	1,2	3	1,60	4,5
>,005mm	0,81	0,88	0,81	0,56	3,78	0,70	2,9	0,3	0,3	3,86	1,14	0,6	0,9	1,3	1,60	7,5
Total	100,24	100,10	100,27	100,27	99,99	100,03	100,00	100,00	99,99	100,00	100,00	100,00	100,00	100,00	99,99	.

* The size distribution of 0,25 to 0,005 mm material was determined by means of a hydrometer by Mr G F Filmlater of the Engineering Geology laboratory, Geological Survey.

- a. Gravel with red soil matrix from Pypklip 362 JP (sampling depth = 6m)
- b. Gravel with clay matrix from Ruigtelaagte (sampling depth = 6m)
- c. Gravel from the "Rooi Sloot" (sampling depth = 4m)
- d. As c (Sampling depth = 2m)
- e. Welverdiend-Grasfontein run on Ruigtelaagte 353 JP (sampling depth = 4m)
- f. As e at sampling depth = 2m.
- g. Near border between Ruigtelaagte 353 JP and Zamenkomst 4IP (sampling depth = 2,5m)
- h. As g at sampling depth of 1 m.
- i. Western side of Pienaar's Pothole - red soil matrix - sampling depth = 10m
- j. Northern side of Pienaar's Pothole - clay matrix - sampling depth = 2m.
- k. Near Zeerust-Lichtenburg road - sampling depth = 3m.
- l. As k at sampling depth of 1m.
- m. Intersection of Welverdiend-Grasfontein and Viakpleats-Uitgevonden run - sampling depth = 2m.
- n. As m at depth of 10 m.
- o. Gravel from sinkhole S₁ - sampling depth 6m.

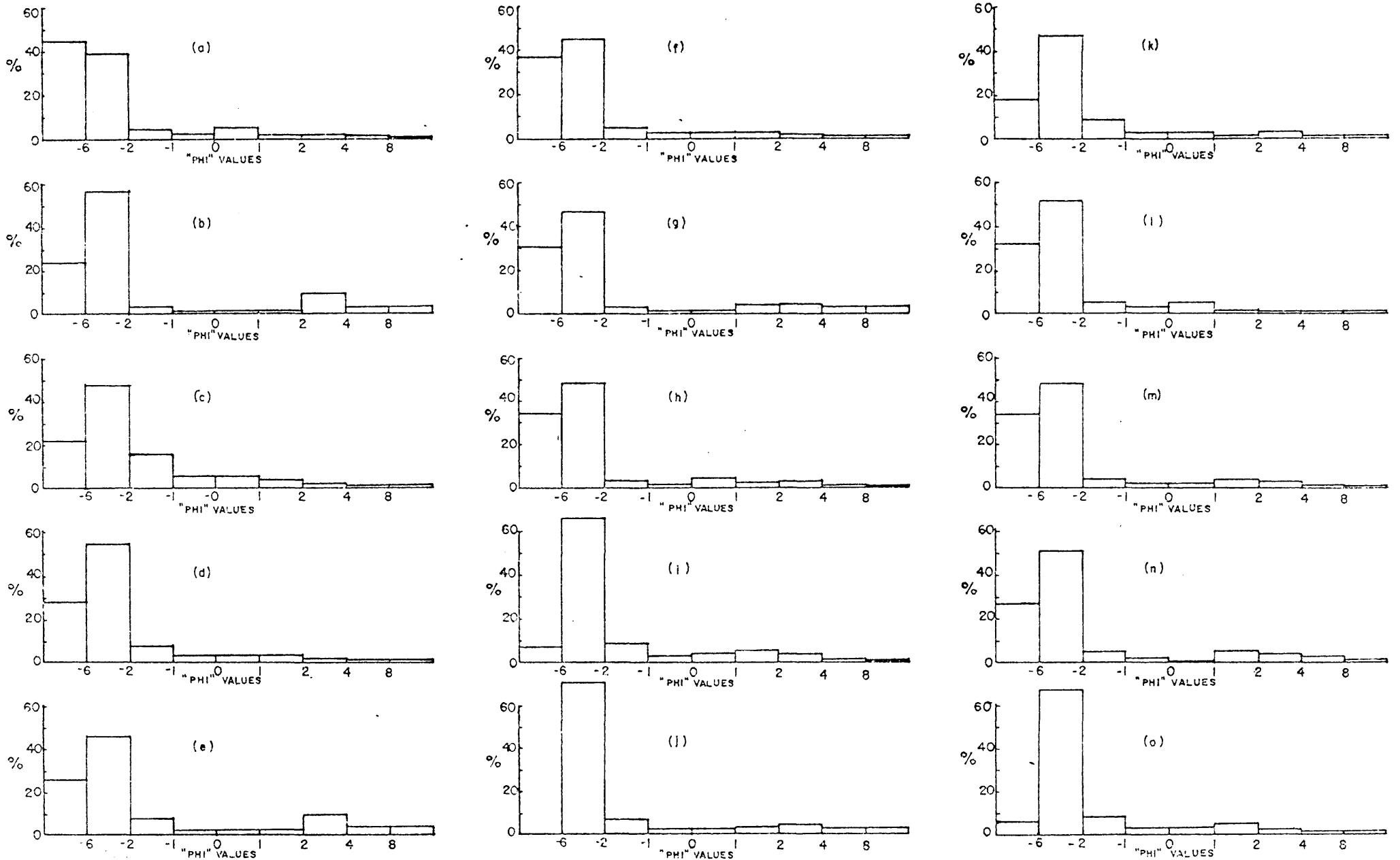


FIGURE 5 HISTOGRAMS OF MASS PERCENT AGAINST "PHI" VALUES FOR GRAVELS COLLECTED ALONG THE PYPKLIP AND WELVERDIEND-GRASFONTEIN RUNS

of the pebbles in the gravel runs is in agreement with the observations of Dal Chin (1968) who found that coarse pebble layers are often without any sign of stratification so that the arrangement of these pebbles is normally very chaotic.

The bimodal character of the lower gravels is evident from the histograms where peaks occur in the pebble and also in the silt sizes.

From cumulative distribution curves drawn for the same data (Figure 6(a)) and 6(b) , the following size parameters were calculated after Folk (1968) and Awasthi (1970).

(1) 'Phi' graphic mean (G_m) which is a measure of the overall mean size.

$$G_m = \frac{(\phi_{84} + \phi_{50} + \phi_{16})}{3} \quad \text{where } \phi_n \text{ denotes the}$$

nth percentile of the cumulative curve. The nth percentile is defined as that value of the variable that divides the sample so that n per cent of the sample is greater (or less) and (100 - n) per cent is less or greater than the value of the nth percentile.

(2) Inclusive graphic standard deviation (S_d) as a measure of sorting

$$S_d = \frac{(\phi_{84} - \phi_{16})}{4} + \frac{(\phi_{95} - \phi_5)}{2(3.3)}$$

The standard deviation is a measure of the dispersion or spread of the cumulative curve in phi units and Folk (1968, p.46) suggests the following classification scale for sorting.

$S_d < 0,35$ very well sorted	1,0 - 2,0 poorly sorted
0,35 - 0,50 well sorted	2,0 - 4,0 very poorly sorted
0,50 - 0,71 moderately well sorted	> 4,0 extremely poorly sorted
0,71 - 1,0 moderately sorted	

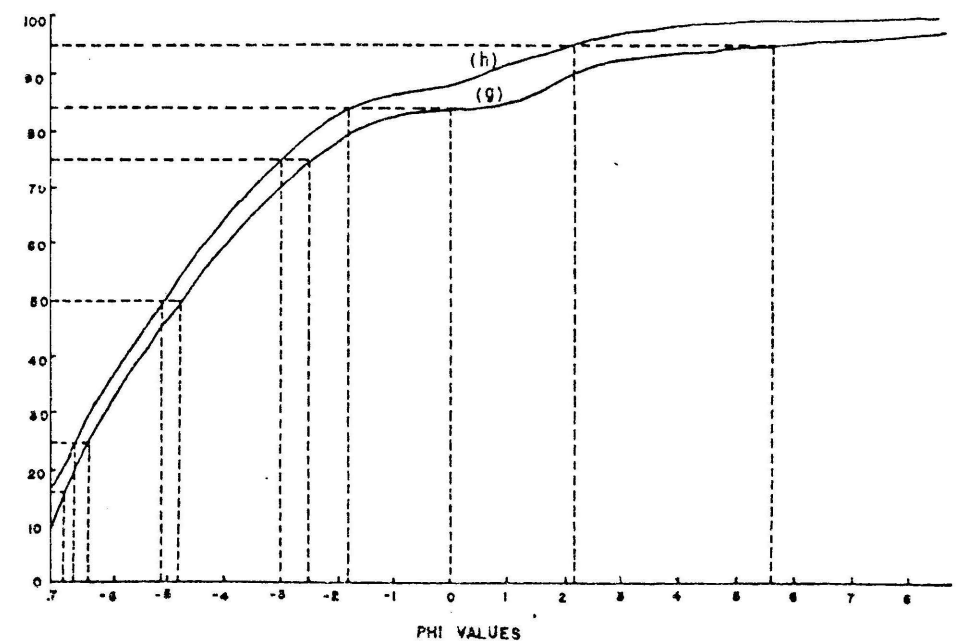
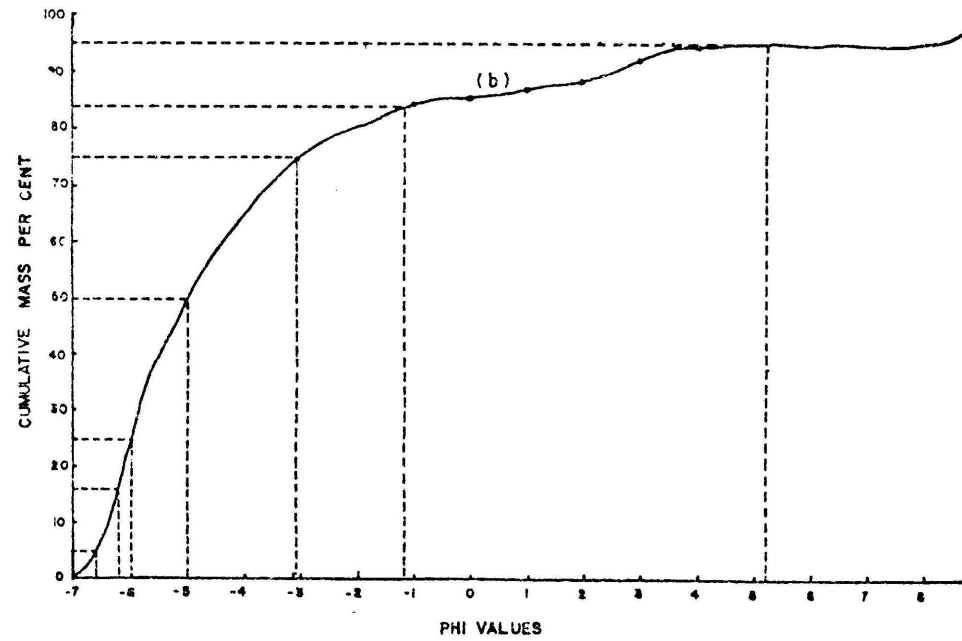
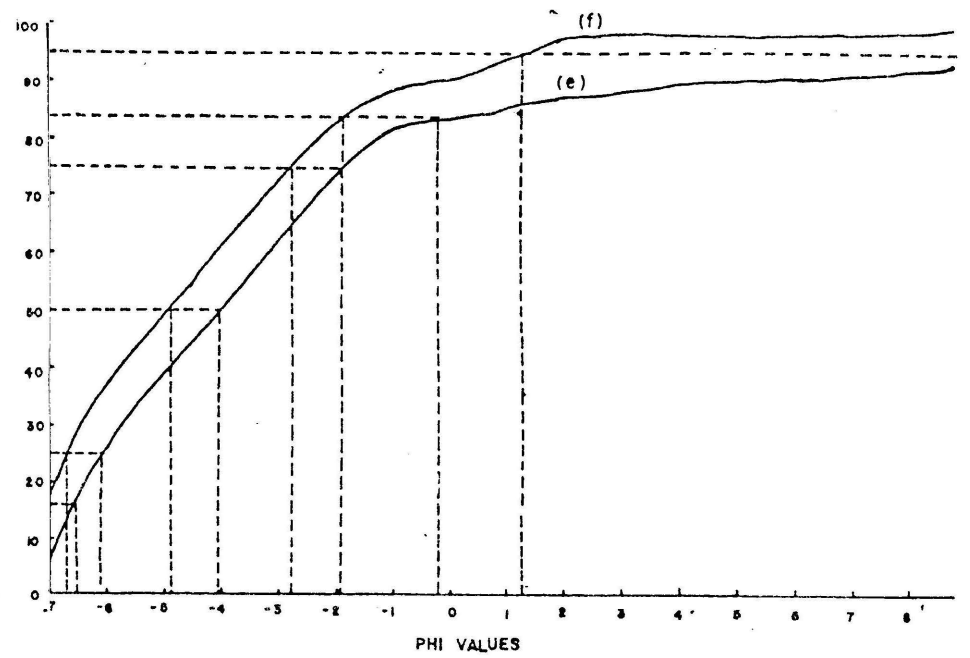
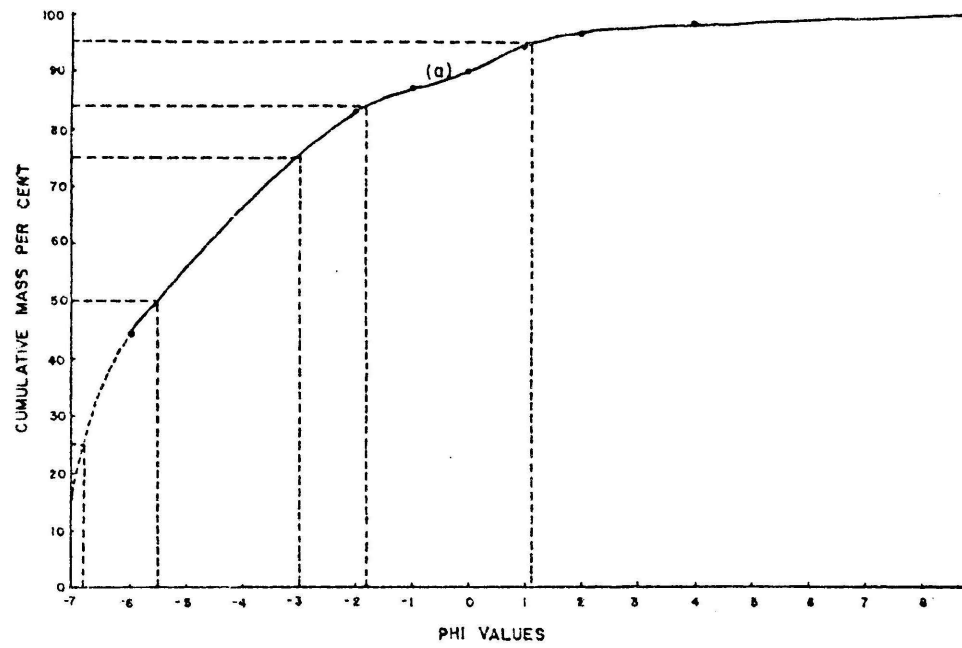


FIGURE 6(a) CUMULATIVE GRAIN SIZE DISTRIBUTION (MASS PER CENT)

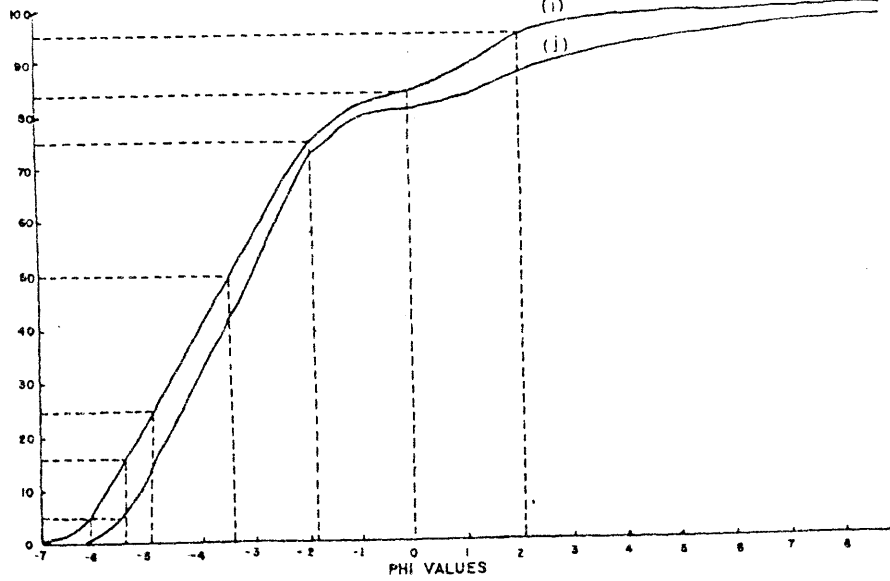
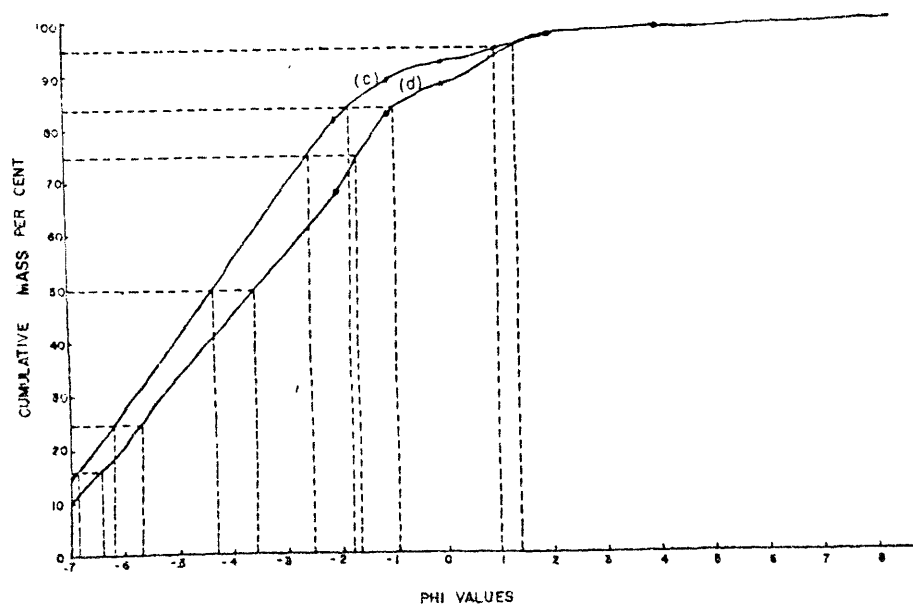
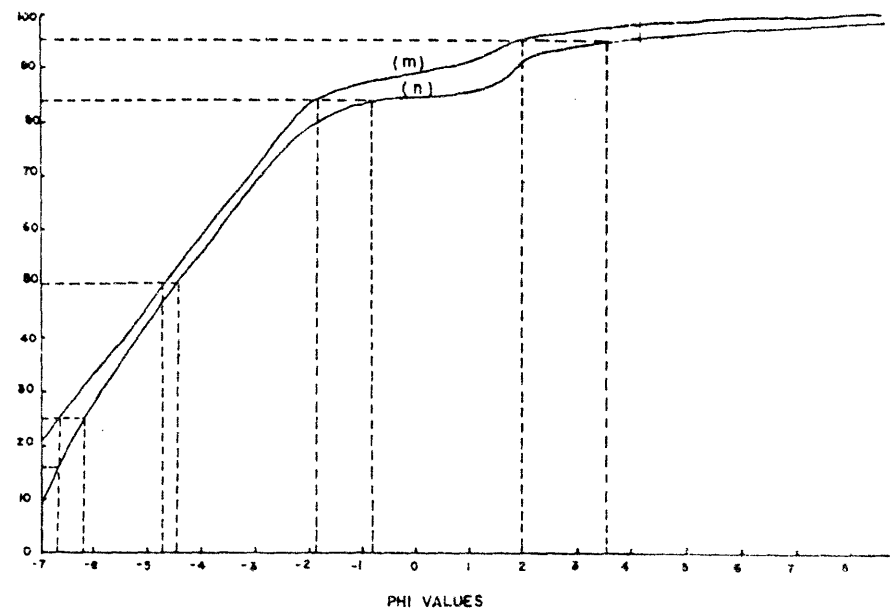
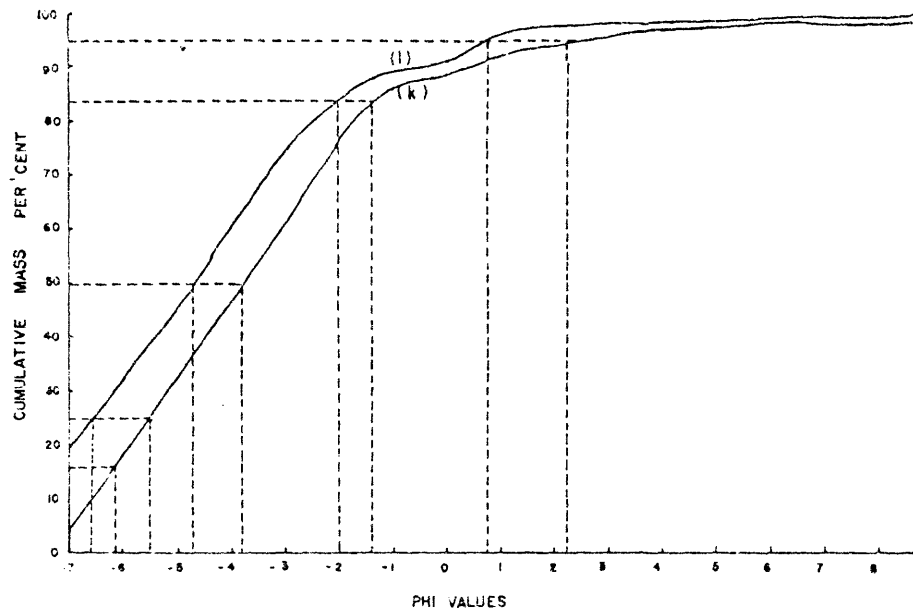


FIGURE 6(b) CUMULATIVE GRAIN SIZE DISTRIBUTION (MASS PER CENT)

- (3) Skewness (S_k) which is a measure of the abundance of sizes finer or coarser than the mean size and thus measures the degree of asymmetry of the distribution curve.

$$S_k = \frac{(\phi_{84} + \phi_{16} - 2\phi_{50})}{2(\phi_{84} - \phi_{16})} + \frac{(\phi_{95} + \phi_5 - 2\phi_{50})}{2(\phi_{95} - \phi_5)}$$

An excess in coarse material results in a positive skewness and vice versa.

Folk (1968, p.47) recommends the following verbal limits on skewness.

$$\begin{aligned} S_k &= +1,00 \text{ to } 0,30 \text{ strongly fine-skewed} \\ &= 0,30 \text{ to } 0,10 \text{ fine-skewed} \\ &= 0,10 \text{ to } -0,10 \text{ near - symmetrical} \\ &= -0,10 \text{ to } -0,30 \text{ coarse-skewed} \\ &= -0,30 \text{ to } -0,100 \text{ strongly coarse-skewed.} \end{aligned}$$

- (4) Kurtosis (K_s) as a measure of the 'degree of peakedness' of the distribution.

$$K_s = \frac{\phi_{95} - \phi_5}{2,44(\phi_{75} - \phi_{25})}$$

this is a calculated measure of the deficiency or excess in the spread between ϕ_5 and ϕ_{95} of the distribution curve when compared to the $\phi_{25} - \phi_{75}$ spread of the curve.

The distribution curve is called platykurtic when it is broader and less peaked than the normal distribution and leptokurtic if it is sharper peaked than the normal distribution.

Folk (1968, p.48) suggests the following limits:

$K_s < 0.67$ very platykurtic; $0.67 - 0.90$ platykurtic; $0.90 - 1.11$ mesokurtic; $1.11 - 1.50$ leptokurtic; $1.50 - 3.00$ very leptokurtic and over 3.00 extremely leptokurtic.

1008429

From the results presented in Table 2 it seems as if two types of gravel representing at least two cycles of deposition are present:

- (1) The lower gravels with a clay matrix can be classified as very coarse and very poorly sorted on the basis of the high negative "phi" mean size ($G_m = -4.13 \phi$ to -2.93ϕ) and the high positive inclusive graphic standard deviation ($S_d = 2.59 \phi$ to 4.02ϕ) respectively. The high positive skewness ($S_k = 0.16$ to 0.43) is due to the excessive amount of fine material which is responsible for the bimodal nature of the lower gravels. The normal distribution curve is classified as leptokurtic ($K_s = 1.06$ to 1.65) which means that it has 1,06 to 1,65 times as large a spread in the tails as for its $\phi_{25} - \phi_{75}$ spread, hence the gravels are more poorly sorted in the large and fine sizes than in the central portion.

- (2) The upper gravels with a terra rossa matrix are also coarse ($G_m = -2,23 \phi$ to $-4,90 \phi$) very poorly sorted ($S_d = 2,43 \phi$ to $2,69 \phi$) but in contrast to the lower gravels they are fine skewed to near symmetrical and platykurtic. This indicates a small excess of fines and a better sorting in the tails than in the central portion.

Since both gravel types are very poorly sorted and coarse it can be assumed that the mode of deposition remained the same but that the nature of the transported material changed. The lower gravel is classified as a coarse muddy gravel and the upper gravel as a coarse muddy sandy gravel (Figure 7; after Folk, 1968, p.29).

The widespread thin blanket of diamictitic material that covers the south-western Transvaal (Von Gottberg, 1970) could have extended further north-east in the past, so that the lower gravels with

TABLE 2 : Grain size parameters of the gravels (after Folk, 1968)

	a	b	c	d	e	f	g	h	i	j	k	l	m	n	o
Graphic mean "Phi" values	-4,90	-4,13	-4,46	-3,36	-3,63	-4,67	-3,87	-4,63	-2,93	-2,23	-3,78	-4,57	-4,63	4,10	-3,17
Inclusive graphic standard deviation "Phi" values	2,43	3,02	2,43	2,65	4,02	2,48	3,61	2,69	2,58	3,18	2,59	2,50	2,56	2,98	2,51
Inclusive graphic skewness	0,50	0,63	0,13	0,09	0,43	0,32	0,53	0,43	0,30	0,47	0,16	0,26	0,27	0,34	0,39
Kurtosis	0,87	1,65	0,93	0,85	1,56	0,97	1,32	1,03	1,06	1,65	0,96	0,67	0,93	1,14	1,10

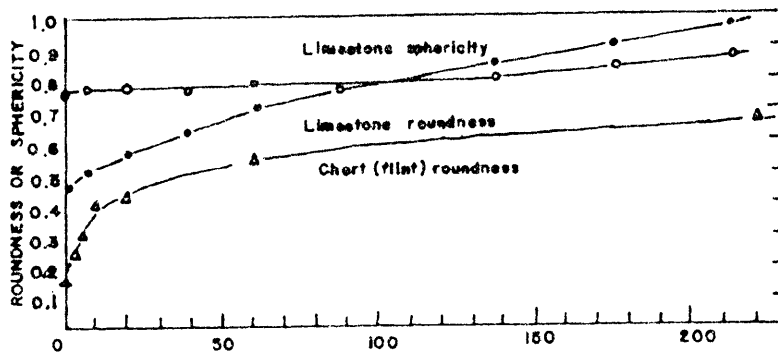
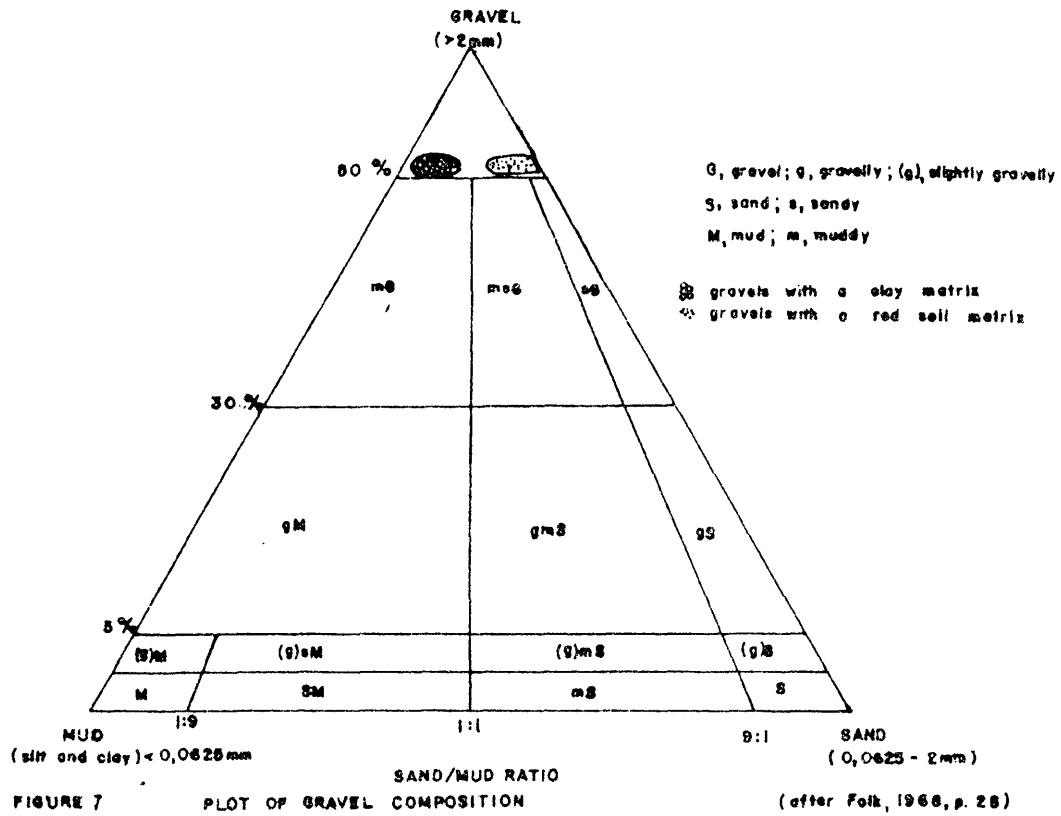


FIGURE 9 RELATION BETWEEN ROUNDNESS OR SPHERICITY OF PEBBLES AND THE DISTANCE OF TRANSPORT IN A CIRCULAR FLUME (KM)

their clayey matrix could have had a diamictite source. The lower gravels on the Welverdiend-Grasfontein run would then represent the first cycle of deposition, followed by the gravels with a red soil matrix, and the "Rooisloot" deposits respectively. Retief (1960) also reached this conclusion. There seems to be no sedimentological difference between the upper gravels and the "Rooisloot" deposits on Ruigtelaagte.

4.2 Roundness of the pebbles

Since roundness should increase with increasing distance of transport the roundness of quartzite pebbles was determined along the Welverdiend-Grasfontein run, in order to establish the direction of transport.

Sampling locations are indicated in Figure 4. Chert pebbles were not considered for this study since this rock type breaks up into angular fragments when transported until a size less than 25 mm is reached (Pettijohn 1957, p.256). Since angular chert was always fed into the river system the unbiased collection of chert pebble samples for roundness determinations is virtually impossible.

The determination of roundness as defined by Wadel (Blatt et al, 1972, p.64) was found to be very time-consuming and thus the Cailleux index as proposed by Van Genderen (1977) was used. This roundness index is calculated as $I_r = 2r/L$ where L is the length of the pebble and $2r$ is twice the radius of the smallest curvature of the pebble. At every locality fifty samples were collected along a line perpendicular to the gravel run and as far as possible only quartzite pebbles from the lower gravels were used. T tests were performed to ensure that enough data were available to ensure meaningful conclusions.

From Figure 8 it is evident that the quartzite pebbles from Pienaar's Pothole (E) are on average much more rounded than the quartzite pebbles along the remainder of the Welverdiend-Grasfontein run. This is a difficult fact to explain but perhaps this could indicate that Pienaar's Pothole, after its initial formation, acted as a real pothole in which gravels were scoured to a higher degree of roundness. The small increase in roundness west of Pienaar's Pothole (H) is ascribed to the fact that the gravels were transported westwards from the Pothole. This conclusion is in agreement with observations by Du Toit (1951) and Retief (1961, p.12) that the Welverdiend-Grasfontein run was formed by streams flowing westwards.

If it is assumed that the rate of abrasion of quartzite pebbles is similar to that of chert pebbles a transport distance of between about 10 and 80 km is obtained from Figure 9 (after Blatt et al, 1972, p.69). However, it should be kept in mind that the quartzite pebbles could have been derived from the diamictite (which could also have comprised fluvio-glacial deposits) and that their presence in the gravel runs should therefore imply at least two cycles of sedimentation. Their actual distance of transport during the formation of the diamondiferous gravels could therefore be considerably less.

4.3 Analysis of heavy minerals and the matrix of the gravels

Garnet and ilmenite were separated from an ilmenite-rich concentrate which was prepared from a depth of about 50 m at Pienaar's Pothole.

These garnet and ilmenite grains were analysed (Kaimmeyer and Frick, 1978) on the scanning electron microscope using a multi-channel analyser. A magnesium-rich almandine garnet (Alm 1) and a kimberlitic ilmenite (Il 5) were used as standards.

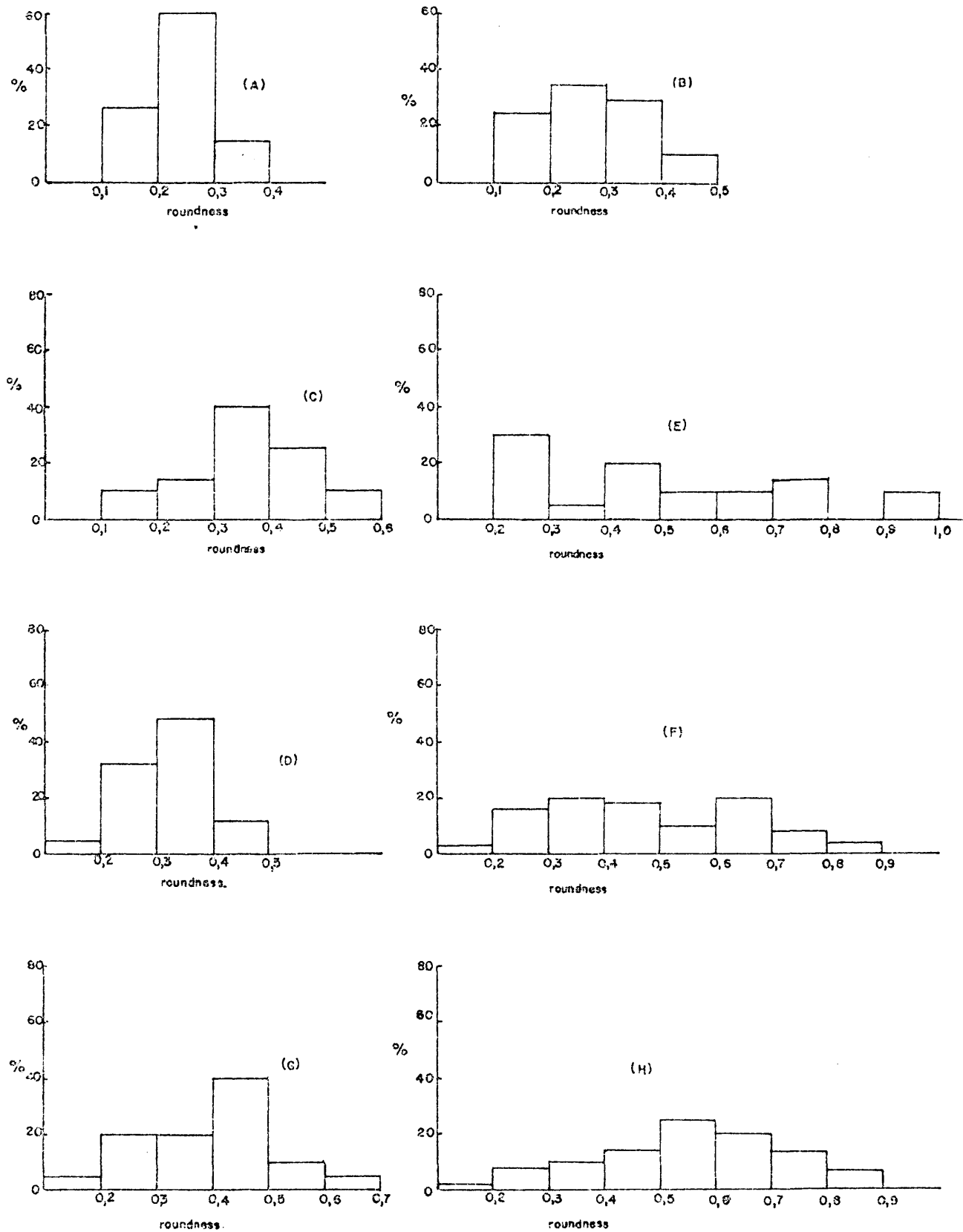


FIGURE 8 Histograms displaying the percentage of pebbles that fall into different roundness intervals for each sample.

Only one of the ilmenite grains analysed closely resembled kimberlitic ilmenite whereas the composition of the other grains was very similar to that of ilmenite from common igneous rocks (Table 4). The analysis of the garnet grains revealed that iron-rich, chromium-poor garnet occurred together with chromium-rich garnet that has a Cr_2O_3 content very similar to chromium-rich kimberlitic garnet. The kimberlitic garnet was purplish red in contrast with the non-kimberlitic garnet that had a mostly red to orange colour. Most grains of the kimberlitic garnet were 2 - 3 mm in diameter. A chromite grain very low in iron and high in magnesium and aluminium was identified by Kammeyer and Frick (1978) as piccotite spinel of possible kimberlitic origin. Figure 10 shows the position of the analysed ilmenite and garnet in relation to the field of kimberlitic ilmenite and garnet. Tables 3 and 5 display the composition and structural formulae of the garnet respectively. As total iron was determined as FeO the partition of iron between Fe^{2+} and Fe^{3+} was not known. Consequently the structural formulas were calculated on the basis of six divalent atoms*, first using Ca, Mg and Mn, and the difference from six was considered to be Fe^{2+} . Any excess iron was taken as Fe^{3+} and grouped with aluminium and chromium. The composition of the kimberlitic garnet in terms of trivalent metals (after Snyman, 1973) is indicated in Figure 11.

Two types of manganese nodules were distinguished in the gravel. The most common one consists mostly of manganese oxide and silica whereas the second type contains notable amounts of barium and smaller amounts of aluminium, silicon, potassium and iron. Kammeyer and Frick (1978) consider the chemical composition of the manganese nodules in the gravel to be very similar to that of manganese ores in the Pretoria Group and that the manganese of these nodules and ores could possibly have originated from the same source, namely the weathering of the Ventersdorp lava.

*which would imply 24 oxygen atoms

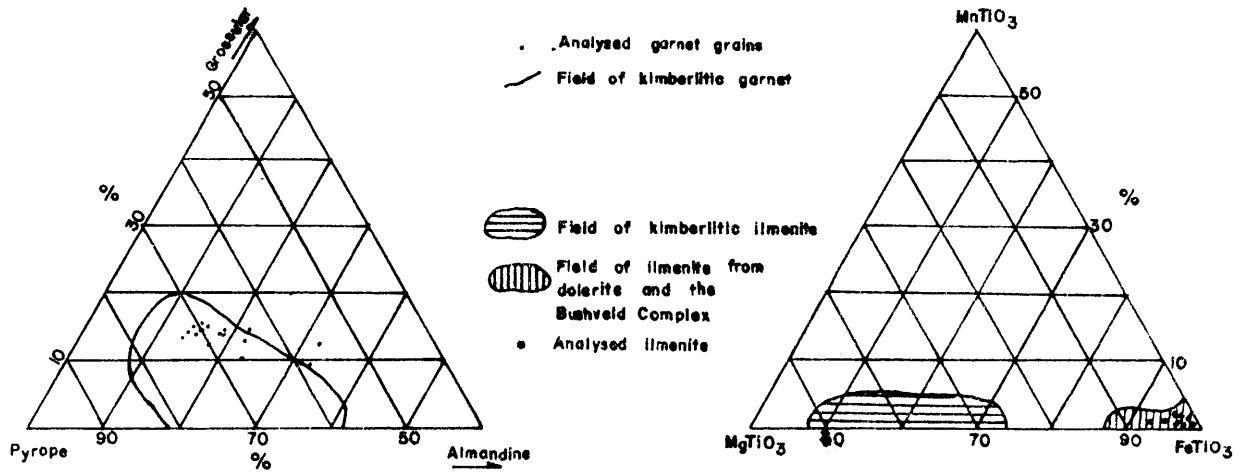


FIGURE 10 Composition of analysed garnet and ilmenite from Pienaar's Pothole

Composition of analysed ilmenite from Pienaar's Pothole

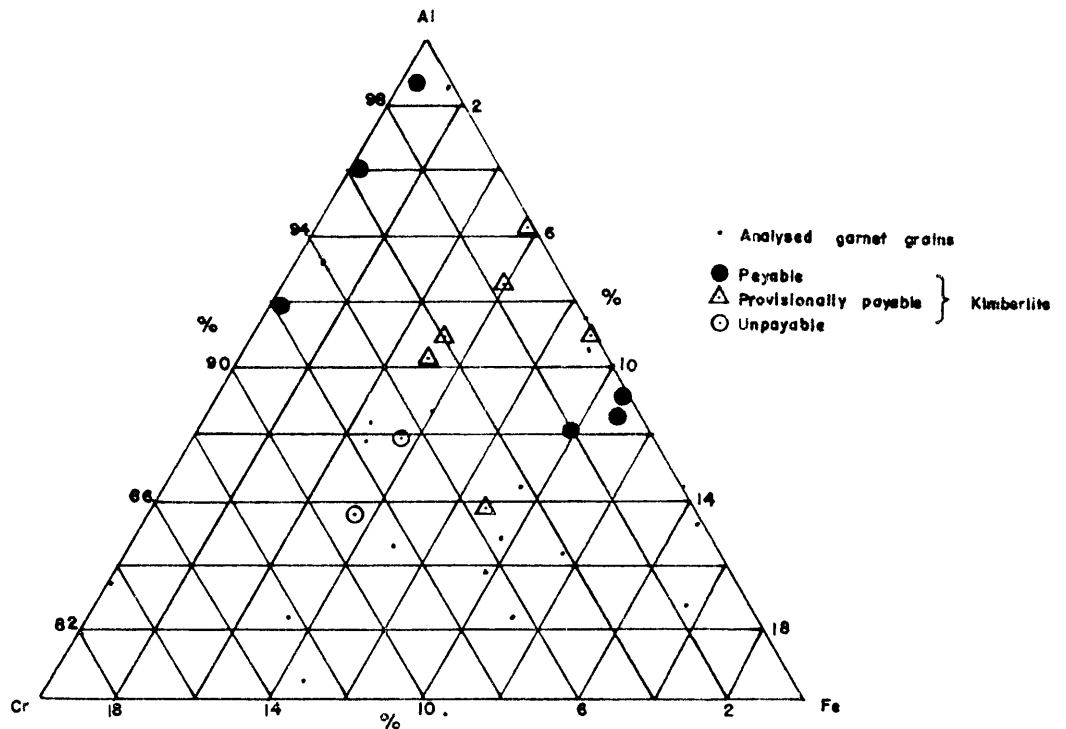


FIGURE 11 Composition of kimberlitic garnet from Pienaar's Pothole in terms of trivalent metals correlated with the composition of garnet from payable, provisionally payable and unpayable kimberlites. (After Snyman, 1973)

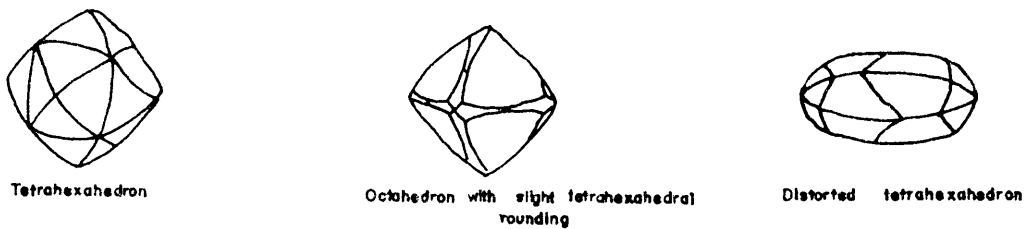


FIGURE 12 Common shapes of diamond from the Lichtenburg diamond fields

TABLE 3 : Chemical analyses of garnet (a-w) from Pienaar's Pothole compared with kimberlitic garnet (A-F)

WEIGHT PERCENT OF THE OXIDES

	a	b	c	d	e	f	g	h	j	k	l	m	n	o	p	q	r	s	t	u
MgO	18,09	18,54	18,86	17,74	18,99	17,16	19,34	19,18	19,37	19,25	19,49	19,24	19,63	20,36	18,85	20,04	19,58	19,14	17,34	19,72
Al ₂ O ₃	21,36	20,98	21,56	22,89	20,95	19,64	20,89	19,98	19,61	20,70	19,44	20,23	19,21	20,48	19,78	20,08	19,46	18,70	19,44	19,35
SiO ₂	42,73	42,74	41,05	41,03	43,43	42,64	40,68	42,53	42,80	42,92	42,59	40,64	42,64	42,49	39,37	41,34	40,09	39,91	39,99	40,81
CaO	4,62	3,93	5,22	4,82	4,78	4,84	5,03	5,31	5,76	4,47	4,83	5,32	5,14	4,62	3,91	4,36	4,33	3,98	3,98	4,35
Cr ₂ O ₃	0,03	0,25	2,15	0,08	1,84	1,90	4,91	1,42	2,78	2,48	3,36	5,87	4,23	2,66	0,58	3,07	4,47	3,33	0,15	2,41
MnO	0,41	0,22	0,13	0,30	0,28	0,13	0,22	0,13	0,14	0,31	0,13	0,21	0,31	0,27	0,07	0,24	0,24	0,28	0,25	0,18
Fe ₂ O ₃ as FeO	11,49	11,42	9,12	11,66	9,20	9,15	8,25	8,56	7,55	7,74	7,65	7,01	6,76	6,28	17,75	11,68	12,14	14,67	18,39	13,71
Total	98,73	98,08	98,09	98,52	99,47	97,46	99,32	97,11	98,41	97,87	97,49	98,52	97,92	97,16	110,31	100,81	100,31	100,01	99,54	110,53

	u	v	w	A	B	C	D	E	F
MgO	18,966	18,88	14,21	20,98	20,15	21,54	16,20	15,40	20,79
Al ₂ O ₃	19,52	17,69	21,14	18,91	23,00	19,83	22,75	21,79	21,55
SiO ₂	40,62	39,42	41,01	41,98	42,86	42,73	41,34	41,30	41,71
CaO	3,90	5,03	6,80	5,21	5,20	4,69	5,17	5,38	5,22
Cr ₂ O ₃	1,40	4,04	0,06	4,02	0,30	2,92	2,96	0,18	2,97
MnO	0,13	0,09	0,27	0,24	0,30	0,33	0,36	0,44	0,31
Fe ₂ O ₃ as FeO	15,35	14,45	17,27	8,68	8,65	8,68	13,60	17,34	8,29
Total	99,88	99,51	100,76	100,02	100,45	100,72	102,76	101,83	100,84

Where A = High chromium kimberlitic garnet B = Low chromium kimberlitic garnet
 C = High magnesium kimberlitic garnet D = Low magnesium kimberlitic garnet
 E = Eclogitic garnet

0000-----0000

TABLE 4 : Composition of a typical kimberlitic ilmenite (A) compared with those of ilmenite from Pienaar's Pothole

	A	1	2	3	4	5	6	7	8	9	10	11	12	13	14	15	16	17	18	19
TiO ₂	55,0	53,7	52,9	52,3	49,0	53,7	50,2	49,2	50,3	54,2	50,8	47,78	49,79	46,31	48,80	49,10	52,03	48,85	48,87	45,2
Fe ₂ O ₃ as FeO	30,0	47,2	41,8	48,2	52,2	43,7	50,6	51,3	50,2	46,0	50,5	49,71	47,00	51,45	48,88	50,40	47,90	51,38	49,12	46,0
MnO	0,2	0,45	1,67	0,47	0,32	2,35	0,64	0,63	1,75	0,50	1,04									
MgO	14,0	0,57	0,20	0,74	1,23	0,10	1,37	1,94	0,10	0,29	0,51	2,10	1,50	1,00	2,40	1,05	0,77	1,29	0,90	7,0
Cr ₂ O ₃	1,0	0,02	0,64	0,07	0,04	0,01	0,01	0,04	0,02	0,02	0,02	0,15	0,10	0,21	0,32	0,05	0,23	0,08	0,06	1,4
T O T A L	100,2	101,94	97,21	101,78	102,79	99,75	102,89	103,11	102,27	101,01	101,87	99,74	98,29	98,97	100,40	100,60	100,93	101,60	98,95	99,6

Table 5 Structural formulas of garnet grains from Pienaar's Pothole

	a	b	c	d	e	f	g	h	i	j	k	l
Si	6,2102	6,2373	5,9995	5,9955	6,2471	6,2489	5,9020	6,2384	6,2111	6,2203	6,2224	5,9318
Al	3,6616	3,6114	3,7167	3,9453	3,5545	3,3949	3,5749	3,4568	3,3567	3,5285	3,3500	3,4828
Cr	0,0034	0,0289	0,2485	0,0092	0,2093	0,2202	0,5634	0,1647	0,3191	0,2843	0,3883	0,6777
Fe	0,0847	0,0678	0,0566	0,0809		0,0822		0,0937	0,0670			
Total	3,7497	3,7081	4,0218	4,0354	3,7638	3,6973	4,1383	3,7152	3,7428	3,8228	3,7383	4,1605
Ca	0,7195	0,6145	0,8175	0,7547	0,7367	0,7600	0,7819	0,8346	0,8957	0,6941	0,7564	0,8320
Mg	3,9102	4,0323	4,1079	3,8633	3,9852	4,1847	4,1817	4,1928	4,1892	4,1578	4,2437	4,1852
Mn	0,0505	0,0272	0,0161	0,0379	0,0341	0,0161	0,0270	0,0162	0,0172	0,0381	0,0161	0,0260
Fe	1,3118	1,3260	1,0585	1,3441	1,1068	1,0392	1,0010	0,9564	0,0879	0,9381	0,9347	0,8557
Total	6,0000	6,0000	6,0000	6,0000	5,8628	6,0000	5,9916	6,0000	6,0000	5,8281	5,9506	5,8589

	m	n	o	p	q	r	s	t	u	v	w
Si	6,2042	6,1751	5,8480	5,9650	5,8650	5,9077	5,800	5,9590	5,9890	5,8970	6,0500
Al	3,2969	3,5110	3,4620	3,4150	3,3550	3,2650	3,4320	3,3300	3,3920	3,1050	3,6750
Cr	0,4868	0,3058	0,0690	0,3500	0,5170	0,3899	0,018	0,2780	0,1630	0,4780	0,0070
Fe			1,0090	0,4210	0,4620	0,7045	0,545	0,6700	0,6900	0,8350	0,3790
Total	3,7837	3,8168	4,5400	4,1860	4,3340	4,3594	4,295	4,278	4,2415	4,418	4,061
Ca	0,8014	0,7195	0,6220	0,6740	0,6790	0,6310	0,6390	0,6810	0,6160	0,8060	1,0870
Mg	4,2567	4,4102	4,1730	4,3090	4,2690	4,2224	3,8710	4,2920	4,1660	4,210	3,1240
Mn	0,0382	0,0332	0,0050	0,0290	0,0290	0,0350	0,0320	0,0230	0,0160	0,0110	0,0340
Fe	0,8226	0,7634	1,1960	0,9880	1,0230	1,1116	1,4580	1,0040	1,2020	0,9730	1,7550
Total	5,9189	5,9263	6,0000	6,0000	6,0080	6,0000	6,0000	6,0000	6,0000	6,0000	6,0000

The most common crystal form of diamond from the Pypklip, Welverdiend-Grasfontein and Vlakplaats-Uitgevonden runs is the tetrahexahedron (Robinson, 1978) and the distorted tetrahexahedron followed by octahedrons with slight tetrahexahedral rounding (Figure 12). Crystal edges of diamond are normally sharp and crystal faces do not seem to display any indications of abrasion (Davis and Prevost, 1977). However, diamond cleavage 'chips' and broken crystals are common.

A quantitative XRD analysis (undertaken by the Geological Survey) of the matrix of the upper and lower gravels revealed the following results:

lower gravels : Quartz 65 per cent; kaolinite 31 per cent; sericite 4 per cent.
upper gravels : Quartz 76 per cent; kaolinite 18 per cent; sericite 4 per cent; hematite 2 per cent.

5. THE GRAVITY SURVEY

All geophysical methods are based on some contrast in the physical properties of different rock materials, e.g. density, magnetisation, electrical properties, elasticity, etc. It should also be borne in mind that geophysical results have to be combined with geological information to provide geologically realistic and useful answers.

Gravity anomalies result from the local variations in density. The success with which the gravity method can be applied depends on the density contrast between the different rock types that have to be differentiated and the size to depth ratio of the anomalous bodies.

The presence of diamondiferous gravel material in leached sinkhole-prone zones in the dolomitic formations, and the occurrence of gravel-filled sinkholes, hidden under a red soil cover has already been discussed.

The problem of locating sinkholes and leached zones in the dolomite is most successfully solved by the application of the gravity method as proved by the following examples, viz the location of sinkhole prone areas on the Far West Rand (Kleywegt and Enslin, 1973); the determination of water-bearing leached zones in the Grootfontein Dolomitic Groundwater Compartment, Rooigrond-Ligtenburg area (Palmer, 1978) and a preliminary investigation of the Bakerville diamond runs (Darracott, 1973). Thus the purpose of the gravity survey was to identify and located these leached structures so that they could be further explored for gravel deposits, particularly those hidden beneath a cover of red soil.

5.1 Fieldwork procedure and data reduction

The area selected for this geophysical investigation on the farm Ruigte=laagte and vicinity (called the Ruigtelaagte area (Figure 2)) was meant to cover the Ruigtelaagte diamondiferous runs, Pienaar's Pothole and sufficient dolomite and chert outcrops to allow the calculation of a realistic regional gravitational field. A station spacing of 50 m was chosen for the survey.

From the Ruigtelaagte beacon Gruishoop 263 with co-ordinates ($Y = 87\ 285,33$ m, $X = 2\ 872\ 973,60$ m) an east-west reference line was determined parallel to the proposed long axis of the area. This simplified the theoretical gravity calculation. To the northwestern corner point of the area, (co-ordinates $Y = 87\ 300,00$ m, $X = 2\ 873\ 000,00$ m/Lo 27° system*) the local co-ordinates $Y = 0$, $X = 0$ were assigned. Locally Y increases to the east and X increases to the south. The local co-ordinates can be transformed to co-ordinates in the Lo 27 system in the following manner:

*The South African co-ordinate system is based on the Gauss conform projection. It consists of belts running N-S, 2° of longitude wide, the central meridian being every odd meridian, i.e. 15°, 17°, 19° ... 31°. Each belt is referred to as Lo 15, Lo 17, etc. In a →Lo system Y is positive to the west of the central meridian.

real y co-ordinate = $A_y - \text{Loc } y$

real x co-ordinate = $A_x + \text{Loc } x$

where:

A_y = y co-ordinate of the northwest corner point (87 300,00 m)

A_x = x co-ordinate of the northwest corner point (2 873 000,00 m)

$\text{Loc } y$ = local y co-ordinate

$\text{Loc } x$ = local x co-ordinate.

For simplicity the local y co-ordinates are denoted y_0, y_1, y_2 etc. and the x co-ordinates are x_0, x_1, x_2, x_3, x_4 etc. (Figure 2). (x_1 indicates a distance of a 100 m from the origin etc.).

The co-ordinates of stations on the perimeter and through the middle of the area were calculated theoretically. After first obtaining the exact co-ordinates of a reference point in the near vicinity of the station by resections (employing the methods of Snellius and Blunt) the position of a particular station in the field was determined by polar computation. By using resections again the co-ordinates of these field stations were obtained and compared with the theoretical values. All station positions determined in this manner are accurate to one metre of the required values. A T2 theodolite and a tellurometer were used for this purpose. The following beacons were used in the co-ordinate determinations:

Gruishoop	263
Delwery	254
The Gat	62
Houthaaldoorns	32

Each individual square kilometre block was thereafter covered with a station spacing grid of 50 m using a theodolite, ranging poles and a plastic cable with a length of 50 m. This was no easy task due to the past activity of the diggers and the vegetation in places so that station

positions inside the area are slightly less accurate owing the already mentioned undulating topography that prevented the measuring cable that was used to space the stations, from being laid horizontally. Wooden pegs marked with local Y/X co-ordinates were used to indicate the gravimeter stations in the field.

On the northern and southern perimeter of the Ruigtelaagte area gravimeter stations with local integer y co-ordinates (e.g. Y12) and in the middle of the area, stations with real y co-ordinates (e.g. Y12,50) were used as gravitational base stations. These base stations were tied in with a La Coste - Romberg gravimeter. For the remaining gravimeter stations a Sharpe gravimeter was used along the north-south lines of each 1 km² block, beginning or ending at either a northern or a southern base station approximately every hour.

Due to a highly undulating topography over the runs, gravimeter stations had in some instances to be moved to minimise terrain corrections. Height determinations of each gravimeter station by precise levelling with a Zeiss automatic level and Nestle levelling staffs, followed the completion of the gravimeter survey on an individual 1 km² block. The accuracy of the level was checked daily when in use. The height of beacon 263 was used as reference from which station (Y0/X10) was tied as starting point.

5.1.1 Gravimeter base stations and drift corrections

A third order Bakerville base station (Figure 1) was tied in from the second order Rooigrond gravimeter base station (Value = 978 602,05 mgal) with a temperature stabilised La Coste-Romberg gravimeter. The Rooigrond base station was tied in from the Pretoria pendulum station making use of a long term drift curve (Palmer, 1978; Maher, 1979(a))

The La Coste-Romberg gravimeter was used in two separate surveys that involved reading it for periods of 4 hours at the Rooigrond and Bakerville base locations alternatively. After earth tide and drift corrections had been applied the absolute gravity value of the Bakerville base was determined as 978 585,65 mgal. From the Bakerville base station primary base stations in the Ruigtelaagte area were established by reading the La Coste-Romberg gravimeter hourly at the Bakerville base station. Later these primary base stations on Ruigtelaagte were instrumental in the determination of the absolute gravity values of the remaining base stations in the area. Due to the fact that hourly readings at base stations could be taken earth tide corrections were ignored.

For the gravity survey a Sharpe gravimeter with a gravimeter constant of 0,09950 mgal/div. was used. The gravimeter sensitivity and levels were checked periodically during the survey. No tidal corrections were applied to these data because they have been taken into account by the hourly drift corrections.

Due to the fact that all gravimeter base stations are tied to the Bakerville base the hourly drift for the La Coste-Romberg and Sharpe gravimeters was calculated as if only the Bakerville base had been used. Thus the absolute gravity values of all the gravimeter stations are tied directly to the Pretoria base station (I.G.S.N. value 978 616,22 mgal) and the Pretoria pendulum station through the work of Maher (1979(a)).

5.1.2 Reduction of gravity data

To be able to compare theoretical gravity values (calculated at sea-level) with absolute observed gravity values, the theoretical values have to be adjusted for height above sea-level and the attraction of the material between the gravity station and sea-level. Thus the application of the

free-air and Bouguer reductions to the theoretical values reduces each theoretical gravity value to station level. The difference between these corrected theoretical gravity values and the corresponding observed gravity values result in Bouguer anomaly values which are applicable to the station level. All gravity values were reduced to Bouguer anomalies. Although terrain effects were significant in a few instances, e.g. around Pienaar's Pothole, no corrections were calculated. All calculations for the reductions were performed by means of a Hewlett-Packard 67 programmable calculator with programs developed by the author.

The free-air correction

The free-air correction considers only the negative effect of the height above sea-level on the theoretical gravity values.

The gravity attraction of a spherical earth on a unit mass, a distance r from the earth's centre is $g = kM/r^2$

where g = gravitational attraction per unit mass

k = gravitational constant

M = mass of the earth.

The gradient of the gravitational attraction due to variations in the distance from the earth's centre is provided by the derivative with respect to the radial distance in the gravitational attraction formula

$$\frac{\partial g}{\partial r} = \frac{-2kM}{r^3} = \frac{-2g}{r}$$

At sea-level the numerical value of the gradient is $-0,3086$ mgal/m. If a spheroidal earth is considered then the vertical gradient according to Heiland (1940) is

$$\frac{\partial g}{\partial r} = -0,30855 (1 + 0,00071 \cos 2\theta) \text{ mgal/m where}$$

θ is the latitude. In the Western Transvaal (Ruigtelaagte 353 JP) the second term only accounts for $-0,000135$ mgal/m and can be neglected.

$$\text{Thus the free-air anomaly} = g_{\text{obs}} + 0,3086h - g_t$$

where g_{obs} = absolute gravity value

h = height above sea-level

g_t = theoretical gravity value.

The Bouguer reduction

The gravity effect of the material between sea-level and the gravimeter station is taken into account in the Bouguer correction which is derived by assuming an infinite horizontal slab of thickness equal to the station elevation in the vicinity of the stations and is given by

$$B_{\text{cor}} = \frac{-3\rho gh}{\rho_m R} = -0,1118 h \text{ mgal/m to a first approximation for}$$

crustal material with a density of $2,67 \text{ g/m}^3$ (Heiland, 1940)

where

ρ_m = mean density of the earth

R = radius of the earth

ρ = density of the crustal slab

h = height of gravimeter in metres above sea-level.

Since the terrain around a gravity station is not flat and deviations from a horizontal infinite slab thus occur terrain corrections have to be applied.

The combined free-air and Bouguer correction amounts to $0,196854 h$ mgal/m where h is the height above sea-level. The idealised Bouguer anomaly (Ervin, 1977) is calculated as

$$g_B = g_{\text{obs.}} - (g_{\text{theor}} - B_{\text{com}}) \equiv (g_{\text{obs.}} + B_{\text{com}} - g_{\text{theor}})$$

where g_{obs} = observed gravity value

B_{com} = combined free-air and Bouguer reduction

g_{theor} = theoretical gravity value.

The Bouguer anomaly map is presented in Figure 13.

Theoretical gravity values

The theoretical gravity values at sea-level were calculated by using the I.G.S.N., 1971 formula

$$g_{\text{theor}} = 978,0318 (1 + 0,0053024 \sin^2\theta - 0,0000058 \sin^2 2\theta) \text{ gal}$$

where θ = latitude of the station

The latitude was calculated from the Lo27 co-ordinates by using the program of Maher (1979(b)).

5.2 Bouguer anomaly map

The Bouguer anomaly values indicate deviations from the idealised (2,67 gm/cc) mass distribution above sea-level and are located at the varying elevations of their respective points of measurement.

The Bouguer anomaly values for the Ruigtelaagte area were plotted and contoured at an interval of 0,1 mgal (Figure 13).

At Y32/X8,5 a restricted area of 300 m by 300 m with more positive Bouguer anomaly values (gravity highs) indicates the possible presence of a dense material which could be due to a type of dolomite, more dense than the average or an

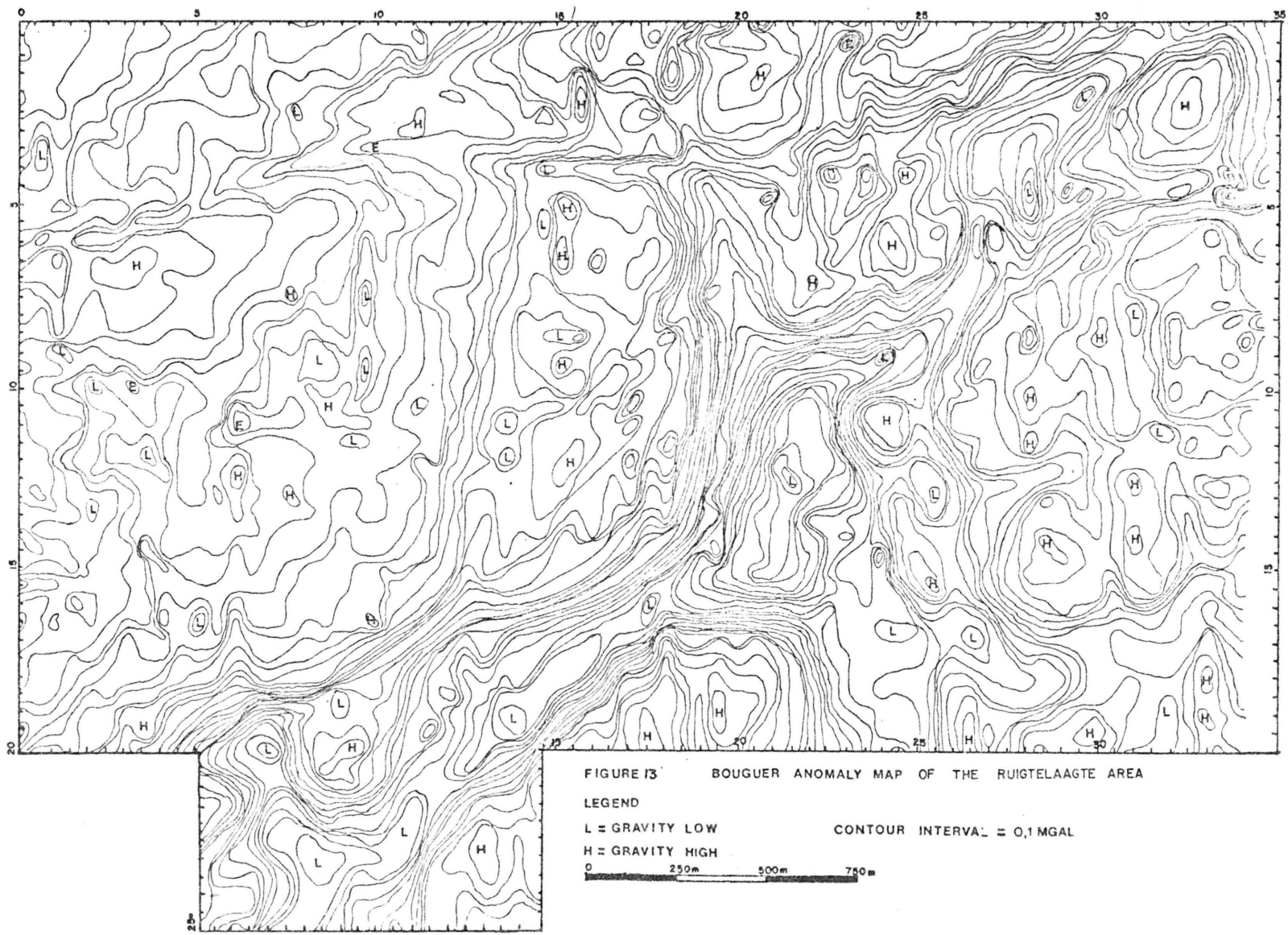


FIGURE 13 BOUGUER ANOMALY MAP OF THE RUIGTEPLAAGTE AREA

LEGEND
 L = GRAVITY LOW CONTOUR INTERVAL = 0,1 MGAL
 H = GRAVITY HIGH

0 250m 500m 750m

igneous intrusion. Only dolomitic chert crops out and no significant magnetic anomalies were observed at this Locality (Figure 14).

Since only a small portion of the Lyttelton Formation was covered by the gravity survey, too little information is available to comment on the possible differentiation between the Lyttelton and Monte Christo formations on the Bouguer anomaly map.

The gravels have a lower density ($1,85 \text{ mg/cm}^3$, Appendix 1) than the dolomitic bedrock ($2,85 \text{ g/cm}^3$; Kleywegt and Enslin, 1973, p.4) and thus areas displaying a negative density contrast (gravity "lows" on the Bouguer anomaly contour map) with respect to solid dolomitic bedrock are of interest.

5.3 Residual gravity anomaly map

To isolate the gravity "lows" on the Bouguer anomaly map a regional or background gravity field is calculated that would have been observed if dolomite cropped out everywhere. Since leached structures, which possess a negative density contrast with respect to the dolomite, influence the gravity values obtained over bordering solid, outcropping, dolomite, very few Bouguer values in the original area could be considered for the calculation of the regional field, so that gravity stations situated on large dolomite outcrops outside the area had to be used as well (Figure 15). A third degree, polynomial surface (Figure 16) gave the best and still realistic representation as regional field when the small size of the area is taken into consideration. The polynomial fit was calculated by a Fortran program available at the Geological Survey. Areas displaying negative density contrasts with respect to the dolomite are isolated when the regional field is subtracted from the Bouguer anomaly values and the remaining gravity field is called the residual gravity field. For the purpose of fitting the regional field to the Bouguer gravity values the more positive Bouguer values over the limited area on the eastern

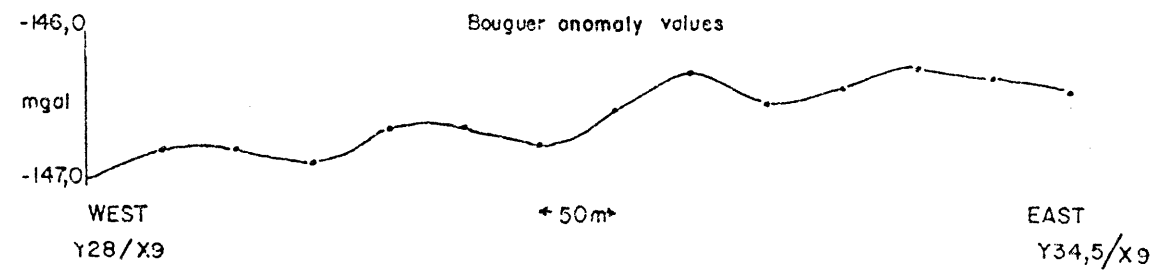
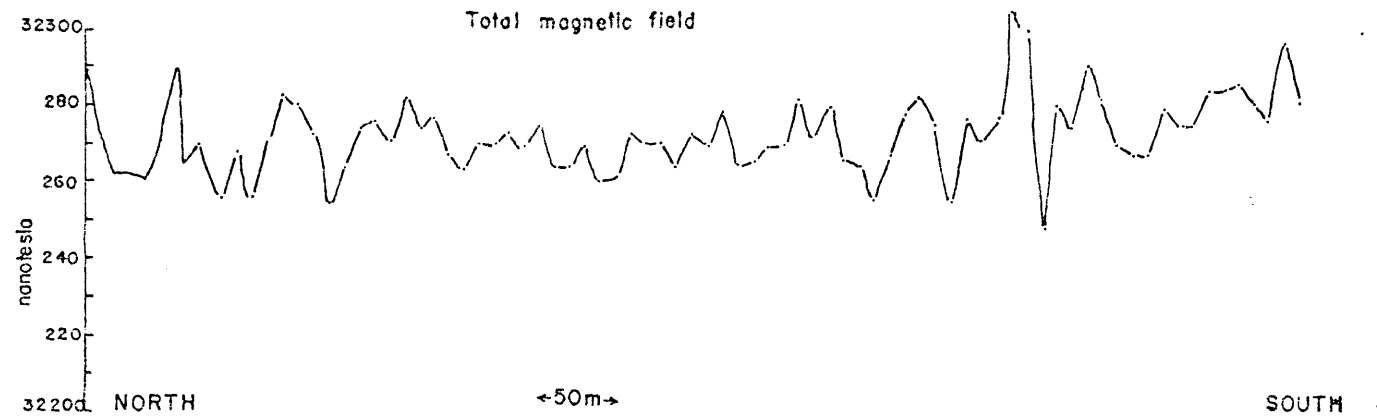
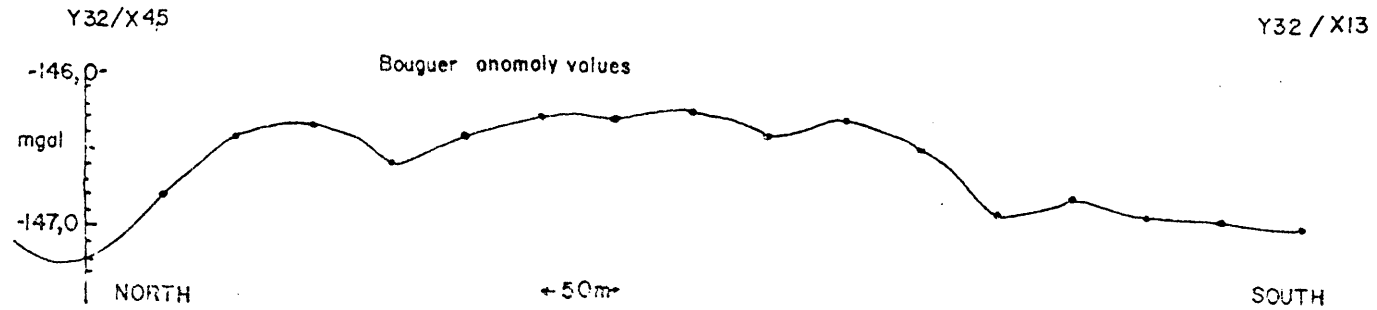


FIGURE 14 Gravity and magnetic profiles across area where possible intrusion occurs

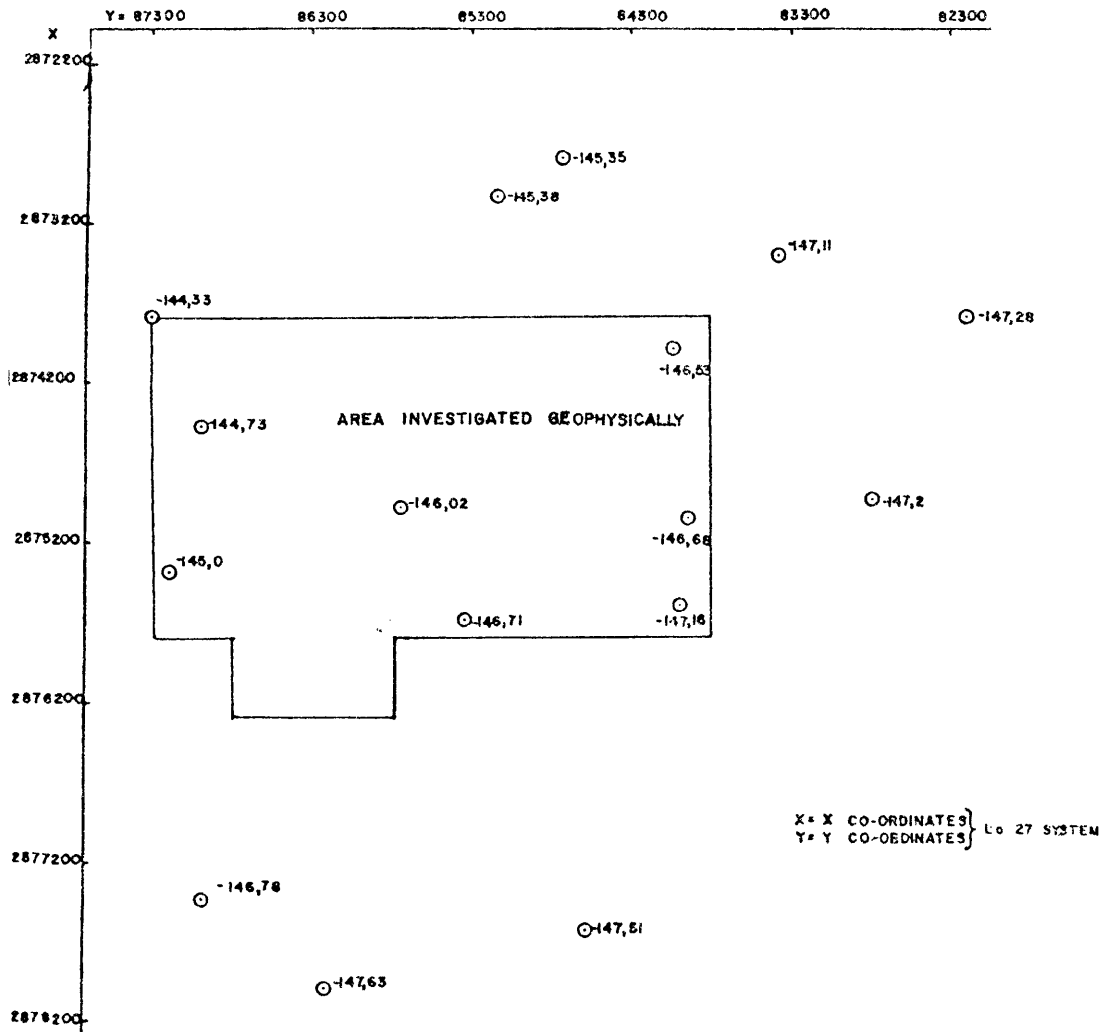


FIGURE 15 GRAVITY STATIONS AND VALUES (MGAL) USED IN THE CALCULATION OF THE REGIONAL GRAVITY FIELD

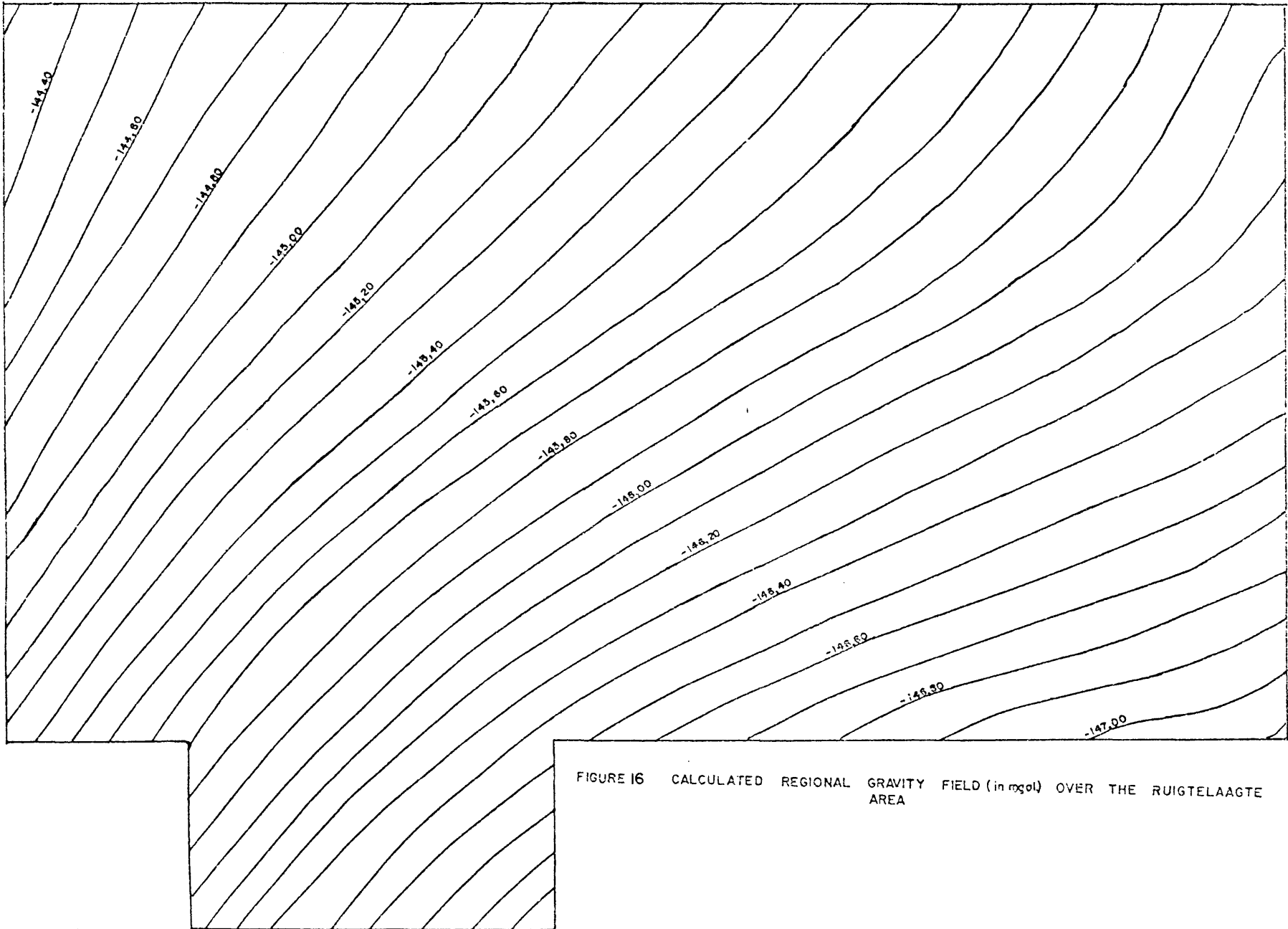


FIGURE 16 CALCULATED REGIONAL GRAVITY FIELD (in mgal) OVER THE RUIGTEPLAAGTE AREA



FIGURE 17 RESIDUAL GRAVITY MAP OF THE RUIGTELAAGTE AREA
 LEGEND
 L = GRAVITY LOW
 H = GRAVITY HIGH
 CONTOUR INTERVAL = 0,1 MGAL
 0 250m 500m 750m

boundary (Y31; X8,5) were considered to be due to dolomite. The resulting residual gravity map is shown in Figure 17.

5.3.1 Qualitative discussion of the residual gravity anomaly map

The negative anomalies on the residual map (Figure 18)* indicate the occurrence of material with a negative density contrast with respect to dolomite. Assuming a constant density contrast increasing negative residual gravity values would reflect an increase in thickness of the anomalous material. Consequently maximum thicknesses of material with a lower density than the dolomitic bedrock are indicated on the residual gravity map by L (for gravity low) and minimum thicknesses by H (gravity high). Since the main concern is the occurrence of leached structures in the dolomite with which diamondiferous gravels are associated, the distribution of large gravity lows is of special interest. However, it must be stressed that virtually no density contrast exists between the gravels and residual products formed by leaching of the dolomite, so that it is impossible to distinguish between the two on the basis of gravity data only.

(1) Dykes

A comparison of the geological map with the residual gravity map (Figure 18) shows that all the dykes in the area coincide with negative residual anomalies. The cores obtained in drilling on the dykes indicate that they all are of basic composition and since dolerite has a higher density than dolomite, the negative residual values over the dykes are attributed to deep weathering.

Owing to the leached zones adjoining the dykes any estimates based on the

*In map holder at back of thesis

residual gravity data about their depth and dip, will be inaccurate. No attempt to determine these parameters have been made since the magnetic data are much better suited for this purpose.

(2) Gravity lows over leached, partly gravel-filled, zones

The most prominent anomaly visible on the residual gravity map is situated roughly parallel to the Ruigtelaagte-Zamenkomst boundary, strikes north-east, and appears to have been displaced by a north-north-west striking gravity low in the vicinity of the Pienaar's Pothole. Smaller gravity lows striking roughly north-south form angles 60° to 90° with the former prominent north-east striking gravity low.

Kleywegt and Enslin (1973) reported the occurrence of a number of widely spaced post-Transvaal tension fractures and faults of limited extent and displacement that facilitated the leaching of dolomitic limestones on the Far West Rand between Carletonville and Westonaria. Jennings (1965) reported leached joints and cracks intersecting at angles of 60° in the dolomite on the Far West Rand and Davis and Prevost (1978) also reported a small fault with a north-south strike direction on Welverdiend 361 JP. The north-east striking gravity low could thus represent a leached post-Transvaal tension fracture and the north-north-west striking gravity low a shear fault that must be older than dyke d_1 , which cuts across it without no displacement.

As the above-mentioned structures form permeable zones which are present on both sides of dykes defining several groundwater compartments it can be accepted that the movement of groundwater takes place along these zones so that sinkhole formation was and still is most prominent along these structures (Enslin et al, 1976; Kleywegt and Enslins, 1973). The intersection of the two major leached zones proved ideal for sinkhole formation, which possibly resulted in the initial formation of Pienaar's pothole

in the late Tertiary. Since surface observations showed that the palaeo-river at least partly exploited these two major leached zones, they form the most important targets for the exploration of virgin gravel. A maximum residual gravity anomaly of -3,0 mgal was encountered about a 100 m north of Pienaar's Pothole.

On the north-east striking gravity low (between Y22; X12 and Y26,5; X4) gravel is present between the Welverdiend-Grasfontein run and Pienaar's Pothole. Near the Ruigtelaagte-Zamenkomst boundary (Y5, X20 and Y9; X25) gravels also occur on the same structure. Two gravel-filled sinkholes were encountered north-east of Pienaar's Pothole on this gravity low (Y22; X11 and Y24,5; X9,5), whilst only thin gravel deposits occur on the north-north-west striking gravity low (X19, X6,5). It thus appears that if the leached zone along the north-east striking structure was better developed than that along the so-called shear fault. Sinkhole S₃, near the Ruigtelaagte-Zamenkomst boundary (Y6,5; X20) which is filled with gravel and clay displays a prominent oval-shaped gravity anomaly with a residual maximum gravity value of -1,8 mgal over its centre. Drilling on this sinkhole revealed possible slump structures (Figure 22) in the gravel, substantiating the sinkhole model of deposition. If the quartz veins (Figures 2 and 18) acted as a aquiclude in the dolomite, groundwater concentrations on the flanks of the quartz veins could have caused the development of sinkholes so that the quartz veins probably played some part in the formation of this sinkhole, although the shape of the residual gravity field suggests joint control.

To the south of sinkhole S₃ (Y7,5; X22,5) only superficial gravel deposits are present on the western side of a shoe-shaped residual gravity contour pattern and this is an example where no major gravel deposits are associated with a major gravity low. However, drilling revealed thick layers of gravel and clay in the area between Y6,5 to Y9 and X23 to X25, charac=

terised by a prominent north-east striking gravity low. A residual gravity low of -1,7 mgal is encountered over this gravel-filled leached structure.

The conspicuous gravity lows associated with dyke d_2 , especially in regions covered with red soil (Y29,5; X12) were also investigated but gravel was only found in small amounts along the flanks at great depth (about 15 m) below layers of red brown soil. Gravels are, however, more abundant on dyke d_2 , just south of the dyke intersection (Y26,5; X5 to X8).

South of dyke d_1 (Y15; X5), the branching of the Welverdiend-Grasfontein gravel run can again be ascribed to karst exploitation. Previously worked gravel deposits, between 3 and 9 m thick, seem to have occurred in small sporadic sinkholes and collapsed channels, but if the size of the residual gravity anomalies are compared to the depth of excavation it seems as if great thicknesses of virgin gravel may still be present under the worked gravels. No drilling could be undertaken here because of the extremely rough terrain.

Agate-bearing gravel was found at a depth of 29 m in a borehole on a small negative gravity anomaly east of the Pienaar's Pothole (Y25,5; X12).

Another interesting negative gravity anomaly centered on (Y23:X4) is characterised by a thick gravel deposit. A comparison between the depth obtained from the gravity anomaly values and the depth (10 m) to which gravel was mined indicates that virgin gravel could still be present here. However, this could not be verified by drilling.

Conclusions which can be drawn from the residual gravity map of the Ruigtelaagte area are as follows:

- (1) Gravity lows obtained adjacent to dykes are likely areas in which gravel-filled sinkholes may occur.

- (2) The more prominent a leached structure, the greater the chance of it containing thick, virgin gravel deposits.
- (3) There is no difference between the residual gravity anomalies over karst structures containing dolomitic debris and those filled with gravel. Only drilling can differentiate between the two and thus the most successful method of prospecting for virgin gravel deposits is to locate the associated leached zones.
- (4) The partly gravel-filled leached zones contain low density material, which is usually porous. If the zones extend below the groundwater level and are permeable they are also important to farm owners or diggers for future water supplies (Enslin et al, 1976).

(3) Residual gravity anomalies not associated with the gravel runs

Positive residual gravity anomaly values of up to 0,2 mgal are encountered over a very limited region along the eastern border (Y34; X6 to X9) of the area under consideration. These resulted due to the limitations in curvature of the third degree polynomial when the regional field was fitted to the Bouguer values. Although the regional field here may be influenced by the already mentioned possible intrusion of a rock type with a density higher than that of dolomite, the residual gravity field should be treated as if no positive residual anomaly exists.

In the limited area under consideration no distinction can be made between the Lyttelton and Monte Christo Formations on the basis of residual gravity patterns because only a very small area of the Lyttelton Formation was covered by the gravity survey.

The quartz veins in the area do not cause any significant gravity anomalies due to their small width (about 10 m).

5.3.2 Three-dimensional gravity modelling by digital computer

Owing to their irregular shape, some of the leached gravel-filled structures on Ruigtelaagte can be better approximated by three-dimensional models.

Consequently a three-dimensional computer approach was resorted to.

Three-dimensional gravity interpretation is well documented in the literature (Talwani and Ewing (1960), Cordell and Henderson (1968), Morgan and Faessler (1972)). New approaches in three-dimensional modelling have mostly been aimed at bringing down the cost of such operations. The Powell (1965) and Marquardt (1963) iteration algorithm; were suggested for reaching faster solutions by Bhattacharyya (1978) and various approximations have been proposed for speeding up the calculation of gravity anomalies due to three-dimensional bodies (Barnett (1976), Mufti (1975), Ku (1977)).

To calculate from the observed residual gravity values a physical model is called the inverse gravity problem and there are two main approaches to solve this problem.

- (1) Trial and error method where the model is constructed on a trial and error basis, e.g. Talwani and Ewing, (1960) or Barnett (1976). The drawback of this approach is that all the corner co-ordinates of the body have to be specified so that data input is very tedious.
- (2) Iteration where the model is constructed of three-dimensional shapes (usually cubes or rectangular parallelepipeds) e.g. Mufti

(1975) and Cordell and Henderson (1968) along the general lines of procedures as suggested by Bott (1960) or Danés (1960) where iteration is used to reach a solution. Iterative methods in general comprise three aspects:

- a) A "starter model"
- b) Calculation of the gravity effect of the tentative starter model, and
- c) A modification of the model, based in some way on the disagreement between the previously calculated gravity anomaly and the observed anomaly (Cordell and Henderson, 1968). Here again care must be taken to keep the modification procedure, which is obviously made without the benefit of human judgement, as short as possible.

A new three-dimensional iterative gravity interpretation program was developed by Kleywegt and Stettler (1979) of which a description and listing appears in Appendix 3. In this program rectangular parallelepipeds are used to build a theoretical model. The gravity effect over a rectangular parallelepiped was calculated after Banerjee and Das Gupta (1977) and the derivation of the formula is presented in Appendix 2.

The procedure adopted in the program is to calculate an initial "starter model" by using the Bouguer slab formula. The exact gravity field caused by the "starter model" is then calculated by employing the formula for the gravity field over a rectangular parallelepiped and compared with the observed gravity anomaly. The iterative process begins where the difference between the two is converted to thicknesses by again using the Bouguer slab formula and these adjustments are added to the thicknesses of the initial starter model. The increase or decrease in the theoretical gravity field due to the

adjustments in thickness of the starter model are calculated by using a formula that approximately describes the gravity field caused by a cylinder (Nettleton, 1978). Thereafter the theoretical and observed gravity anomalies are again compared and the difference converted to thickness so that the whole iterative process follows again. After three iterations the iterative process is followed by the calculation of the exact gravity field due to the adjusted model whereafter this gravity field is again compared with the observed field and a new cycle of iterations with cylinders begins.

The program converges very rapidly and normally only six cylinder iterations are sufficient to produce a solution to the inverse gravity problem.

5.3.3 Structure of the gravel runs based on residual gravity anomalies and borehole data

Residual gravity values over known gravel-filled karst structures were selected and interpreted using this iterative computer approach. It must be borne in mind that the computer result provides a solution for the observed residual gravity values. Owing to the fact that the influence of gravity lows bordering the areas selected is not compensated for in the interpretation, the depth to the bedrock on the perimeter of each selected area will be in error. To overcome this problem a larger area than is required must be digitised and fed to the computer.

A density contrast of 1 g/cm^3 (see Appendix 1) was used and since no significant density contrast exists between the gravels and the weathered dolomitic material the interpreted thickness to dolomitic bedrock incorporates both.

(1) Southern boundary of Ruigtelaagte 353 JP

The residual gravity field over this area is displayed in Figure 19, the numerical values are given in Table 6 and the calculated structure of the dolomitic bedrock over the gravel deposits near the Ruigtelaagte-Zamenkomst boundary is depicted in three-dimensional form in Figure 20. The calculated depths to dolomitic bedrock are indicated in Table 7 and the difference between the observed and calculated gravity values are given in Table 8. After only six cylinder iterations (i.e. two exact iteration cycles) an extremely good fit between the observed and calculated gravity values was achieved.

The distribution of gravel as determined by drilling is shown in Figure 21 and coincides with the major north-south leached zone depicted on Figures 19 and 20. Sinkhole S_3 formed at the intersection of this zone and a south-west striking leached structure. This again suggests that the formation of sinkholes was controlled by joints and that these joints and sinkholes were exploited by palaeorivers.

An interpretation of the drilling results is shown as sections in Figures 22, 23 and the borehole locations in Figure 21. Over the centre of sinkhole S_3 a maximum depth of 70 m to the dolomitic bedrock was calculated. With drilling large thicknesses of wad and leached dolomite were encountered beneath the gravel layers but due to the frequent collapse of the boreholes the exact depth to the dolomitic bedrock is not known.

The gravel deposits south of sinkhole S_3 (Y6,5 to Y9 and X23 to X25) most likely also extend into Zamenkomst 4 IP. Gravel thicknesses of up to 40 m were encountered by drilling (Figure 22, Section C) while the greatest calculated depth to bedrock is 73 m. Owing to the frequent collapse of boreholes this calculated depth could not be verified either.

The diamond content of gravel layers was determined from samples obtained from boreholes with a diameter of 0,75 m, sunk by means of a Masserenti

X18,0
Y5,0

X18,0
Y12,0

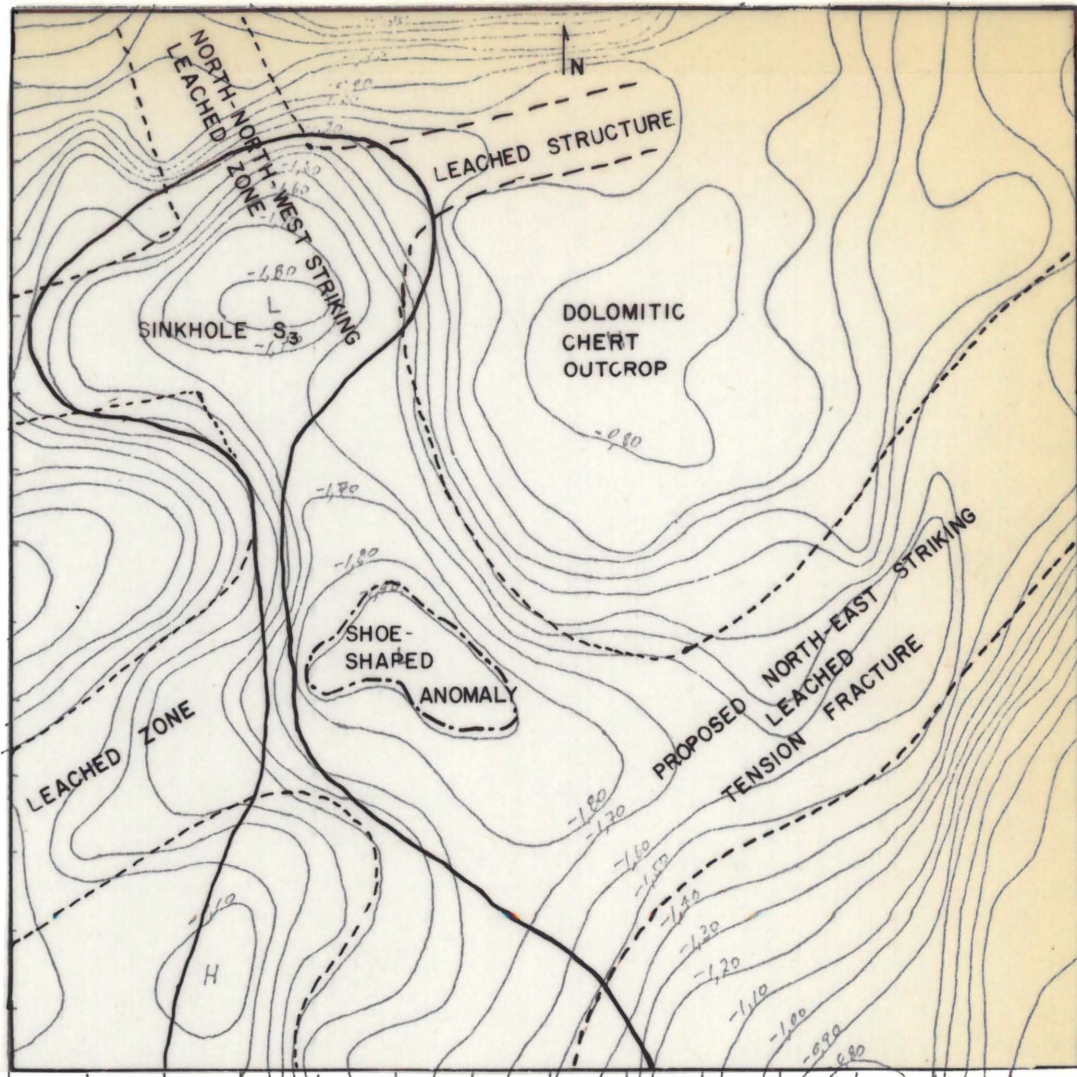


FIGURE 19 RESIDUAL GRAVITY FIELD IN THE VICINITY OF SINKHOLE S₃, NEAR THE SOUTHERN BOUNDARY OF RUIGTELAAGTE 353 JP

0 50m 100m 200m

Residual gravity field in mgal.

TABLE 6: Residual gravity field (in mgal) near the Ruigteoogs-Zamenkomst boundary used for the calculation of the depth to the dolomitic bedrock

	Y5	Y5,5	Y6	Y6,5	Y7	Y7,5	Y8	Y8,5	Y9	Y9,5	Y10	Y10,5	Y11	Y11,5	Y12
X18	-0,34	-0,37	-0,68	-0,52	-0,34	-0,30	-0,37	-0,26	-0,36	-0,87	-0,92	-1,09	-1,27	-1,49	-1,48
	-0,59	-0,54	-0,76	-0,68	-0,81	-0,84	-0,83	-1,03	-1,08	-0,96	-0,83	-1,01	-1,27	-1,37	-1,34
X19	-0,84	-1,28	-0,79	-1,27	-1,46	-1,13	-1,18	-1,05	-1,11	-0,93	-1,02	-1,00	-1,31	-1,33	-1,52
	-1,04	-1,33	-1,26	-1,73	-1,66	-1,30	-0,95	-0,92	-0,97	-0,75	-0,85	-1,19	-1,28	-1,02	-1,41
X20	-1,21	-1,55	-1,70	-1,82	-1,81	-1,26	-1,08	-0,97	-0,73	-0,69	-1,05	-1,13	-1,27	-1,43	-1,51
	-1,30	-1,50	-1,58	-1,62	-1,57	-1,50	-1,00	-0,73	-0,76	-0,86	-0,91	-1,08	-1,40	-1,42	-1,54
X21	-1,02	-0,99	-1,11	-1,41	-1,61	-1,55	-1,16	-0,96	-0,82	-0,80	-0,96	-1,14	-1,49	-1,43	-1,42
	-0,78	-0,78	-0,85	-1,20	-1,73	-1,75	-1,45	-1,03	-0,94	-1,18	-1,31	-1,17	-1,66	-1,43	-1,19
X22	-0,63	-0,80	-0,92	-1,28	-1,85	-1,94	-1,70	-1,34	-1,45	-1,34	-1,35	-1,54	-1,68	-1,34	-0,86
	-0,67	-1,09	-1,45	-1,62	-1,94	-1,89	-1,94	-1,79	-1,71	-1,62	-1,46	-1,64	-1,60	-1,03	-0,62
X23	-1,13	-1,18	-1,46	-1,44	-1,71	-1,76	-1,89	-1,87	-1,80	-1,67	-1,62	-1,52	-1,44	-0,66	-0,40
	-1,08	-1,32	-1,31	-1,23	-1,38	-1,59	-1,79	-1,80	-1,67	-1,49	-1,48	-1,32	-1,12	-0,54	-0,48
X24	-1,02	-1,17	-1,12	-1,07	-1,35	-1,53	-1,74	-1,68	-1,57	-1,31	-1,27	-1,15	-0,95	-0,41	-0,44
	-1,02	-1,12	-1,10	-1,08	-1,51	-1,59	-1,73	-1,63	-1,44	-1,16	-1,05	-0,94	-0,85	-0,43	-0,36
X25	-1,15	-1,17	-1,12	-1,19	-1,69	-1,72	-1,65	-1,52	-1,24	-1,13	-0,98	-0,77	-0,84	-0,40	-0,33

TABLE 7 : Interpreted thickness (in metres) to the dolomitic bedrock near the boundary between Ruigtelaagte and Zamenkomst

	Y5	Y5,5	Y6	Y6,5	Y7	Y7,5	Y8	Y8,5	Y9	Y9,5	Y10	Y10,5	Y11	Y11,5	Y12
X18	7,40	6,88	19,58	11,24	5,31	4,25	6,29	2,18	2,47	26,54	26,13	34,95	43,21	64,05	76,29
X18,5	13,54	7,32	17,09	10,12	15,34	19,20	18,02	33,23	36,10	24,67	14,80	20,95	30,61	44,54	39,23
X19	16,75	54,55	7,01	35,14	55,09	24,48	34,87	26,35	34,12	21,31	29,38	18,17	42,92	31,60	67,64
X19,5	26,03	36,36	20,50	57,67	55,37	32,64	16,47	20,66	27,10	14,02	14,98	34,83	34,79	9,24	52,92
X20	35,50	51,96	58,76	64,48	79,82	21,86	27,77	15,38	14,77	11,99	31,43	26,02	29,74	43,06	61,21
X20,5	47,92	49,62	47,72	43,50	36,92	47,32	17,00	12,21	16,38	21,53	18,47	21,94	41,57	33,86	64,65
X21	28,84	16,75	19,09	33,97	45,05	42,82	21,56	21,44	16,37	13,27	18,60	23,40	46,56	34,97	52,86
X21,5	19,42	14,63	13,12	19,65	57,39	55,14	36,48	16,00	14,36	31,07	40,01	15,92	64,76	37,89	34,41
X22	12,27	15,01	13,14	21,02	64,93	68,22	47,33	21,61	41,96	28,67	28,92	45,56	61,46	37,03	16,62
X22,5	21,63	26,18	50,16	49,72	72,92	54,45	66,53	54,42	50,30	47,59	30,73	52,96	56,42	19,37	11,61
X23	39,99	25,25	45,52	30,09	51,32	44,41	57,05	55,75	55,08	47,67	49,73	41,62	50,46	8,09	6,71
X23,5	31,29	42,69	34,66	23,76	27,03	36,46	51,02	51,69	43,91	33,83	41,86	32,47	28,31	8,07	11,20
X24	28,16	30,30	34,47	18,21	30,22	34,21	51,04	43,77	43,22	27,55	32,89	29,56	24,02	6,00	10,58
X24,5	28,27	27,67	25,39	17,44	45,48	39,00	53,89	46,13	38,18	23,57	23,55	21,62	22,02	7,97	8,36
X25	50,26	40,81	33,68	33,21	84,39	76,03	65,14	56,14	33,81	34,99	28,83	17,59	28,40	7,99	8,10

- 58 -

Table 8 : Difference between observed and calculated residual gravity values after two iterations (in mgal)

	Y5	Y5,5	Y6	Y6,5	Y7	Y7,5	Y8	Y8,5	Y9	Y9,5	Y10	Y10,5	Y11	Y11,5	Y12
X18	-0,0004	-0,0013	0,0000	-0,0000	0,0016	0,0013	0,0015	-0,0012	-0,0018	0,0020	-0,0014	0,0060	-0,0001	0,0656	0,1582
	-0,0015	-0,0054	-0,0054	0,0009	-0,0070	0,0007	-0,0066	0,0066	0,0129	-0,0018	0,0023	-0,0008	-0,0290	-0,0200	-0,0479
X19	-0,0128	0,0945	0,0069	-0,0298	0,0556	-0,0228	0,0231	-0,0123	0,0085	-0,0063	0,0181	-0,0090	0,0280	-0,0415	0,1071
	-0,0128	-0,0175	-0,0474	0,0718	0,0043	-0,0090	-0,0027	-0,0019	0,0048	0,0011	-0,0054	0,0148	0,0038	0,0013	0,0249
X20	-0,0193	0,0097	0,0294	0,0342	0,1064	-0,0283	0,0123	-0,0002	-0,0010	-0,0030	0,0191	-0,0049	-0,0190	-0,0060	0,0548
	0,0336	0,0199	0,0069	-0,0199	-0,0460	0,0379	-0,0017	0,0017	-0,0008	0,0046	0,0020	-0,0035	0,0160	-0,0485	0,0822
X21	-0,0016	-0,0058	-0,0044	-0,0074	-0,0037	-0,0095	-0,0104	0,0072	0,0029	0,0001	0,0000	-0,0068	0,0148	-0,0428	0,0422
	-0,0002	0,0025	0,0111	-0,0106	0,0269	0,0064	-0,0094	0,0085	0,0024	0,0070	0,0381	-0,0190	0,0893	-0,0281	-0,0042
X22	0,0019	0,0021	0,0020	-0,0330	0,0415	0,0444	-0,0089	-0,0267	0,0229	-0,0161	-0,0176	-0,0024	0,0483	-0,0082	-0,0036
	-0,0051	-0,0109	0,0448	0,0129	0,0873	-0,0245	0,0524	0,0149	0,0014	0,0200	-0,0354	0,0175	0,0378	-0,0166	0,0025
X23	0,0332	-0,0275	0,0268	-0,0327	0,0297	-0,0295	0,0094	0,0001	0,0190	0,0050	0,0269	-0,0188	0,0434	-0,0008	0,0000
	-0,0065	0,0281	0,0047	0,0040	-0,0049	-0,0141	0,0045	0,0023	-0,0057	-0,0166	0,0138	-0,0117	-0,0074	-0,0002	-0,0007
X24	-0,0015	-0,0021	0,0017	0,0054	-0,0533	-0,0250	0,0085	-0,0226	0,0117	-0,0047	0,0091	0,0039	0,0010	0,0007	-0,0063
	-0,0150	-0,0179	-0,0038	-0,0131	-0,0561	-0,0673	-0,0155	-0,0247	-0,0073	-0,0089	-0,0008	0,0000	-0,0019	-0,0000	-0,0001
X25	0,0620	0,0124	-0,0040	-0,0267	0,1848	0,1155	0,0597	0,0452	-0,0152	0,0132	0,0075	-0,0042	0,0125	-0,0012	0,0001

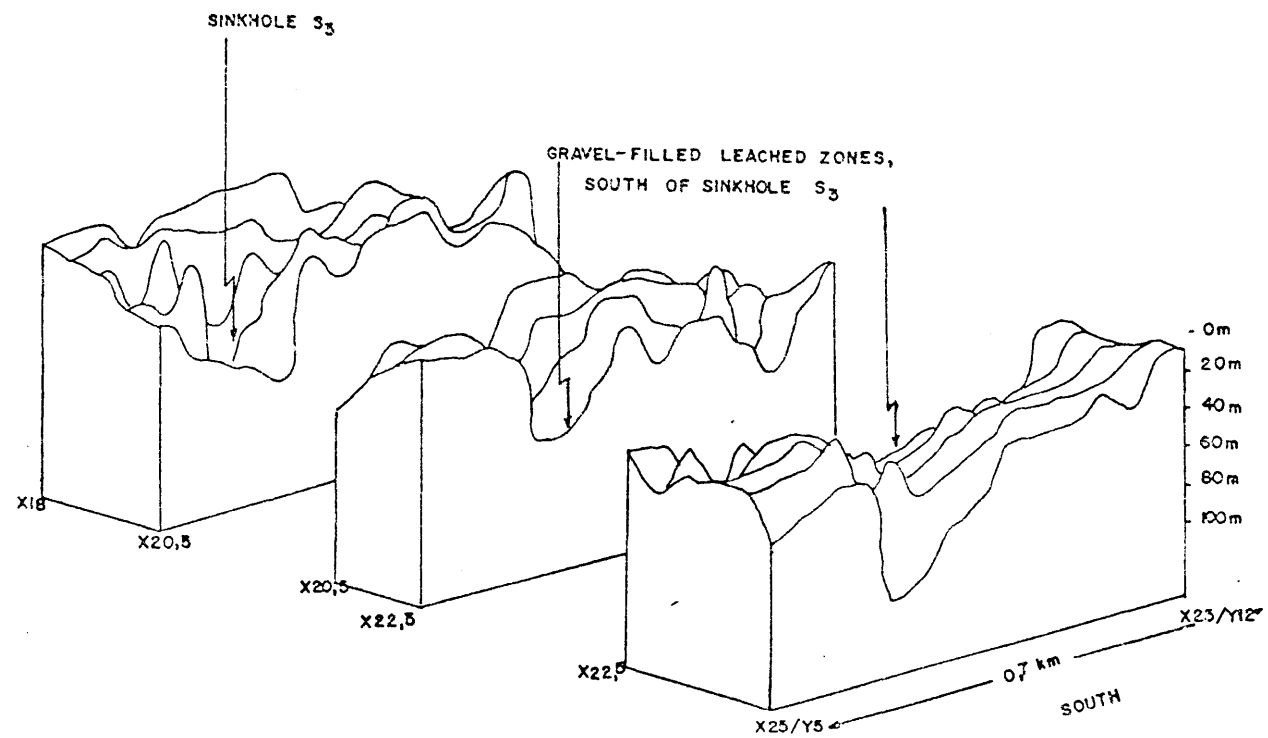
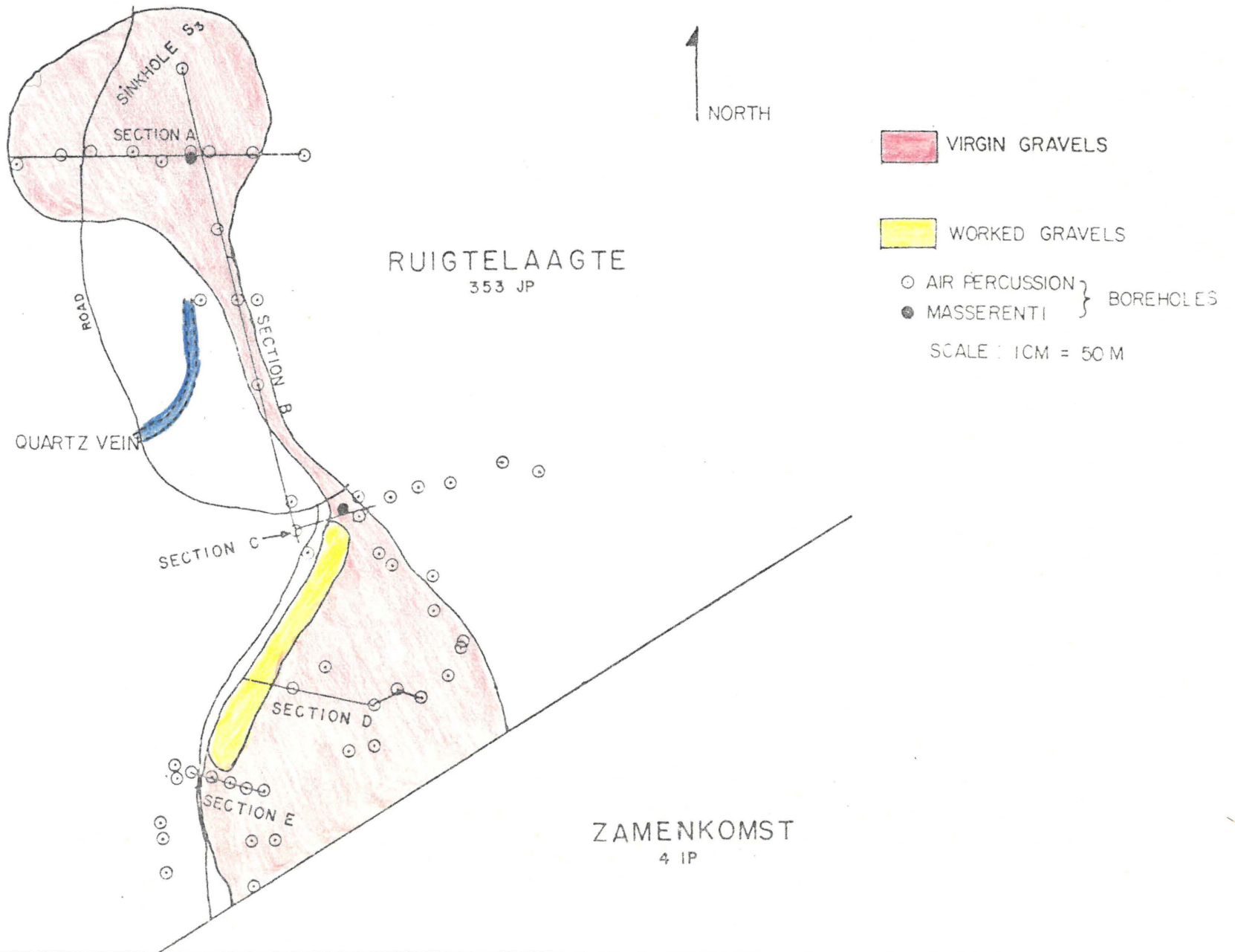
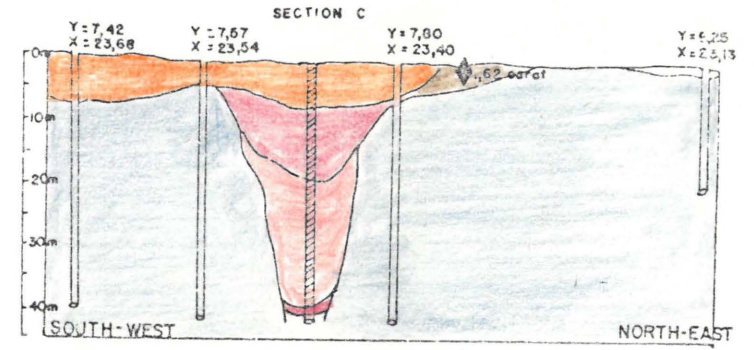
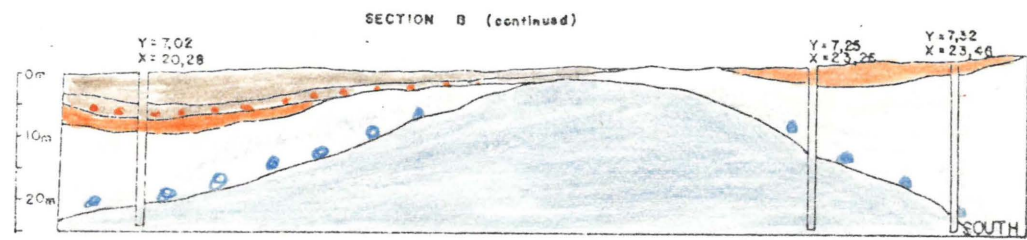
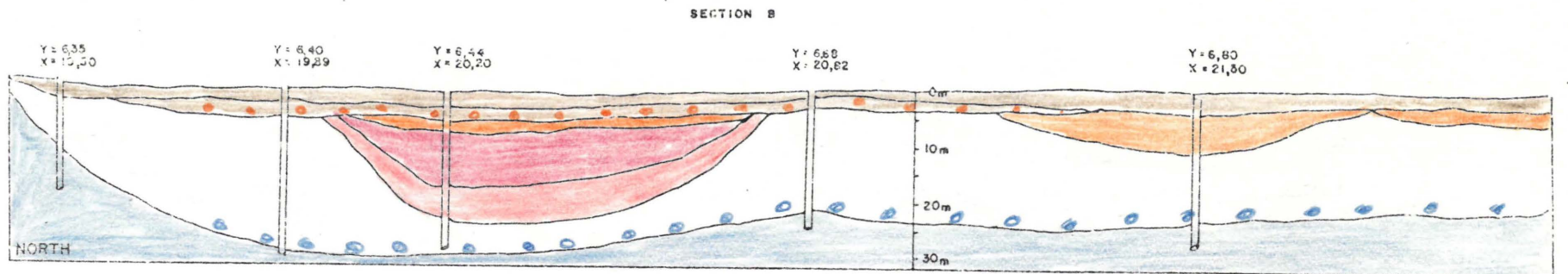
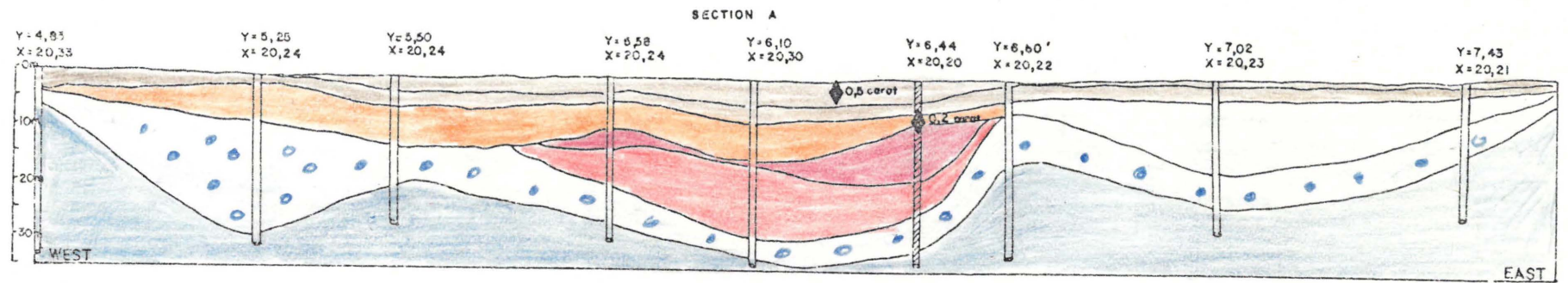


FIGURE 20 DOLOMITIC BEDROCK CONFIGURATION IN THE VICINITY OF SINKHOLE S₃ AS CALCULATED FROM THE RESIDUAL GRAVITY FIELD

FIGURE 21 DISTRIBUTION OF GRAVEL AS DETERMINED BY THE GRAVITY METHOD AND DRILLING





- | | | |
|---|--|--|
| RED SANDY SOIL | DARK CHERT GRAVEL WITH A CLAY MATRIX | WAD AND LEACHED CHERT |
| RED SOIL AND MANGANESE NODULES | DARK CHERT GRAVEL AND AGATE IN A CLAY MATRIX | JOINTED AND PARTLY LEACHED DOLOMITIC CHERT |
| CHALKY WEATHERED CHERT GRAVEL WITH RED SOIL MATRIX - UPPER GRAVEL | CLAY AND CHERT GRAVEL | MASSERENTI BOREHOLE |
| | | DIAMONDS |

FIGURE 22 SECTIONS A, B AND C BASED ON THE DRILLING RESULTS IN THE VICINITY OF SINKHOLE S₃

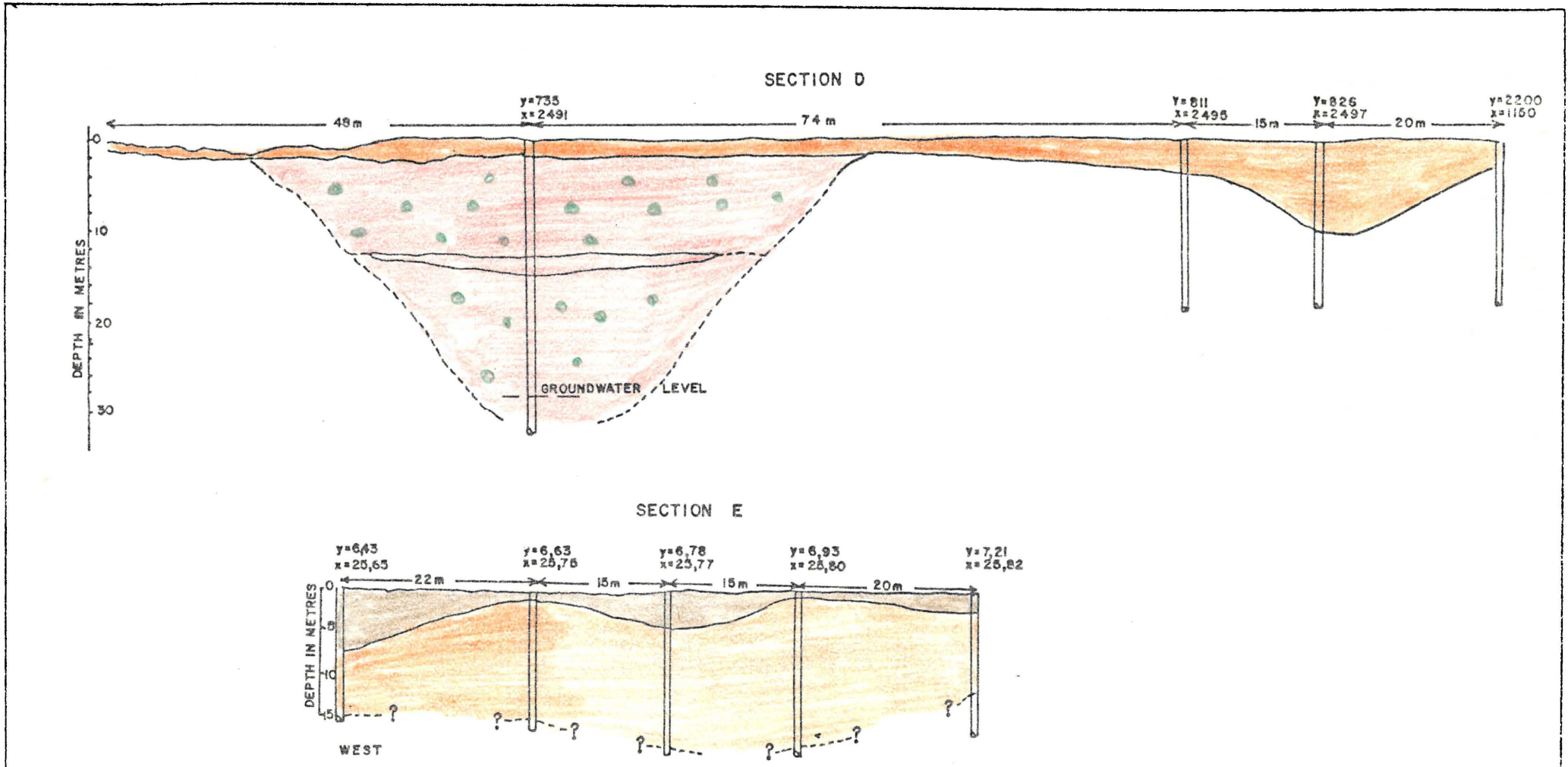


FIGURE 23 INTERPRETATION OF THE DRILLING RESULTS NEAR THE SOUTHERN BOUNDARY OF RUIGTELAAGTE (FOR LEGEND SEE FIGURE 22)

drill. Since the diamonds are often concentrated in pockets, the diamonds found in the these Masserenti boreholes cannot be used to calculate the actual diamond content of the specific gravel layers in carat/ton but should rather be regarded as proof that these layers are diamondiferous.

(2) Pienaar's Pothole and sinkholes S₁ and S₂

No terrain corrections were applied to gravity readings taken on the perimeter of Pienaar's Pothole.

The residual gravity values from Y17 to Y26,5/X7,5 to X17 were digitised (Table 9) and the overburden thickness was calculated. The residual gravity field over Pienaar's Pothole is depicted in Figure 24 while the calculated depths to dolomitic bedrock and the difference between the observed and calculated values are given in Tables 9 and 10 respectively. From the calculated depths to dolomitic bedrock depicted in the three-dimensions in Figure 25, it is evident that Pienaar's Pothole is also situated on the intersection of two gorge-like leached zones. The largest calculated depth to dolomitic bedrock is 122 m, occurs 100 m north-east of Pienaar's Pothole and corresponds to a residual gravity value of -3,01 mgal.

Gravel occurrences and borehole positions in the vicinity of the Pienaar's Pothole are indicated in Figure 26. A very narrow (2 m wide) gravel-filled channel possibly connects sinkhole S₂ with Pienaar's Pothole and in boreholes on this channel gravel was found to a depth of 47 m. The drill could not penetrate any further and the gravels probably extend even deeper.

Over sinkhole S₁ a maximum depth of 111 m to dolomitic bedrock was calculated. Gravel thicknesses of up to 45 m were encountered. Interpretations of the borehole results over sinkhole S₁ are shown as sections F to J in Figures 27 and 28'.

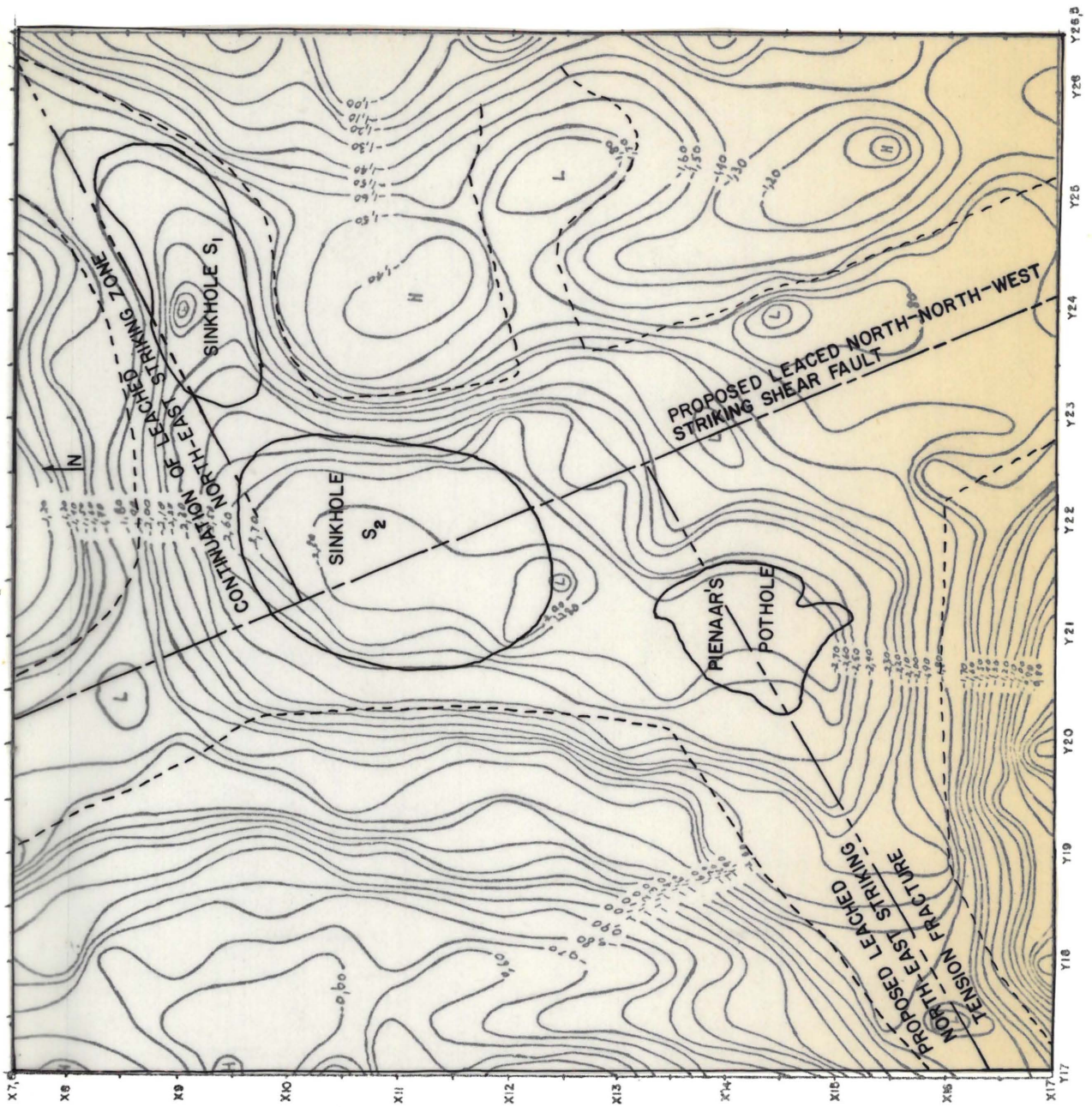


FIGURE 24 THE RESIDUAL GRAVITY FIELD (in mgal) OVER PIENAAR'S POTHOLE AND SINKHOLES S₁ AND S₂

TABLE 9 : Residual gravity values (in mgal) over Pienaar's Pothole and vicinity used for the calculation of the depth to the Jolomitic bedrock

	Y17	Y17,5	Y18	Y18,5	Y19	Y19,5	Y20	Y20,5	Y21	Y21,5	Y22	Y22,5	Y23	Y23,5	Y24	Y25	Y25,5	Y26	Y26,5	
X7,5	-0,62	-0,78	-0,97	1,17	1,77	1,66	1,79	1,65	1,23	1,14	1,14	1,16	1,34	1,40	1,38	1,33	1,69	1,75	1,75	1,49
X8	-0,59	-0,74	-1,13	0,99	1,30	1,61	1,73	1,73	1,38	1,26	1,29	1,56	1,54	1,75	1,67	1,53	1,84	1,87	1,6	1,24
	-0,69	-0,74	-0,63	0,96	1,16	1,54	1,78	1,87	1,74	1,69	1,79	1,95	1,82	1,78	1,77	1,92	2,06	1,89	1,51	1,17
X9	-0,71	-0,54	-0,75	0,84	1,17	1,53	1,57	1,92	2,06	2,18	2,31	2,29	2,33	2,14	2,42	2,14	2,01	1,72	1,38	0,98
	-0,48	-0,57	-0,61	0,78	1,01	1,59	1,81	2,17	2,40	2,49	2,69	2,53	2,44	2,31	2,15	2,05	1,94	1,38	1,16	0,83
X10	-0,58	-0,57	-0,62	0,84	0,99	1,57	1,83	2,35	2,44	2,71	2,77	2,71	2,38	1,87	1,65	1,67	1,68	1,40	1,24	1,14
	-0,81	-0,60	-0,60	0,73	1,20	1,74	1,96	2,41	2,72	2,89	2,86	2,71	2,26	1,45	1,39	1,42	1,61	1,29	0,95	0,97
X11	-0,34	-0,51	-0,71	0,73	1,16	1,69	1,95	2,42	2,73	2,89	2,84	2,69	2,23	1,49	1,33	1,43	1,65	1,35	1,01	0,96
	-0,51	-0,67	-0,51	0,82	1,39	1,64	1,76	2,44	2,65	2,88	2,76	2,75	2,39	1,68	1,41	1,34	1,60	1,55	1,24	1,10
X12	-0,32	-0,72	-0,59	0,92	1,33	1,47	1,89	2,43	2,98	2,88	2,77	2,72	2,61	1,99	1,68	1,72	1,83	1,70	1,40	0,86
	-0,39	-0,86	-0,64	0,87	1,24	1,68	1,78	2,52	2,75	3,01	2,78	2,47	2,59	2,17	1,78	1,60	1,80	1,82	1,57	1,27
X13	-0,40	-0,86	-0,74	0,98	1,57	1,70	2,44	2,67	2,75	2,78	2,53	2,50	2,34	2,10	1,62	1,39	1,67	1,80	1,58	1,32
	-0,61	-1,01	-0,81	1,19	1,51	1,42	2,30	2,75	2,73	2,66	2,19	2,15	2,05	2,02	1,64	1,38	1,52	1,66	1,46	1,12
X14	-0,82	-1,20	-1,05	1,40	1,92	2,00	2,50	2,57	2,73	2,73	2,44	2,09	2,14	1,88	1,68	1,38	1,26	1,41	1,32	1,00
	-0,87	-1,28	-1,27	1,82	2,20	1,80	2,59	2,56	2,73	2,73	2,43	2,08	1,84	1,79	2,05	1,35	1,17	1,23	1,31	1,18
X15	-1,00	-1,41	-1,62	1,97	2,16	2,42	2,53	2,70	2,73	2,54	2,28	1,92	1,79	1,75	1,88	1,45	1,12	1,14	1,31	1,17
17	-1,46	-1,84	-1,81	1,98	2,17	2,12	2,24	2,36	2,29	2,35	2,02	1,96	1,84	1,72	1,84	1,72	1,21	1,00	1,33	1,23
X16	-1,62	-2,02	-1,79	1,91	2,08	1,95	1,84	1,84	1,79	1,85	1,86	1,55	1,83	1,75	1,77	1,73	1,50	1,30	1,45	1,38
19	-1,80	-1,83	-1,38	1,41	1,44	1,01	1,22	1,27	1,28	1,39	1,54	1,69	1,82	1,77	1,78	1,75	1,77	1,48	1,45	1,48
X17	-1,66	-1,30	-0,62	0,95	0,96	0,76	0,40	0,72	0,73	0,99	1,14	1,53	1,69	1,72	1,68	1,70	1,67	1,48	1,36	1,47

TABLE 10 : Calculated depth (in metres) to the solid dolomite bedrock over Pienaar's Pothole area and vicinity

	Y17	Y17,5	Y18	Y18,5	Y19	Y19,5	Y20	Y20,5	Y21	Y21,5	Y22	Y22,5	Y23	Y23,5	Y24	Y24,5	Y25	Y25,5	Y26	Y26,5
X7,5	17,35	21,20	26,77	35,20	102,01	66,28	82,79	69,14	29,04	30,21	39,66	26,69	41,21	42,24	39,68	30,50	69,33	71,75	82,30	72,50
X8	14,02	15,50	42,06	15,47	26,54	43,34	46,67	50,71	22,97	20,70	19,77	41,97	31,20	56,52	44,41	23,54	54,92	59,28	44,03	28,97
X8,5	19,33	18,96	8,76	22,41	22,22	40,82	54,18	56,79	40,19	34,64	41,28	56,90	37,93	34,31	33,26	54,46	74,02	61,76	36,62	31,29
X9	22,53	10,11	19,31	16,85	27,67	41,84	23,52	48,94	53,02	61,63	73,77	68,23	82,33	59,71	111,27	66,69	63,26	47,94	34,60	21,41
X9,5	10,71	13,37	12,54	15,92	16,73	47,82	46,60	66,31	76,31	74,25	59,53	77,49	78,80	78,68	68,10	63,62	66,91	21,21	22,77	14,64
X10	14,65	13,04	13,69	20,70	14,92	40,10	36,77	78,96	60,60	87,08	91,59	94,13	70,95	3-,16	27,35	36,56	46,85	33,77	34,52	41,69
X10,5	31,00	13,59	12,70	13,27	28,79	56,44	46,69	75,37	62,51	102,00	95,91	89,42	62,53	12,23	23,90	26,61	49,98	27,32	14,60	26,00
X11	5,70	10,45	18,96	12,54	21,00	47,33	44,87	71,80	85,30	96,60	80,71	84,56	58,01	17,10	22,87	32,16	56,47	31,42	17,60	26,34
X11,5	12,28	19,41	8,61	15,48	43,21	42,83	03,12	76,62	70,16	92,74	75,71	93,39	74,77	24,61	23,22	18,96	42,93	46,97	28,36	26,12
X12	5,65	19,64	10,96	20,33	35,03	23,56	41,99	70,60	122,39	91,70	97,30	88,56	01,29	47,29	37,07	52,71	63,56	51,86	36,28	11,66
X12,5	7,39	28,09	11,39	16,78	21,68	44,27	17,16	79,60	82,17	117,09	88,55	54,66	96,70	66,24	43,76	33,16	56,56	61,72	46,00	41,34
X13	6,80	23,63	13,72	17,05	52,77	33,92	100,41	90,76	82,39	86,01	64,23	77,50	70,43	62,33	29,58	20,73	47,09	62,00	46,76	43,70
X13,5	12,21	30,37	11,79	24,39	31,49	5,52	66,56	99,04	81,56	78,77	27,69	43,78	43,49	61,66	36,91	26,38	39,94	64,87	39,99	27,66
X14	16,16	38,96	16,33	26,86	64,73	50,60	86,46	67,46	76,39	93,86	72,31	43,62	71,30	46,76	40,79	27,66	23,29	33,11	33,69	21,63
X14,5	17,71	35,56	18,37	56,73	84,36	9,13	98,60	67,99	69,93	98,48	74,54	60,86	36,82	40,30	94,86	23,03	22,66	26,17	36,86	36,51
X15	17,16	32,10	37,72	58,94	63,84	92,26	87,42	01,40	103,71	62,41	64,69	38,31	36,66	39,07	63,82	29,33	16,87	24,40	37,49	33,90
X15,5	58,75	67,76	46,93	56,70	69,17	51,82	63,36	76,73	66,48	83,23	47,34	59,17	49,71	37,31	57,23	57,20	19,09	12,82	37,66	27,07
X16	56,28	84,73	48,22	61,33	81,18	64,67	47,09	46,06	39,36	47,43	54,79	18,18	64,86	42,17	46,61	48,92	26,64	26,86	42,61	46,11
X16,5	64,86	70,26	24,23	30,37	36,83	9,51	24,34	26,26	26,22	29,76	36,08	49,34	57,38	47,60	60,88	48,98	63,36	36,31	37,49	59,44
X17	61,92	34,21	3,43	20,53	21,56	14,90	2,46	13,37	11,64	22,44	24,23	56,53	66,54	67,96	61,50	66,28	67,23	60,71	41,24	73,93

TABLE 11 : Difference between the calculated and observed gravity values (in mgal) over Pienaar's Pothole area after two iterations

	Y17	Y17,5	Y18	Y18,5	Y19	Y19,5	Y20	Y20,5	Y21	Y21,5	Y22	Y22,5	Y23	Y23,5	Y24	Y24,5	Y25	Y25,5	Y26	Y26,5
X7,5	-0,0000	-0,0041	-0,0221	-0,0240	0,2987	0,0490	0,1423	0,1034	-0,0092	0,0149	0,0209	-0,0074	0,0228	0,0026	0,0044	-0,0288	0,0835	0,0571	0,1372	0,1424
X8	0,0010	-0,0075	0,0481	-0,0045	-0,0278	-0,0311	-0,0451	0,0027	-0,0101	0,0189	0,0019	0,0224	-0,0284	0,0639	0,0169	-0,0456	-0,0201	-0,0160	-0,0423	-0,0367
X8,5	-0,0016	-0,0009	-0,0033	0,0054	-0,0072	-0,0038	0,0350	0,0355	-0,0134	-0,0238	-0,0334	0,0150	-0,0531	-0,0573	-0,0756	-0,0176	0,0556	0,0215	-0,0313	0,0027
X9	0,0044	-0,0020	0,0018	-0,0002	0,0024	0,0207	-0,0368	-0,0193	-0,0193	-0,0298	-0,0175	0,0203	-0,0251	0,0753	-0,0377	0,0137	0,0011	-0,0041	0,0002	-0,0016
X9,5	-0,0006	-0,0006	-0,0015	0,0012	-0,0023	0,0370	-0,0053	0,0261	0,0261	-0,0244	0,0964	-0,0263	0,0160	0,0705	0,0373	0,0148	0,0717	-0,0244	-0,0055	-0,0046
X10	-0,0048	-0,0013	-0,0011	0,0068	0,0007	0,0014	-0,0599	0,0655	-0,1005	0,0017	0,0105	0,0552	0,0056	-0,0492	-0,0299	-0,0246	0,0010	-0,0054	0,0074	0,0408
X10,5	0,0189	-0,0037	-0,0011	0,0004	0,0002	0,0597	-0,0390	0,0226	0,0503	0,0639	0,0256	0,0259	-0,0047	0,0129	0,0128	-0,0208	0,0360	-0,0133	0,0030	-0,0031
X11	-0,0021	-0,0023	0,0018	0,0025	-0,0164	0,0200	-0,0283	0,0011	0,0037	0,0227	-0,0145	-0,0006	-0,0327	0,0029	0,0135	-0,0031	0,0634	-0,0137	0,0020	-0,0027
X11,5	-0,0008	-0,0006	-0,0009	-0,0050	0,0337	0,0292	-0,0479	0,0435	-0,0933	0,0065	-0,0850	0,0482	0,0332	-0,0325	0,0063	-0,0151	-0,0208	0,0089	-0,0171	0,0262
X12	-0,0007	-0,0036	-0,0016	-0,0028	0,0158	-0,0166	-0,0073	-0,0131	0,2011	0,0005	-0,0553	0,0283	0,1573	-0,0401	-0,0231	0,0407	0,0510	-0,0009	-0,0144	-0,0026
X12,5	-0,0023	0,0088	-0,0026	0,0010	-0,0210	0,0318	-0,0508	0,0203	-0,0435	0,1611	0,0356	-0,1279	0,1433	0,0261	0,0001	-0,0300	0,0160	0,0277	-0,0150	0,0136
X13	-0,0000	-0,0051	-0,0005	-0,0076	0,0705	-0,0557	0,2016	0,0427	-0,0354	0,0286	-0,0297	0,0616	0,0266	0,0282	-0,0221	-0,0054	-0,0038	0,0381	-0,0163	0,0206
X13,5	-0,0018	0,0069	0,0035	0,0000	-0,0295	0,0188	-0,0349	0,0794	-0,0340	0,0147	-0,1099	-0,0419	-0,0653	0,0428	-0,0093	-0,0046	-0,0003	0,0375	-0,0088	-0,0068
X14	-0,0044	0,0297	0,0065	-0,0385	0,0548	-0,0326	0,0573	-0,1068	-0,0159	0,0644	0,0337	-0,0538	0,1088	-0,0195	-0,0182	-0,0042	-0,0082	0,0044	-0,0069	-0,0077
X14,5	0,0030	0,0194	-0,0104	0,0206	0,1370	-0,0054	0,1291	-0,1090	0,0053	0,0818	0,0246	-0,0065	-0,0299	-0,0359	0,2633	-0,0139	0,0088	-0,0022	0,0005	0,0193
X15	-0,0093	-0,0289	-0,0344	-0,0097	-0,0328	0,1304	0,0459	0,1004	0,1149	0,0223	-0,0021	-0,0486	-0,0136	-0,0303	0,0668	-0,0295	0,0059	0,0027	0,0027	-0,0065
X15,5	-0,0076	0,0561	-0,0478	-0,0377	0,0053	-0,0909	-0,0375	0,0331	-0,0241	0,0976	-0,0544	0,0634	0,0174	-0,0353	0,0270	0,0604	-0,0019	0,0137	-0,0022	-0,0086
X16	-0,0349	0,1091	-0,0371	0,0231	0,1183	0,0545	-0,0206	-0,0165	-0,0374	-0,0153	0,0445	-0,0339	0,0316	-0,0322	-0,0235	-0,0122	-0,0183	-0,0174	0,0009	0,0159
X16,5	0,1244	0,0631	-0,0404	-0,0236	-0,0136	0,0013	-0,0085	-0,0020	-0,0011	-0,0102	-0,0099	-0,0024	-0,0006	-0,0471	-0,0313	-0,0517	-0,0468	-0,0444	-0,0502	0,0464
X17	0,2326	-0,0461	0,0029	-0,0017	-0,0037	0,0004	0,0016	0,0027	0,0041	0,0036	-0,0223	0,0458	0,0634	0,0713	0,0325	0,0580	0,0728	0,0158	-0,0288	0,1558

60

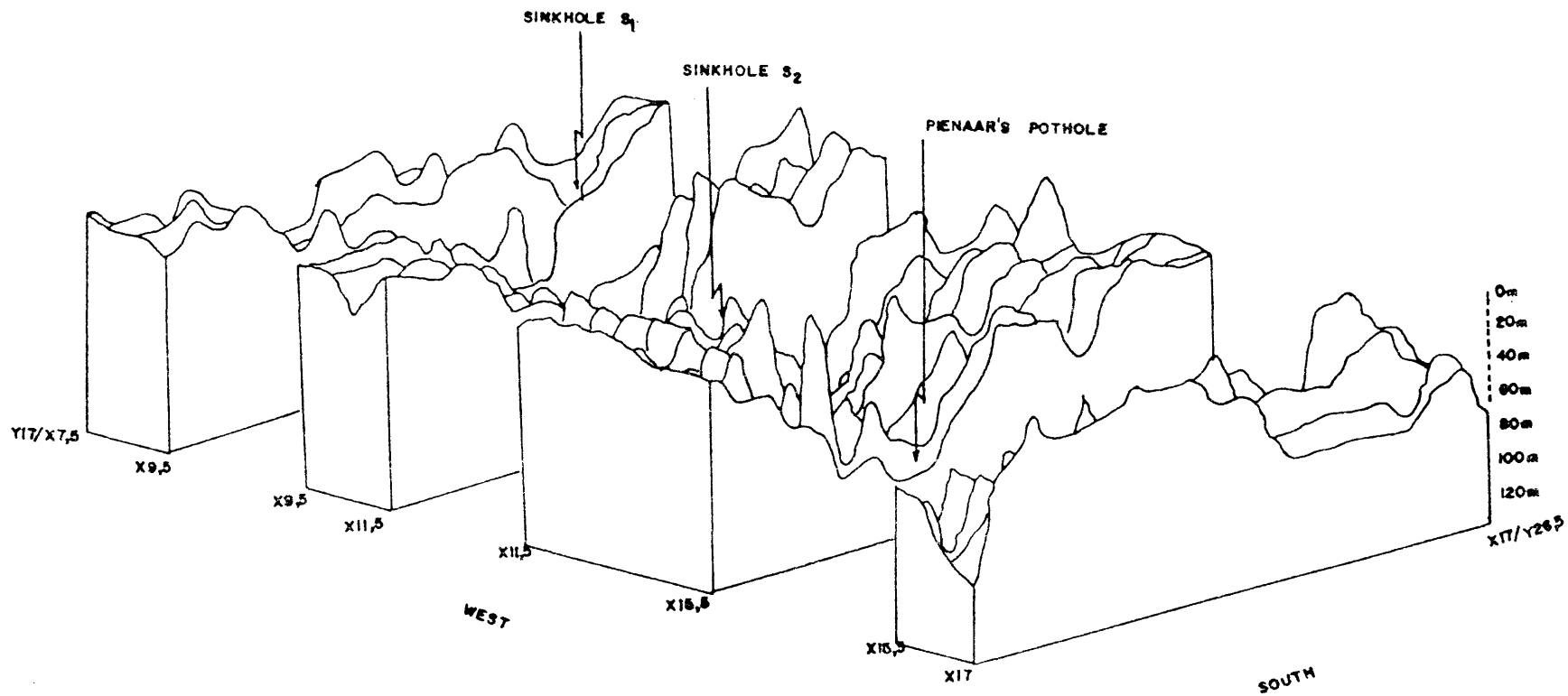


FIGURE 25 DOLOMITIC BEDROCK CONFIGURATION AT PIENAAR'S POTHOLE AND VICINITY
AS CALCULATED FROM THE RESIDUAL GRAVITY VALUES

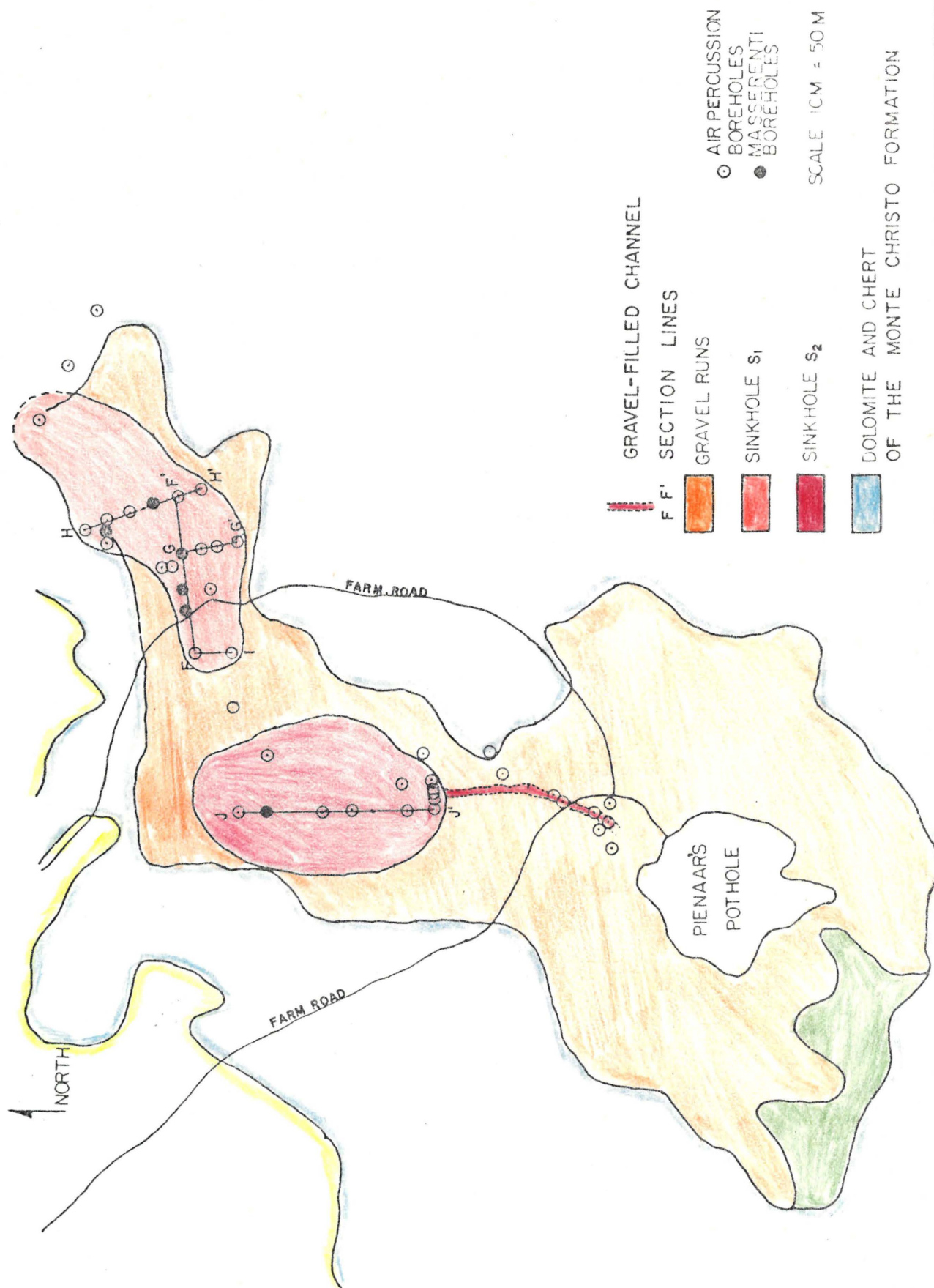


FIGURE 26 . GRAVEL OCCURRENCES AND BOREHOLE POSITIONS IN THE VICINITY OF PIENAAR'S POT HOLE AND SINKHOLES S₁ AND S₂

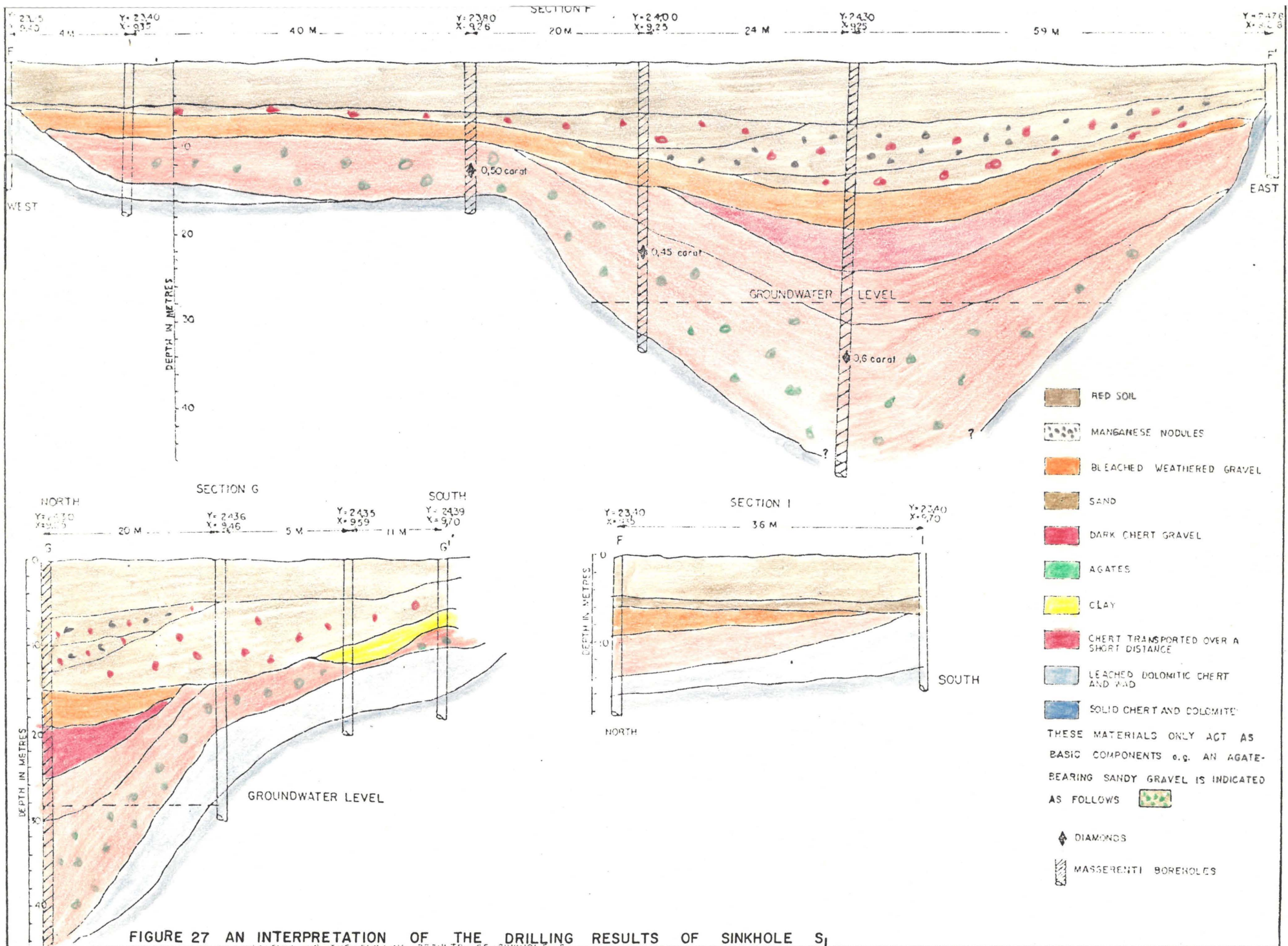
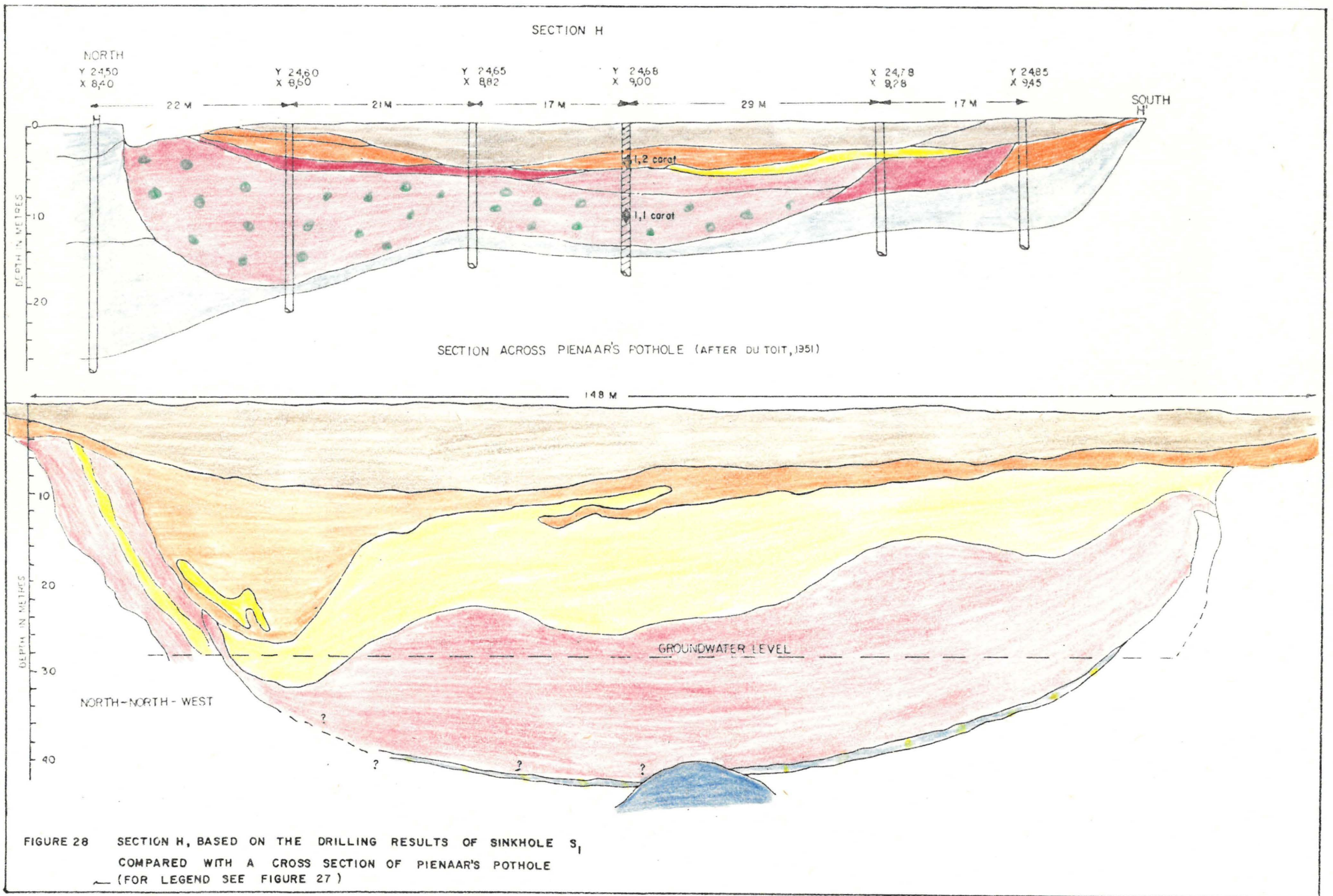


FIGURE 27 AN INTERPRETATION OF THE DRILLING RESULTS OF SINKHOLE S₁



Over sinkhole S_2 the calculated depth varies between 25 m and 70 m. Gravel thicknesses of 30 m were obtained so that a leached zone of up to 30 m thick should theoretically occur under the gravels. Borehole sections across sinkhole S_2 are depicted as Section J in Figure 29.

The Welverdiend-Grasfontein run

The residual gravity values (Figure 30, Table 12) from Y11,5 to Y18,5/X2 to X6 were used to calculate the thickness of the material overlying the dolomitic bedrock. Directly over the Welverdiend-Grasfontein run the calculated depths to bedrock vary from 18 to 45 m (Table 13). The structure of the dolomitic floor as calculated, is indicated in Figure 31. The difference between the calculated and observed gravity values are given in Table 14. At right angles to the run a north-east striking leached zone prone to sinkhole formation extends to the south. Many gravel-filled sinkholes occur along this zone but unfortunately no borehole information is available over this area.

On the Welverdiend-Grasfontein run at Y21 to Y24,5/X2,5 to X6 where the three dykes intersect an oval-shaped gravity anomaly is visible on the residual gravity map. No borehole information is available on this structure but the area over which the anomaly occurs was worked intensively in the past. The calculated structure of the dolomitic bedrock here is also shown in Figure 31. The maximum calculated depth to bedrock varies between 19 and 90 m.

6. MAGNETIC SURVEY

The success with which the magnetic method can be applied depends on the contrast in magnetic properties of the rock types concerned. These mag=

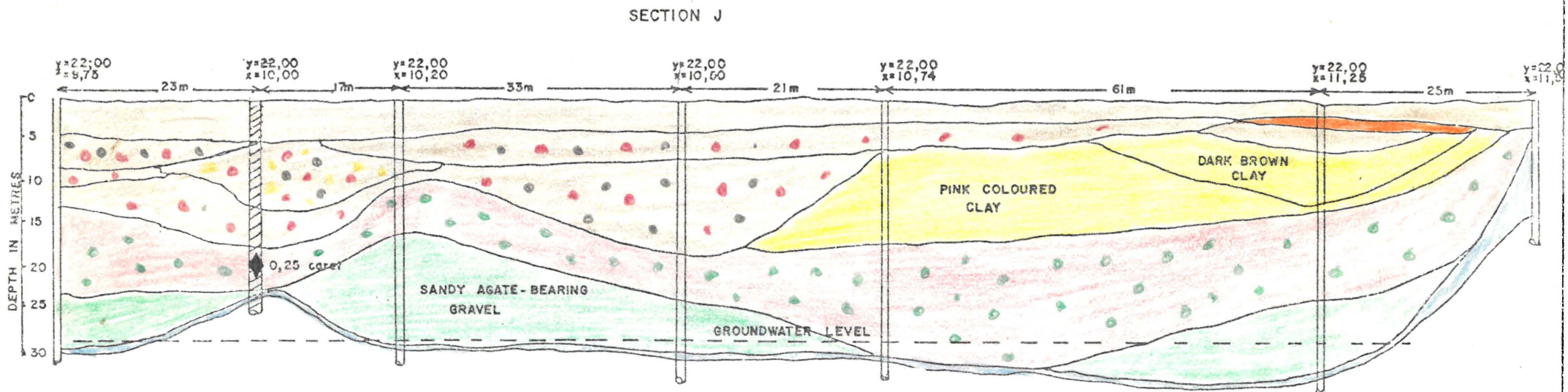


FIGURE 29 INTERPRETATION OF THE DRILLING RESULTS ON SINKHOLE S₂
(FOR LEGEND SEE FIGURE 27)

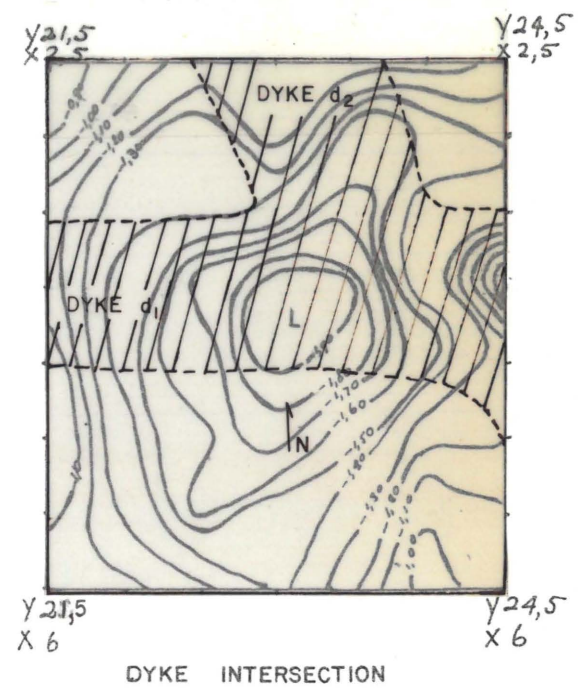
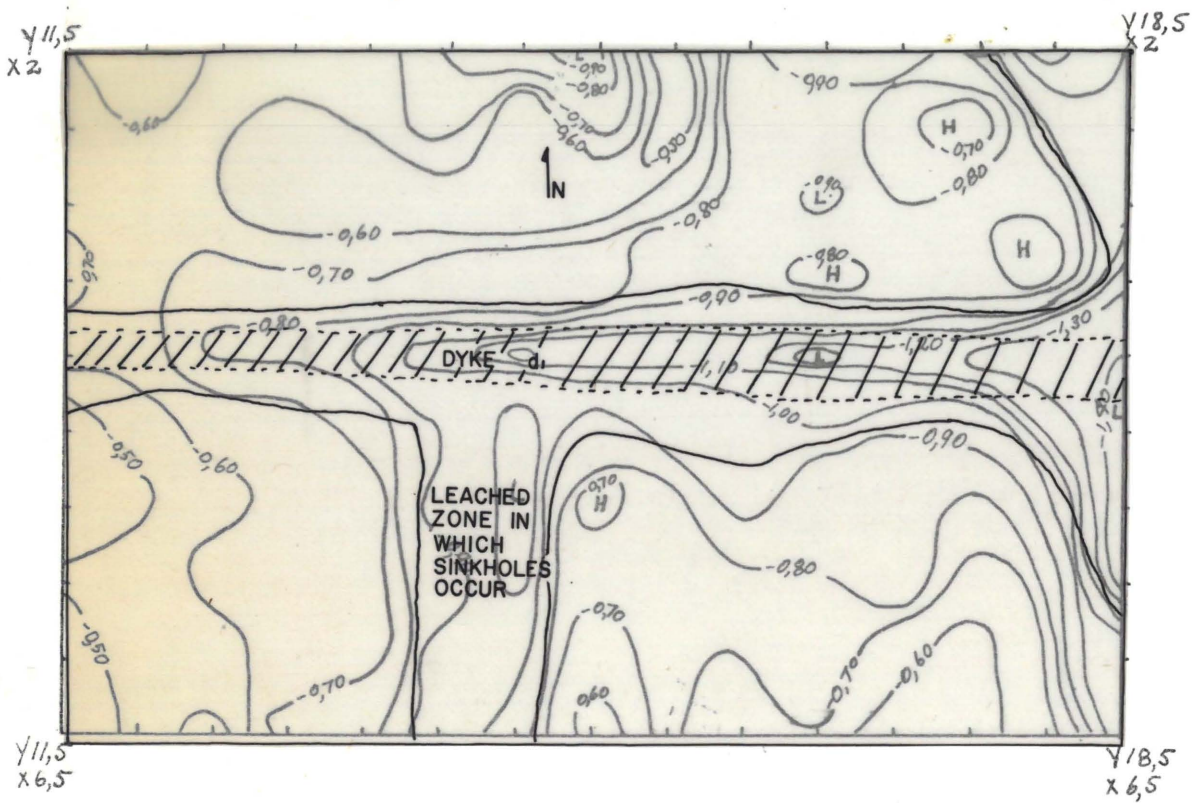


FIGURE 30 THE RESIDUAL GRAVITY FIELD OVER TWO PARTS OF THE WELVERDIEND-GRASFONTEIN RUN

TABLE 12 : Residual gravity values (mgal) obtained over the Welverdiend-Grasfontein run and used for the calculation of the depth to the dolomitic bedrock

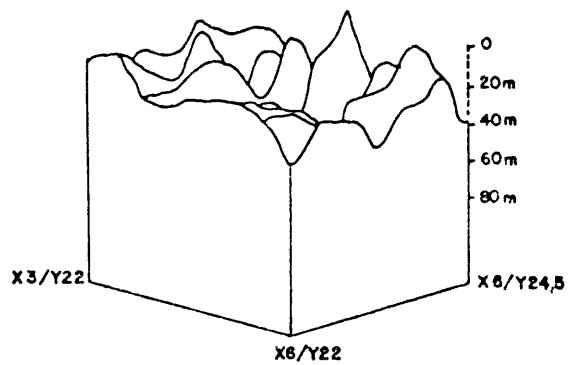
	Y11,5	Y12	Y12,5	Y13	Y13,5	Y14	Y14,5	Y15	Y15,5	Y16	Y16,5	Y17	Y17,5	Y18	Y18,5
X2	-0,61	-0,55	-0,61	-0,69	-0,61	-0,80	-0,88	-0,91	-0,46	-0,89	-0,93	-0,93	-0,90	-1,25	-1,10
	-0,66	-0,60	-0,63	-0,56	-0,60	-0,72	-0,48	-0,76	-0,46	-0,83	-0,86	-0,77	-0,66	-1,00	-1,02
X3	-0,65	-0,64	-0,61	-0,55	-0,56	-0,57	-0,57	-0,55	-0,52	-0,67	-0,83	-0,92	-0,80	-0,82	-1,05
	-0,74	-0,63	-0,76	-0,74	-0,70	-0,75	-0,76	-0,73	-0,87	-0,84	-0,75	-0,83	-0,87	-0,73	-1,26
X4	-0,65	-0,69	-0,81	-0,84	-0,95	-0,07	-0,21	-1,13	-1,17	-1,19	-1,24	-1,19	-1,31	-1,39	-1,40
	-0,44	-0,53	-0,64	-0,66	-0,75	-0,91	-1,04	-0,85	-0,96	-0,96	-1,00	-0,91	-0,95	-1,23	-1,48
X5	-0,41	-0,49	-0,57	-0,63	-0,62	-1,00	-1,02	-0,62	-0,72	-0,92	-0,83	-0,86	-0,77	-1,00	-1,42
	-0,51	-0,52	-0,63	-0,64	-0,68	-0,85	-1,01	-0,76	-0,79	-0,79	-0,79	-0,82	-0,67	-0,84	-1,42
X6	-0,49	-0,57	-0,57	-0,64	-0,68	-0,95	-0,92	-0,62	-0,75	-0,70	-0,75	-0,67	-0,55	-0,69	-1,07
X6	-0,48	-0,52	-0,48	-0,71	-0,77	-0,96	-0,87	-0,59	-0,74	-0,55	-0,70	-0,58	-0,57	-0,69	-1,07

TABLE 13 : Calculated depth (in metres) to the dolomitic bedrock over the Welverdiend-Grasfontein gravel run

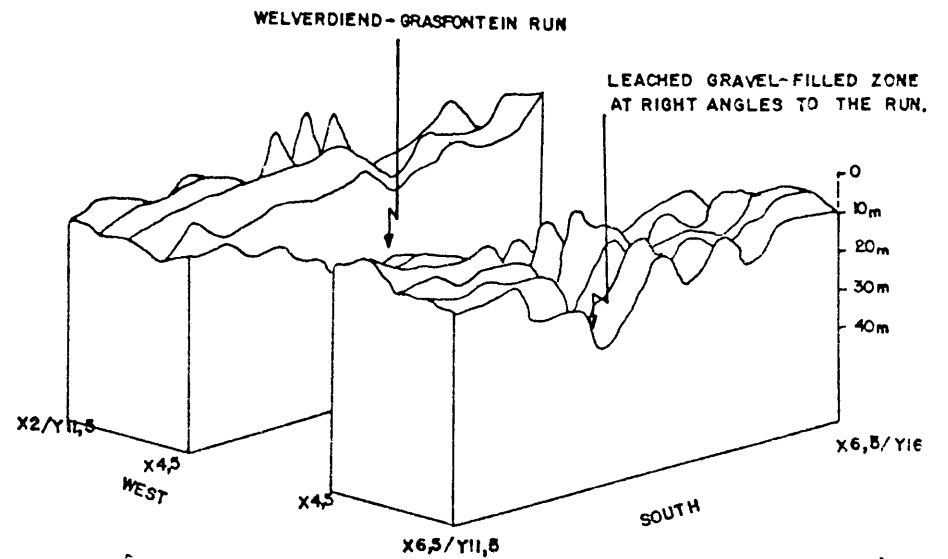
	Y11,5	Y12	Y12,5	Y13	Y13,5	Y14	Y14,5	Y15	Y15,5	Y16	Y16,5	Y17	Y17,5	Y18	Y18,5
X2	18,48	13,88	15,47	21,18	14,89	25,14	29,94	33,79	6,98	30,40	29,67	29,98	24,08	57,96	43,65
X2,5	19,30	14,40	16,21	12,46	13,97	19,42	6,92	21,08	6,65	21,42	20,46	15,06	9,40	24,94	29,41
X3	17,58	15,93	14,13	11,75	12,15	11,84	11,30	9,1E	14,57	20,57	26,41	17,32	23,17	14,65	32,86
X3,5	23,53	13,80	20,68	18,49	15,11	16,30	15,48	13,51	20,29	16,63	11,22	15,25	15,87	6,25	51,11
X4	18,31	17,76	23,09	22,73	28,47	33,61	45,53	35,98	38,78	39,68	45,22	37,19	47,86	49,37	54,43
X4,5	10,19	11,97	15,20	14,38	16,16	19,65	27,52	15,98	23,84	20,75	23,94	17,39	16,79	30,06	64,95
X5	9,74	11,42	13,22	15,08	11,44	30,90	29,91	94,43	14,14	25,94	17,95	21,20	14,22	18,52	61,34
X5,5	13,87	12,26	16,52	15,48	15,07	21,30	30,99	17,17	20,38	19,06	18,92	21,87	13,00	14,45	71,47
X6	12,67	14,90	13,62	15,29	14,08	27,46	24,90	11,35	19,33	16,54	19,27	15,43	10,36	11,44	33,73
X6,5	13,32	13,97	11,00	21,48	21,41	33,88	26,99	12,71	23,22	12,02	20,88	14,12	13,84	15,63	48,14

TABLE 14 : Difference between the observed and calculated gravity values (mgal) over the Welverdiend-Grasfontein gravel run after two iterations

	Y11,15	Y12	Y12,5	Y13	Y13,5	Y14	Y14,5	Y15	Y15,5	Y16	Y16,5	Y17	Y17,5	Y18	Y18,5
X2	0,0011	0,0007	-0,0003	0,0035	-0,0015	-0,0004	0,0013	0,0168	-0,0030	0,0086	0,0014	0,0061	-0,0199	0,024	0,0266
X2,5	0,0015	0,0010	0,0019	0,0005	0,0009	0,0002	-0,0009	-0,0030	0,0011	-0,0020	-0,0042	-0,0003	0,0037	-0,0152	-0,0162
X3	-0,0011	0,0019	0,0011	0,0018	0,0023	0,0019	0,0020	0,0023	0,0023	0,0008	0,0096	-0,0000	0,0069	-0,0048	-0,0100
X3,5	0,0051	0,0001	0,0018	0,0007	-0,004	-0,0031	-0,0066	-0,0032	-0,0060	-0,0070	-0,0038	-0,0059	-0,0122	-0,0061	0,0370
X4	0,0000	0,0001	0,0026	-0,0006	0,0048	0,0041	0,0429	0,0068	0,0146	0,0157	0,0386	0,0019	0,0395	0,0110	0,0184
X4,5	0,0007	0,0011	0,0008	0,0014	0,0017	-0,0066	-0,0066	-0,0042	-0,0009	-0,0091	-0,0056	-0,0037	-0,0058	-0,0432	0,0765
X5	0,0004	0,0010	0,0005	0,0019	0,0009	0,0120	0,0028	0,0027	-0,0000	0,0095	0,0013	0,0023	0,0044	-0,0256	0,0625
X5,5	0,0008	0,0005	0,0015	0,0018	0,0038	-0,0066	0,0093	0,0008	0,0030	-0,0002	-0,0005	0,0013	0,0007	-0,0146	0,1454
X6	0,0003	0,0010	0,0010	0,0013	0,0005	-0,0012	-0,0047	-0,0016	-0,0003	0,0008	-0,0001	-0,0010	0,0018	-0,0030	-0,0268
X6,5	0,0003	0,0007	0,0001	0,0030	-0,0046	0,0154	0,0023	0,0013	0,0058	-0,0009	0,0029	-0,0008	0,0000	-0,0128	0,0623



DOLOMITIC BEDROCK CONFIGURATION
WHERE THE DYKES INTERSECT, AS
CALCULATED FROM THE RESIDUAL
GRAVITY FIELD



DOLOMITIC BEDROCK CONFIGURATION
BENEATH THE WELVERDIEND-GRASFONTEIN RUN

FIGURE 31 DOLOMITIC BEDROCK CONFIGURATIONS BENEATH PORTIONS OF THE WELVERDIEND-GRASFONTEIN RUN

netic properties arise from the presence in the rock of magnetic minerals such as magnetite, pyrrhotite, ilmenite, franklinite and specular hematite. By far the most common and the most magnetic of these is magnetite, and it is true to say that the magnetic properties of most rocks are controlled almost entirely by their magnetite content (Richards, 1978).

Crustal rock material becomes magnetised by the influence of the earth's main magnetic field on the magnetic minerals in the crustal material so that they generate their own magnetic fields which modify the magnetic field of the earth. This causes anomalies in the smoothly varying field of the earth itself.

The main magnetic field generated in the earth's core and that induced in the crust are both vector quantities which interact with each other and on the surface of the earth only the magnitude of the resultant force is measured by the Proton magnetometer. A further complication is that the magnetic field present in the rocks in the crust of the earth consists of two parts, a remanent or permanent field and a temporarily induced field. The strength of the induced field is proportional to the earth's magnetic field and has a direction which is parallel to the earth's field. Remanent magnetisation represents a remnant of the magnetic field induced during an earlier stage in the earth's history.

In the 7,5 km² area selected for the geophysical investigation a total field magnetic survey was carried out:

- (1) to locate dykes unknown at that stage
- (2) to provide a better understanding of the interrelationship between the individual dykes
- (3) to determine the relation between gravels and the dykes

- (4) to determine if a contrast exists in the magnetic contour pattern of areas underlain by gravel, outcropping dolomite and weathered dolomite with no gravel present and
- (5) to correlate gravity lows with dyke positions.

Although it is known that not all kimberlites are magnetic, it was hoped that possible kimberlite occurrences would show up during the magnetic survey.

6.1 Qualitative discussion of data

Except for the high amplitude anomalies caused by the various dykes only noise was registered over the remainder of the Ruigtevlei experimental area. The dyke positions as determined from the magnetic data have been marked on the geological map (Figure 2).

The displacement of dyke d_2 in the north-eastern portion was probably caused by the intrusion of dyke d_1 at a later stage in the geological history of the area (Figure 2). Drilling revealed that both dykes are deeply weathered. Whether dyke d_3 is contemporaneous with either d_1 or d_2 could not be established.

Variations in amplitudes and widths of anomalies along individual dykes seems to indicate differences in depths of weathering, thickness and magnetite concentration. The anomaly amplitudes along dyke d_1 normally decrease where the dyke is flanked by heavily leached zones in the dolomite.

The regional magnetic field is very quiet and it is only disturbed by the magnetic field of the dykes. No effort was made to remove the regional field as it does not show up any magnetic disturbances which could be ascribed to deep-seated structures. The area is also too small to observe

any regional trends. It seems as if a higher magnetic noise occurs over the Lyttelton Formation than over the Monte Christo Formation.

No single magnetic anomaly was encountered in the area that could possibly indicate the presence of kimberlite pipes or dykes. Over Pienaar's Pothole only magnetic noise was encountered. The fact that kimberlite intrusions mostly favour weak zones in the crust is well documented (Frick 1976; Dawson 1971 and Richards 1979) and likely areas for kimberlite intrusion are major joints and along dykes and their intersections. If kimberlites do occur in the Lichtenburg area they are probably deeply weathered owing to the high water content of the dolomite along leached joints and dykes and this would be very difficult to detect magnetically

Over the small part (Y32/X4,5 to X13) of the Ruigtelaagte area where the positive residual anomaly values were obtained, very little disturbance of the magnetic field was encountered. However, if it is kept in mind that not all kimberlites cause a disturbance in the magnetic field this gravity anomaly is still interesting.

No correlation was found between gravel occurrences and disturbances in the magnetic field. However, the magnetic data proved valuable pinpointing the positions of the dykes so that interesting gravity lows next to the dykes could be explored for gravels.

6.2 Quantitative discussion of the magnetic data

Presently two procedures exist for the interpretation of magnetic data, namely the solution of the so-called direct and indirect cases. The indirect problem deals with theoretically calculated anomalies based on a postulated model which are altered and compared with the observed magnetic anomaly until a reasonably "good fit" is obtained. When the magnetic body para=

meters are calculated directly from the observed magnetic field a direct interpretation approach is used.

Magnetic profiles obtained over the three dykes in the Ruigtelaagte experimental area were interpreted using the direct approach of Koulomzine, et al (1970) and the indirect method as described by Reford (1964). Dyke-sill combinations were modelled after the approach of Talwani and Heirtzler (1964).

When considering the following magnetic interpretations it must be borne in mind that the accuracy of any quantitative magnetic analysis is reduced by three main factors, namely

- (1) imperfect geometry, e.g. deviations from a flat top and parallel sides and a finite depth extension and along the strike
- (2) heterogeneity of the magnetic susceptibility, e.g. chilled margins will be finer grained and thus of a lower susceptibility
- (3) presence of remanent magnetism.

No information about the remanent magnetisation of the dykes is available. The Nilsen and the Hanning filter (Davis, 1973, p.269), upward continuation and low pass filters in the frequency domain were used to try to smooth the magnetic anomalies. None of them provided very satisfactory results and smoothing by hand had to be resorted to.

6.2.1 Method of Koulomzine, Lamontagne, Nadeau (1970)

A tabular body of infinite length and depth, orientated in any direction is considered in this method. From a total field anomaly across a dyke the thickness (W), depth (d) to the top of the dyke and inclination (θ) of

the dyke can be calculated.

No previous knowledge or assumption concerning the zero datum level or body centre is required as the determination of both these parameters has a sound mathematical basis.

Two sets of conjugate points indicated as F_1' and F_2' and F_1'' and F_2'' in Figure 32 are located on the total field magnetic curve in such a manner that, $F_{\max} - F_2'' = F_1'' - F_{\min} = E''$ and $F_{\max} - F_2' = F_1' - F_{\min} = E'$. The determination of the zero datum level ($\Delta F = 0$) and the body centre ($\Delta F(o)$) by construction is depicted in Figure 32. The field curve is then divided into a symmetrical and an asymmetrical component as shown in Figure 33). By determining the parameters:

$$\begin{aligned}\delta &= \frac{X_{1/2}}{X_{3/4}} \text{ of the symmetrical curve} \\ \mu &= \frac{X_{\max}}{X_{1/2_{\max}}} \text{ of the asymmetrical curve} \\ \xi &= A_{\max}/S_{\max}\end{aligned}$$

where $X_{1/2}$, $X_{3/4}$, X_{\max} , $X_{1/2_{\max}}$, A_{\max} and S_{\max} are as indicated in Figure 33 and using the master curves (Koulomzine et al 1970, p.825) an estimate of the width, depth and dip is obtained from the symmetrical and asymmetrical curves. When considering the validity of the interpreted results the fact that the width times the susceptibility of the dyke is constant, introduces ambiguity.

When a dyke has a length of more than 10 times its width or more than 10 times the depth to its flat top (whichever is the greatest) and a similar extent in depth, calculations show that conditions rather rapidly tend towards the limiting case of the infinite dyke (Koulomzine et al, 1970).

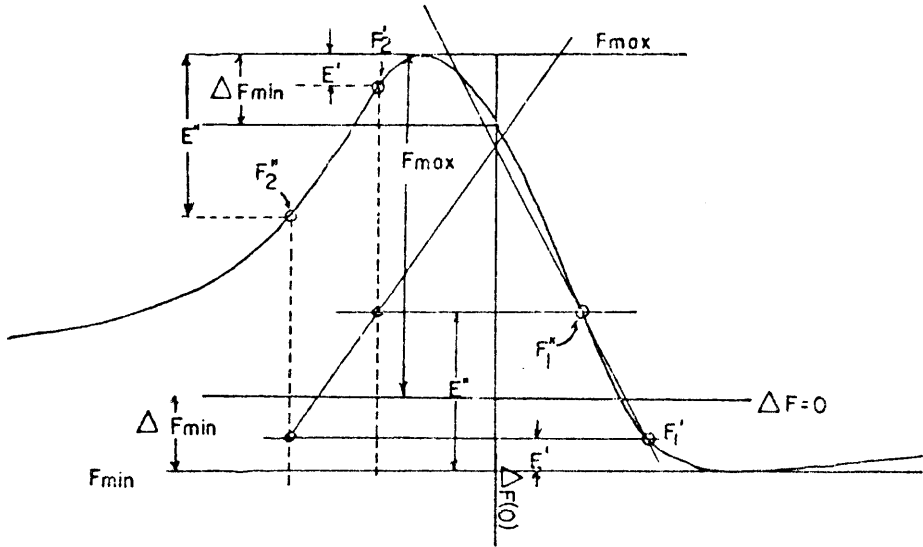


FIGURE 32 DETERMINATION OF THE MIDPOINT POSITION OF A DYKE AND THE DATUM LEVEL FROM A TOTAL FIELD MAGNETIC PROFILE, BY CONSTRUCTION.

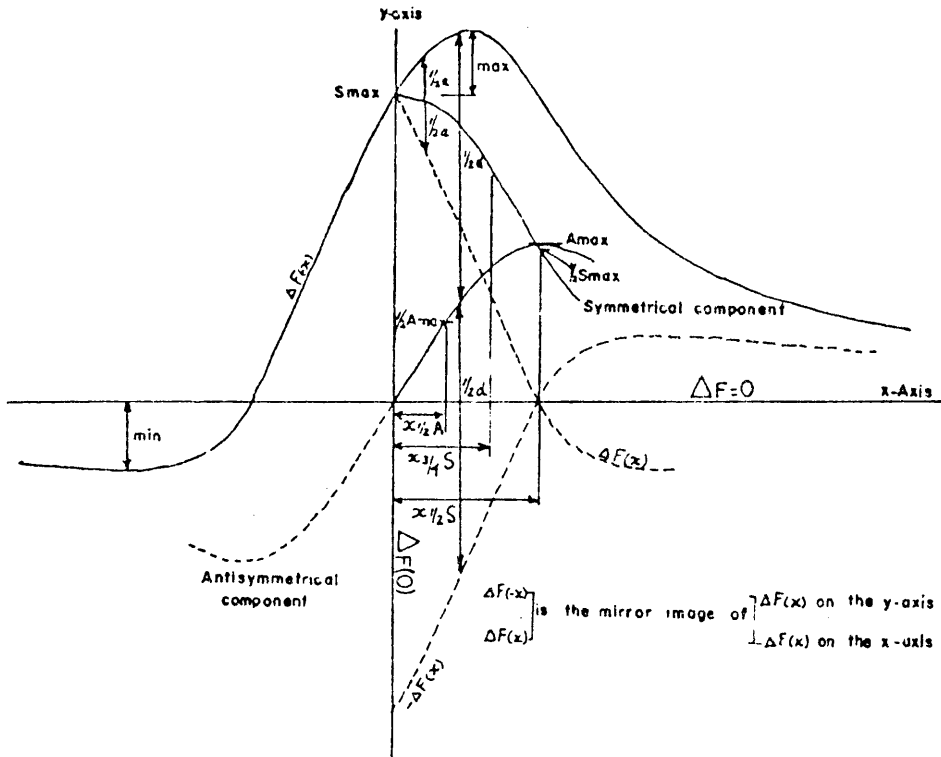


FIGURE 33 DECOMPOSITION OF THE FIELD CURVE INTO A SYMMETRICAL AND ASYMMETRICAL COMPONENT

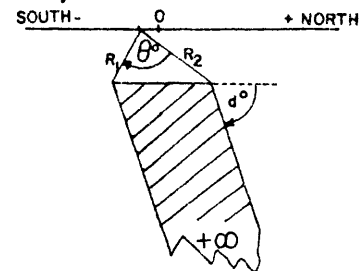
Three total field magnetic profiles across dykes d_2 and d_1 were interpreted by using the Koulomzine et al method and appear in Figures 35 (a, b and c) and are discussed in Section 6.2.3.

6.2.2 Methods of Reford (1978) and Talwani and Heirtzler (1964)

A dyke is considered as thin when its depth to width ratio is greater than unity. Reford (1978) quotes a separate formula for the thick and the thin dyke. Only the thick dyke formula was used to determine the dyke parameters.

The formula for the thick dyke is

$$\Delta T = 2kTb^2 \sin(d) \left(\ln \frac{R_2}{R_1} \cos(2I-d) + \theta \sin(2I-d) \right)$$



where $b^2 = (1 - \cos^2 i \cdot \sin^2 A)$

i = inclination of the earth's magnetic field

A = traverse strike direction as determined from true north and positive clockwise

T = total inducing magnetic field

k = susceptibility contrast of the dyke

d = dip of the dyke as measured from the positive side

$I = \tan^{-1} \left(\frac{\tan i}{\cos A} \right)$

θ = angle between R_1 and R_2 (see Figure above)

As the methods of Koulomzine et al and Reford only consider a simple dyke model, total magnetic profiles which displayed the presence of more than one magnetic body had to be interpreted by using the Talwani and Heirtzler (1964) approach. A polygonal two-dimensional body can be interpreted with this method.

In order to compute the magnetic profile over a two-dimensional polygonal body as shown in Figure 34(a) the following procedure is adopted. Each face is assumed to be the edge of a horizontal slab extending to infinity in the +X direction. The horizontal, vertical and total field components of the magnetic anomaly caused by a two dimensional slab (Figure 34(b)) are given by Talwani and Heirtzler (1964) as:

$$\begin{aligned} \text{Horizontal field: } \Delta H &= 2J_x \sin \psi (\sin \psi (\theta_2 - \theta_1) - \cos \psi \cdot \log(r_2/r_1)) \\ &\quad + 2J_z \sin \psi (\sin \psi \cdot \log(r_2/r_1) + \cos \psi (\theta_2 - \theta_1)) \end{aligned}$$

$$\begin{aligned} \text{Vertical field : } \Delta V &= 2J_x \sin \psi (\sin \psi \cdot \log(r_2/r_1) + \cos \psi (\theta_2 - \theta_1)) \\ &\quad + 2J_z \sin \psi (\cos \psi \cdot \log(r_2/r_1) - \sin \psi (\theta_2 - \theta_1)) \end{aligned}$$

$$\text{Total field : } \Delta T = \Delta V \sin I + \Delta H \cos I \sin \alpha$$

where J_x = horizontal component of total intensity of magnetisation

J_z = vertical component of total intensity of magnetisation

ψ = acute angle between slab face and horizontal

r_1, r_2 = distances from observation point to slab corners

θ_1, θ_2 = angles between lines connecting observation point to slab corners, and horizontal

α = acute angle between traverse strike and magnetic north

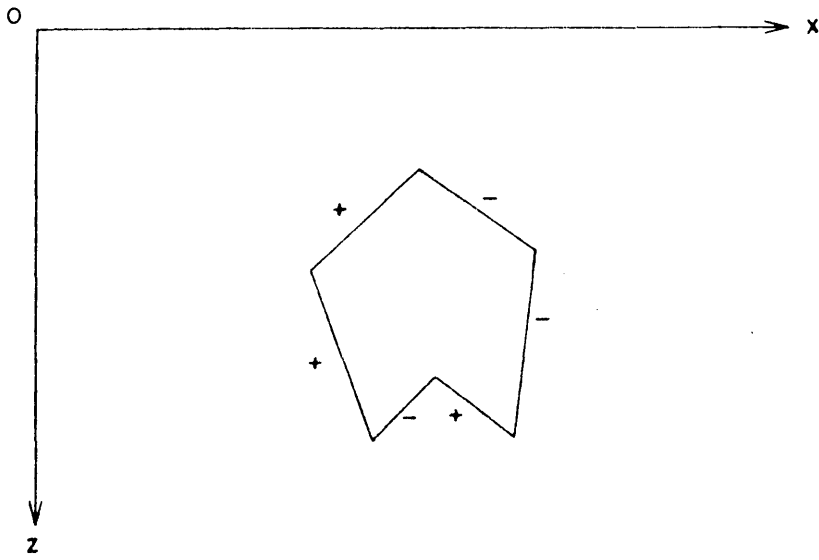


FIGURE 34a POLYGONAL BODY SHOWING SIGNS OF FACES.

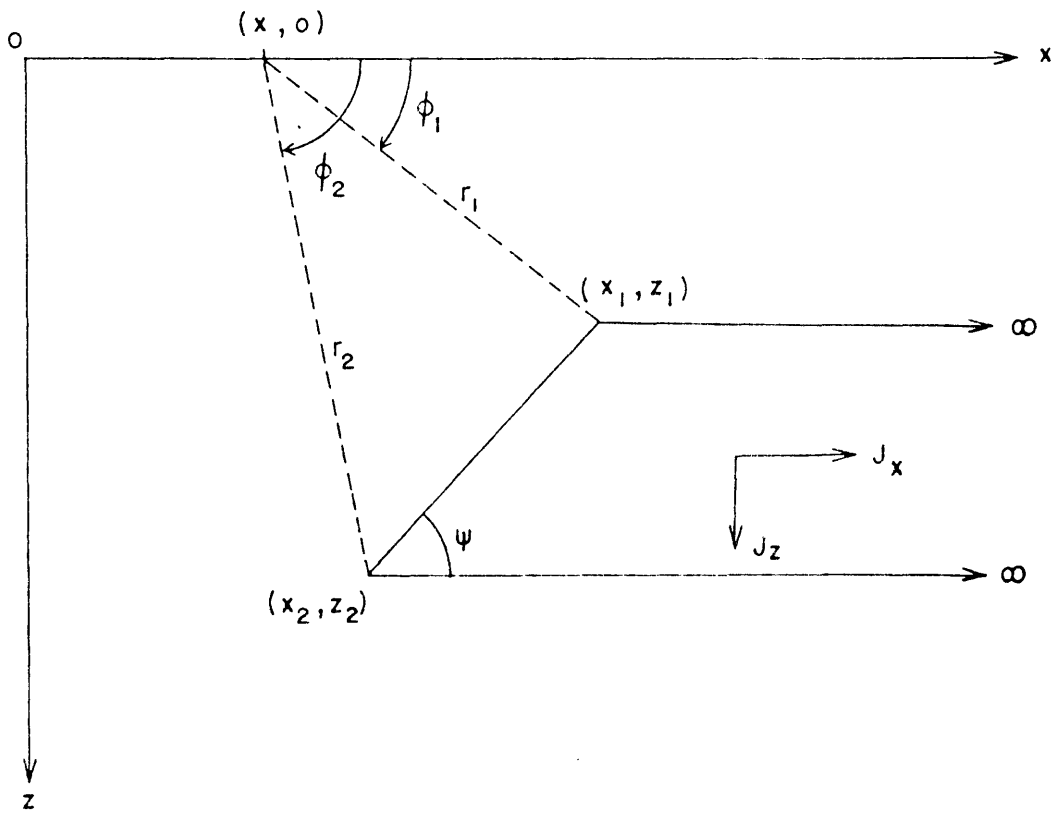


FIGURE 34b SEMI - INFINITE HORIZONTAL SLAB.

J_x and J_z are the already stated horizontal and vertical components of the total magnetisation vector and can be due to a purely induced magnetisation or to a combination of induced and remanent magnetisations.

The magnetic anomalies due to slabs formed from polygon sides which face in the +X direction are subtracted from the magnetic anomalies due to slabs formed from polygon sides which face in the -X direction (Figure 34(a)).

6.2.3 Results

Four typical total magnetic field profiles obtained over the dykes present on the Ruigtelaagte area are depicted in Figures 35(a) to (d).

Figure 35(a) displays a total magnetic field profile obtained over dyke d_1 . The profile is very noisy and except for the anomaly caused by a simple dipping dyke model a dyke-sill combination also fits the observed data. The ordinary dyke parameters were calculated by the methods of Reford (1978) and Koulomzine et al (1970). Except for the calculated dip, the width and depth to the top of the dyke agree quite well for the two interpretation methods (Figure 35(a)). The dyke-sill model was calculated with the Talwani and Heirtzler approach and the parameters used are indicated in Figure 35(a). Since it appeared on quite a few profiles across dyke d_1 as if more than one body contributed to the anomalous magnetic field a diamond drill hole was sunk through dyke d_1 to look for possible kimberlite intrusions along its northern flank. Unfortunately no kimberlite was intersected.

Total magnetic field profiles across dyke d_2 in the southern and northern sector are depicted in Figures 35(b) and (c) respectively. Good correlations between the methods of Reford and Koulomzine et al were obtained

FIGURE 350 TOTAL FIELD MAGNETIC ANOMALY OBTAINED OVER DYKE D_1

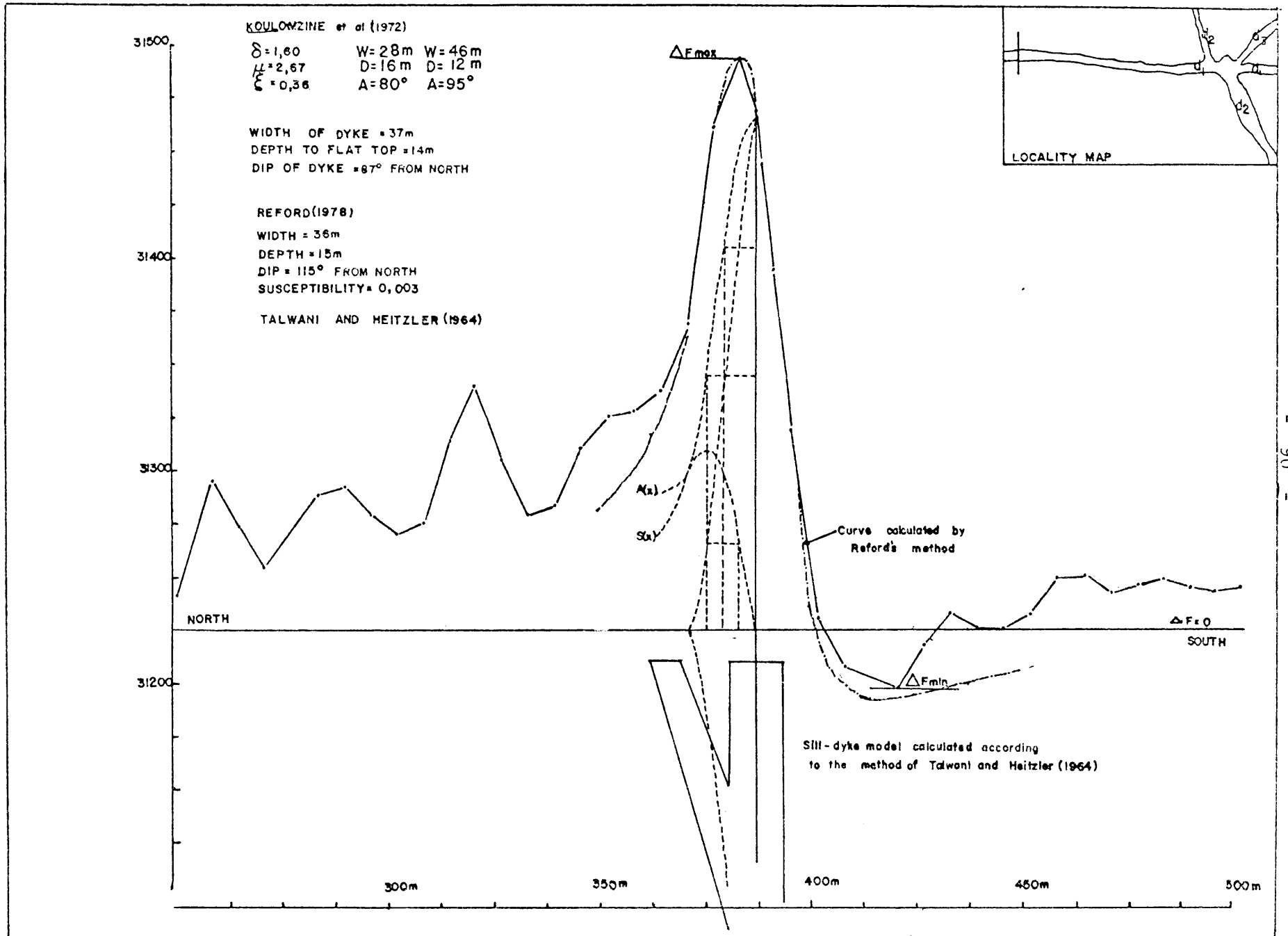


FIGURE 350 TOTAL FIELD MAGNETIC ANOMALY OBTAINED OVER DYKE d₂

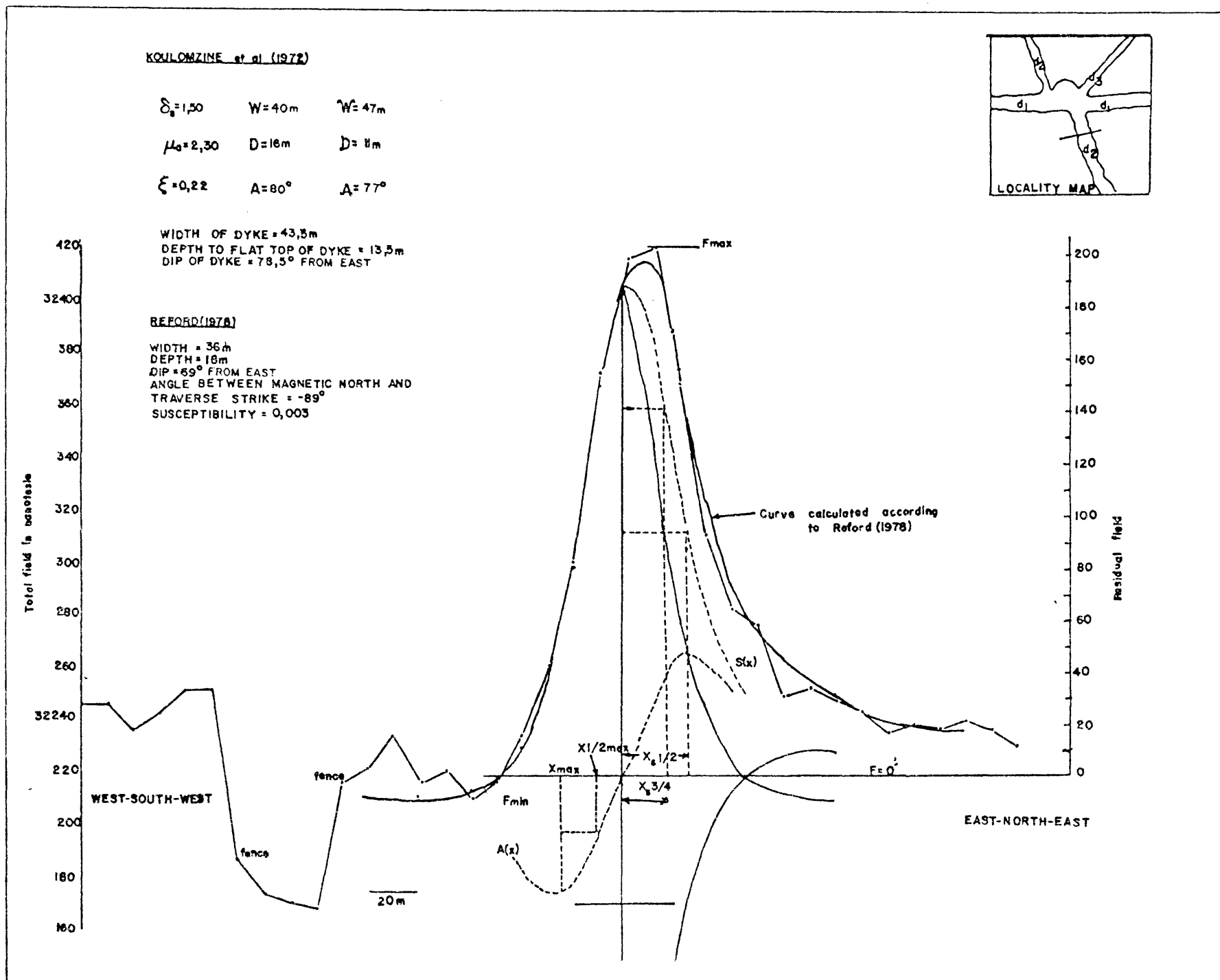


FIGURE 35c: TOTAL FIELD MAGNETIC ANOMALY OBTAINED OVER DYKE d₂

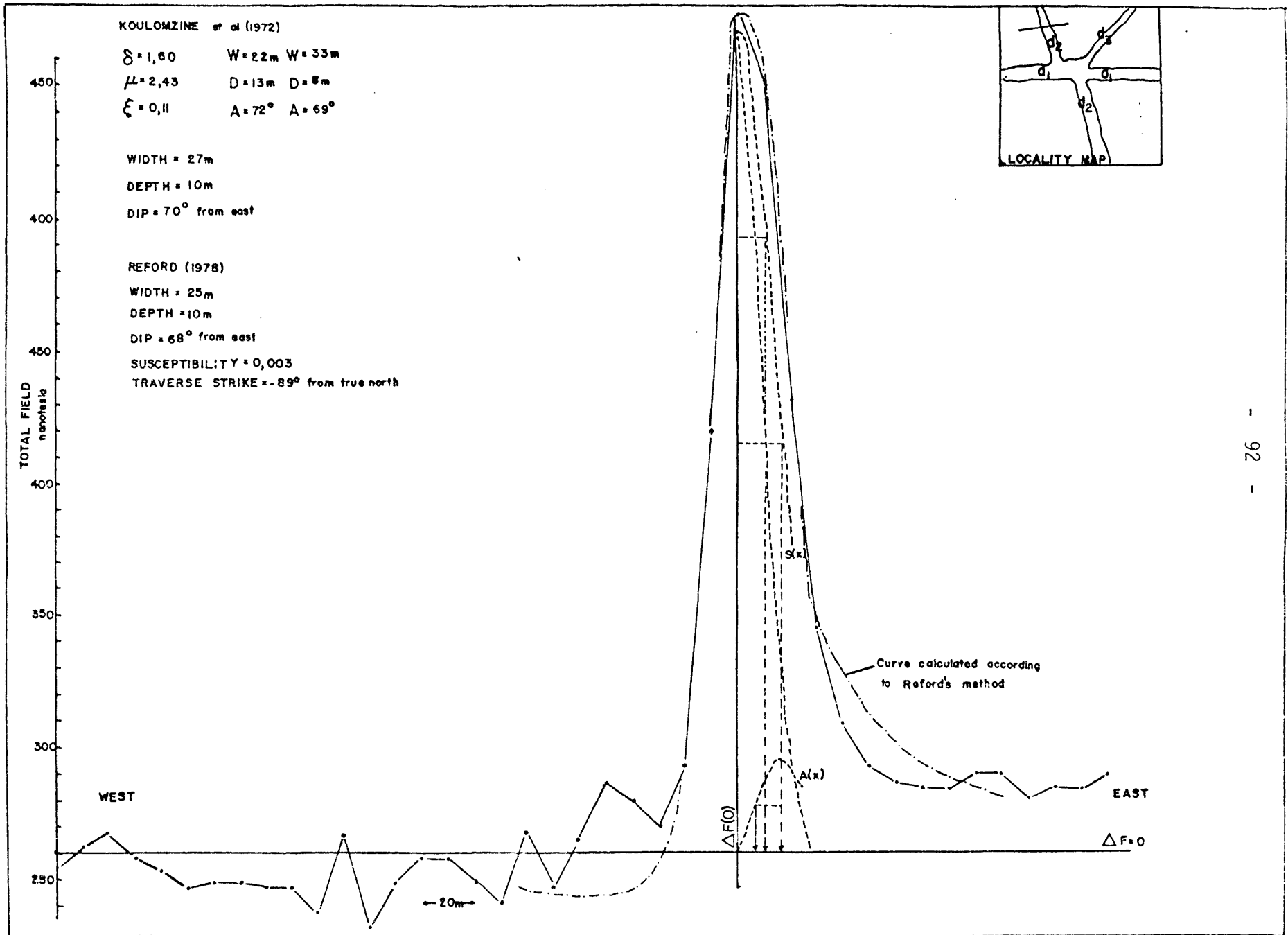
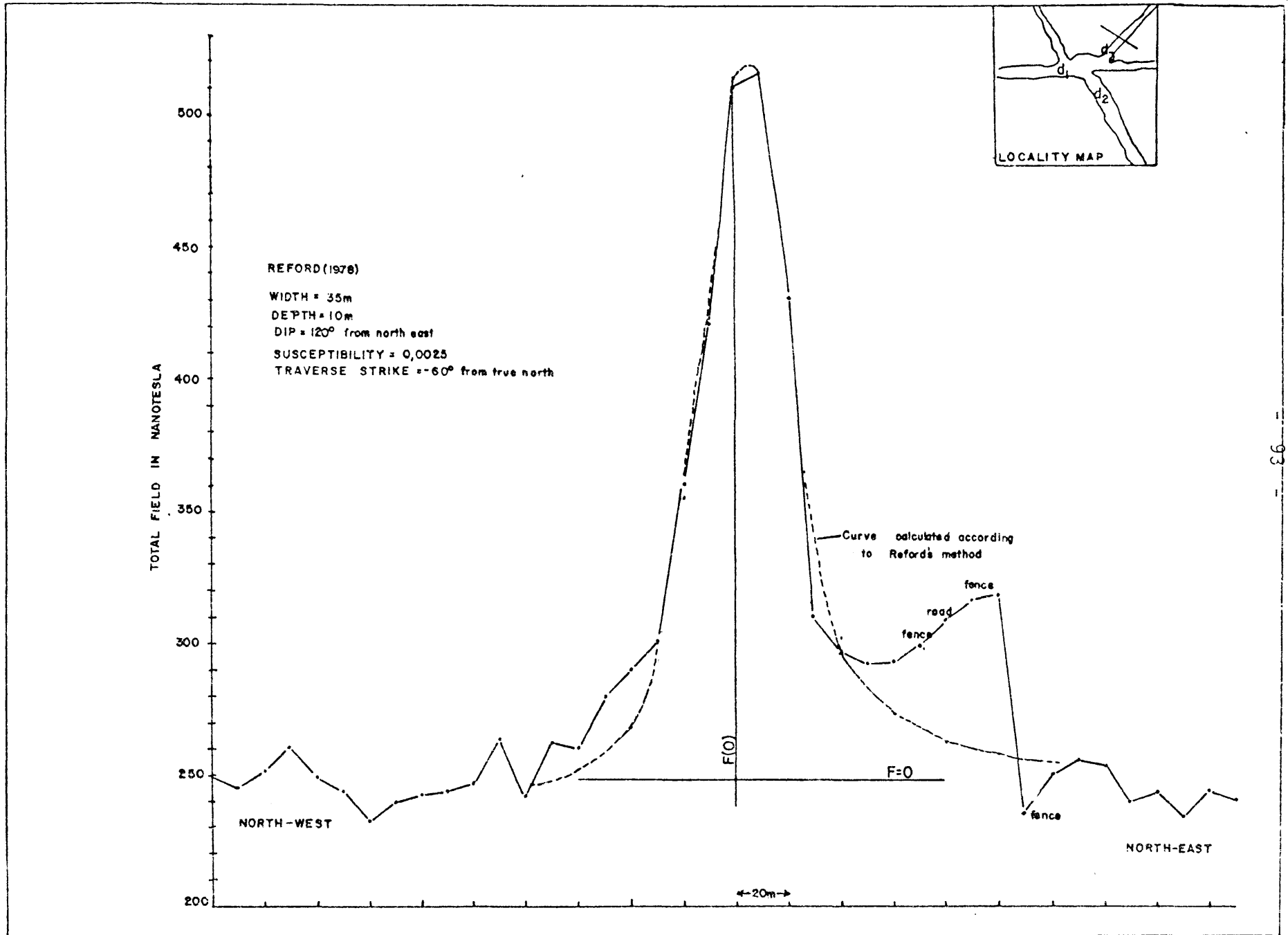


FIGURE 35D TOTAL FIELD MAGNETIC ANOMALY OBTAINED OVER DYKE d_3



(Figure 35(b) and (c)). Although the part of dyke d_2 in the southern sector is thicker than the one in the northern sector, they both have a similar dip and the displacement assumption seems valid.

A total field magnetic profile across dyke d_3 is given in Figure 34(d). A possible additional body, situated on the north-eastern flank of dyke d_3 , causes a disturbance in the magnetic field. Since the position of the body also corresponds with the position of the main dirt road to Carlisonia and three fences are present in the same area it is difficult to establish if the observed anomaly is caused by more than one intrusion. On profiles of magnetic data across dyke d_3 further removed from the road it seems as if only one intrusion is present. Only the Reford method was used to determine the dyke parameters (Figure 35(d)).

Drilling on the dykes indicated that fresh dyke material is only reached at a vertical depth of more than 20 m. However, a clay consisting of decomposed basic material was usually encountered at a depth of 15 m from the surface. Since magnetite weathers more slowly than the basic material itself the magnetite content in the clay could thus be responsible for the erroneous depth estimation.

7. MODE OF DEPOSITION OF THE DIAMONDIFEROUS GRAVELS

The Lichtenburg diamondiferous gravel runs are by no means unique. Similar gravel runs occur at various places in the Western Transvaal and also in western Yakutia, the Urals, Siberia, Australia, Borneo and Brazil where they are referred to as diamond placers (Dorofeyeva, 1963).

Furthermore these diamond placers seem to have many common characteristics

and are described as accumulations of different types of rock fragments of all sizes (boulders to clay) with different degrees of rounding and sorting, which resembles flood plain or glacial deposits. As a rule the deposits lie far removed from the present day valleys and drainage patterns. They are found on formerly exposed rock surfaces, in channels or in sink-holes and the thicknesses can vary from 3 to more than 30 m.

The major factor that facilitated the deposition and preservation of the diamondiferous gravels in the Western Transvaal was the presence of karst landforms in the dolomite.

Martini and Kavalieris (1976) recognised at least four periods of karst formation of the dolomite of the Chuniespoort Group, dating from just after its deposition to recent. The erosion of the dolomite therefore started long before the deposition of the diamondiferous gravels in the Western Transvaal since they are at most of late Tertiary age (Du Toit, 1951). Marker (1972) recognised several Quaternary climatic fluctuations in which water would have been available during wet periods for the dissolution of dolomite.

7.1 Karst formation in the Dolomite

The main process involved in karst formation is the widening of fissures, joints and faults by solution. A prerequisite is that the water table must be well below the surface to allow surface water to percolate through the rock along joints and especially joint-intersections (Sparks 1972, p.190; Sweeting 1972, p.1.).

The rate of dolomite solution is affected inter alia by the state of equilibrium between the carbon dioxide content of the water, the partial

pressure of carbon dioxide in the gas phase of the carbon dioxide-water system (Bögli, 1960) the amount of free carbon dioxide in the atmosphere, soil or underground atmosphere and the temperature (Sweeting 1972, p.31-40).

For the formation of karst a large area of massive, crystalline, well-bedded and jointed dolomitic limestone of considerable thickness must exist below the elevation of throughflowing rivers, otherwise hydrological constraints, denudation of karst features, intercalated lithologies of other rock types and the lack of full circulation of underground water will hinder the development of a full karst scenery. There should also be enough rainfall to promote solution (Sparks, 1972).

Solution channels will form and their shape will depend largely on the control exercised by the minor structural features of the rock. Two main types of solution holes have been distinguished; funnel-shaped depressions with a hole at the centre (sinkholes) and gorge or shaft-like holes (called "ponor" or "evens"). Both types may enlarge and in places several may coalesce to form larger, compound solution holes. These result in underground caverns in the phreatic zone of permanent saturation and between the phreatic and vadose zone, which is only occupied by water when the water table is high. The action of chemical and normal erosion on the surface leads to the thinning of the roofs of the solution caves so that infiltration through joints in the roofs results in their weakening and collapse.

7.2 River action

River action forms an integral part in the development and completion of the karst cycle.

Rivers that initially flowed on thin rock formations underlain by dolomite will eventually entrench themselves into the dolomite and cause a water saturation of the dolomitic rock. Consequently solution caves develop as described in the previous section and because of erosion of the surface, the area of dolomitic limestone that outcrops, will increase. Due to the abstraction of surface water, rivers subsequently flowing on the dolomite will partly flow on the surface and partly underground, thus the majority of river valleys will become dry and the rivers that survive receive their water from springs. The thinning of the roofs of solution caverns (through erosion) and the following water infiltration through joints in cave roofs cause their collapse.

Karst formation stops when impermeable rock formations are encountered. As the dolomite thickness is lowered, solution caves just above these impermeable beds will eventually form open karst structures and gorges, along which river flow will again take place. River entrenchment in the impermeable bed follows and the dolomitic cover is reduced to a few outliers that eventually will disappear.

7.3 Mode of deposition

The problems concerning the origin, accumulation and enrichment of the Lichtenburg diamond gravels have been extensively treated in the literature and diamond enrichment by ordinary alluvial processes (Du Toit 1951; Retief 1960; Stratten 1973) and flashfloods (Beetz, 1930) have been proposed.

The diamictite occurrences of probably Dwyka age south of Lichtenburg (Von Gottberg, 1970) could have extended further north and eastwards during the early Tertiary so that the area underlain by the

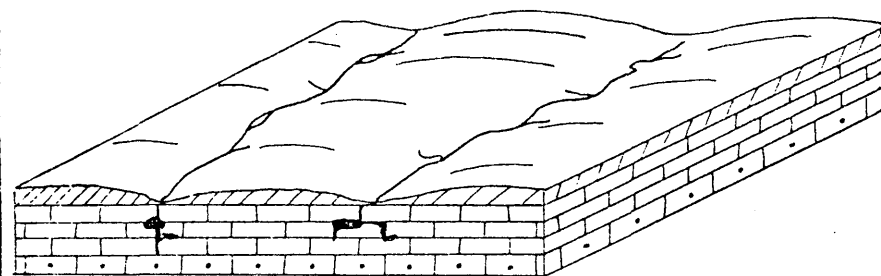
dolomite of the Malmani Subgroup north of Lichtenburg was covered by a diamictite veneer.

Thus, north of Lichtenburg the ideal condition for sinkhole formation existed viz. a chert-poor jointed dolomite overlain by Karoo sediments and underlain by the impermeable chert-rich upper chert rich zone of the Monte Christo Formation (Figure 36, stage 1).

Due to erosion and entrenchment of rivers, dolomite, outcropped with the result that karstification of the dolomite began and underground caves were formed by solution along weak zones (Figure 36, stages 1 and 2).

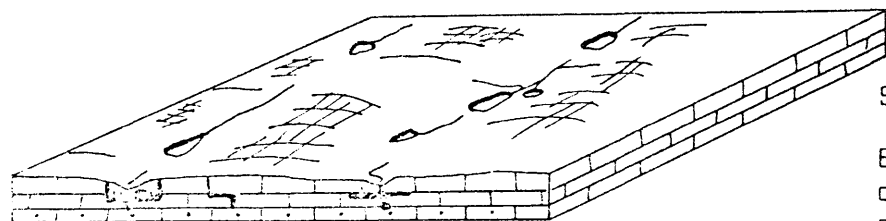
During the late-Tertiary period the uplift of the Griqualand-Transvaal axis as proposed by Du Toit (1933) or a similar tectonic disturbance caused the lowering of the water-table in the dolomitic limestones. Cavern roofs were weakened by the lowering of the dolomite surface, and the subsequent water infiltration through cave roofs. This caused the collapse of solution caves, which resulted in the exploitation by the palaeorivers of the collapsed sinkholes in the Lyttelton Formation (Figure 36, Stage 3).

Open karst landforms thus existed in which diamondiferous gravel was deposited while the water flow continued underground to resurface again as springs. Due to the fact that the rivers frequently lost their freight in karst areas during their youth, subrounded to well rounded pebbles (Blatt et al, 1972, p.64) present in the lower gravels in sinkholes could be of diamictitic origin, since the apparent short distance of fluvial transport cannot account for the rounding of these gravels. Furthermore the unconsolidated nature of weathered diamictite as described by Von Gottberg (1970) probably enhanced its introduction into the palaeoriver system that transgressed it. Rapid drainage of the water into leached

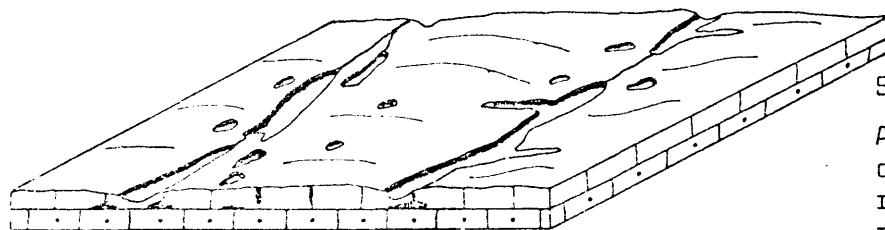


DIAMICTITE VENEER
 LYTTTELTON FORMATION
 MONTE CHRISTO FORMATION

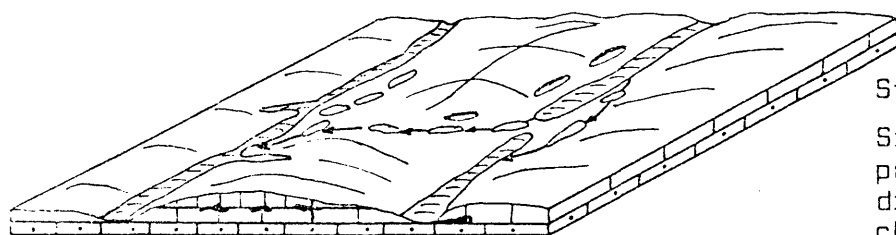
Stage 1.
 The erosion of the diamictite veneer and the entrenchment of rivers into the dolomitic limestone of the Lyttelton Formation. Due to ground water infiltration the widening of joints takes places.



Stage 2.
 Extensive development of solution cavities. Water movements continuous underground and springs develop. Transported material of diamictitic origin is deposited into sinkholes.



Stage 3.
 A tectonic disturbance causes lowering of watertable in the dolomite. Increased water infiltration and thinning of cave roofs cause their collapse. Open karst gorges appear in which river gravels of diamictitic and local origin are deposited by fluvial action and flash floods. Karst formation is hindered in the Monte Christo Formation due to its chert layers.



Stage 4.
 Sinkholes appearing next to the runs are exploited by the palaeorivers and secondary runs appear. After depletion of diamictite source, material consisting of predom nantly local chert is deposited.

Figure 36 : Development of the diamondiferous gravel runs

jointed zones underneath sinkholes caused clay of possible diamictitic origin, initially in suspension, to also drain away until voids and pores were sufficiently blocked with fine material to result in the clayey matrix of the lower gravels. Due to the further intermittent collapse of gravel filled sinkholes the gravels were probably re-arranged when moving down the normally funnel-shaped sinkholes. This resulted in the vertical orientation of the long axis of individual pebbles as already mentioned.

To explain the great number of unconnected gravel patches and gravel-filled sinkholes situated next to the gravel runs, the original palaeorivers must have changed course continuously so that gravel-filled sinkholes were temporarily by-passed as gravel was deposited in new sinkholes. Further collapse of the old, already gravel-filled sinkholes brought the river back to a previous course (Figure 36, Stage 4). This would also explain the fact that so much variation exists between bordering gravel deposits e.g. sinkhole S_1 and S_2 (Figures 27 and 28 and 29). The discordant layer of dolomitic chert detritus present in places in gravel-filled sinkholes, was probably deposited by debris flows (Rodine and Johnson, 1976) during periods when the palaeorivers by-passed these sinkholes.

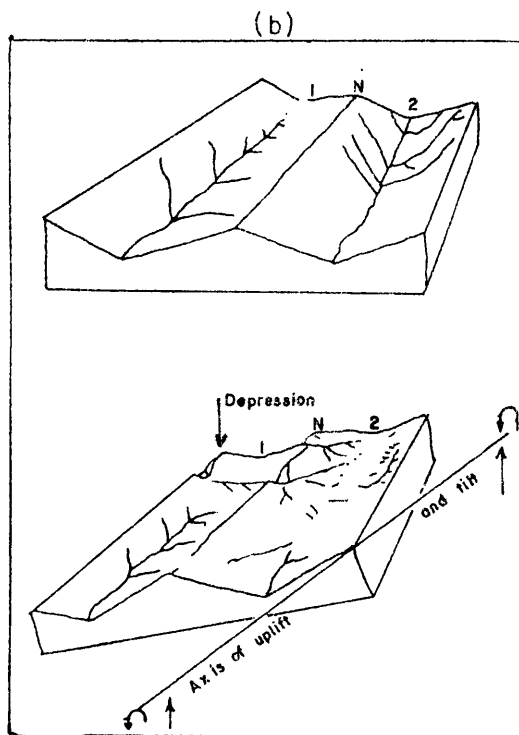
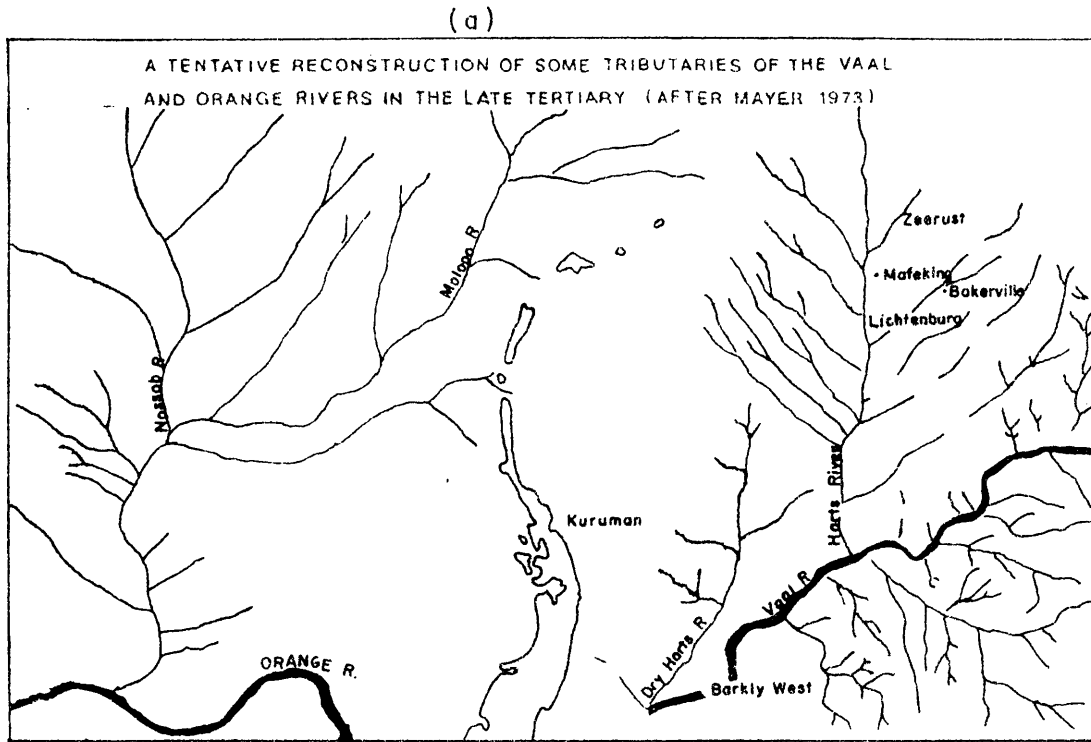
The deposition of the lower clayey gravels was followed by the deposition of the upper gravels with a red soil matrix. This indicates that the diamictitic source must have been depleted or that a change in the drainage pattern due to the diastrophic uplift of the Transvaal axis (Du Toit 1933; Mayer 1973) must have taken place. The alternative assumption that these upper gravels represent reworked lower gravels does not seem acceptable since allochthonous pebbles except for diamonds, are rarely seen in the upper gravels.

The upper gravels were followed by the deposition of the "Roosloot" gravel which is considered to represent the last cycle of deposition by Retief (1961).

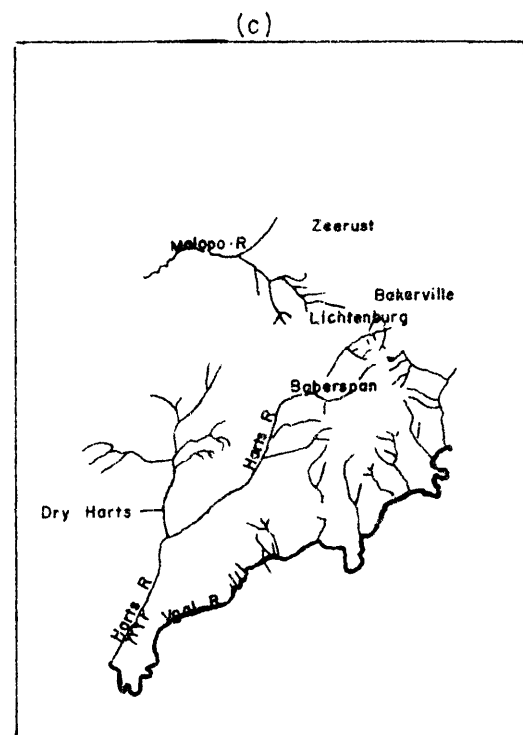
Mayer (1973) proposed that the Welverdiend-Grasfontein run during its mature stage formed a tributary of the Harts River (Figure 37(a)). Due to the uplift of the Griqualand-Transvaal axis, tributaries of the Molopo River cut off the headwaters of the palaeo Harts River so that the "Welverdiend-Grasfontein-La Rys Stryd" tributary was directed towards the northwest and the diamondiferous alluvials of the Dry Molopo were deposited (Figure 37(b) and (c)), remnants of which are present near Mafeking. Du Toit (1951, p.10) states that the well-defined depression of the Dry Molopo River extends across the farm Elizabeth 357 S0 almost to La Rys Stryd and describes the presence of allochthonous pebbles of possible Pretoria Group origin in the Dry Molopo diamondiferous gravels. The diamonds that were found here were of a good quality which indicates a longer transport distance. The author is also aware of agate-bearing gravels that were found in boreholes on the farm Grootfontein 115 J0 which substantiates Mayer's proposal.

The uplift of the Griqualand-Transvaal axis probably caused a dramatic change in the drainage pattern in the Western Transvaal so that the palaeo-river system of which the gravel runs north of Lichtenburg formed part, did not survive. Depressions in the gravel runs and gravel-filled sinkholes were thus filled with red sandy soil and dolomitic surface rubble.

Due to the continued lowering of the dolomitic surface in the Western Transvaal the gravel runs which are more resistant to erosion formed chains of small mounds.



LINKAGE OF THE HARTS RIVER WITH THE DRY HARTS RIVER DUE TO UPLIFT IN THE LATE TERTIARY TO EARLY PLEISTOCENE



PRESENT REGIONAL SETTING OF THE HARTS RIVER

FIGURE 37 PROPOSED DEVELOPMENT OF THE HARTS RIVER (AFTER MAYER 1973)

The erosion of the gravel runs introduced diamonds into the surface rubble flanking the runs. A clear example of this is observed around King's Pothole where gravels were only present in the Pothole but diamonds were also found among the surface rubble surrounding it.

The greatest speculation applies to the origin of the diamonds. Since the Swartruggens kimberlites are of post-Karoo age (Allsopp and Barrett, 1975) they could not have acted as a source for possible diamonds in the diamictite. No diamonds have ever been reported from the diamictite south of Lichtenburg. Du Toit (1951) reported the occurrence of tourmaline and spinel, possibly from the Swartruggens field, on Witstinkhoutboom 9 IP (Figure 1). However, it is doubtful if diamonds could have been transported approximately 80 km by normal river action from the Swartruggens fields to Bakerville since the alluvial diggings from the Swartruggens fields only extend at most a distance of 5 km from the Swartruggens kimberlite dykes. Alluvial diamonds from the Cullinan pipe were only transported 13 km along the Elandsriver by fluvial action.

It is therefore proposed that a local yet unidentified diamondiferous kimberlitic source should exist in the immediate vicinity to the east or north of Lichtenburg. This proposal would account for the facts that the gravel runs are all diamondiferous but were fed from different directions from north-north-west to south, that the diamonds from neighbouring runs vary widely in quality, that diamonds show no signs of abrasion and that fair amounts of board and cleavage "chips" are present on the runs. Du Toit (1951, p.32) stressed that the top and not the bottom layers of the gravel runs, had the highest diamond content. A reworking of the "lower" gravels could explain this fact but it could also be attributed to the kimberlite source becoming more exposed, that resulted in an increase of the diamond content of the transported load since a fair

amount of boart is also present in the "upper" gravels. The fact that very little kimberlitic ilmenite was found does not rule out the possibility of nearby kimberlite occurrences since the Bellsbank and Sover kimberlite dykes also contain very little ilmenite.

8. SUMMARY AND CONCLUSION

The fluvial model where individual palaeoriver courses were governed by sinkhole formation in the dolomite is the only model that can explain the trapping and preservation of the diamondiferous gravels reasonably well. The direction of flow of the palaeorivers can also be accepted as being from the north, north-east or east and south (Manana run).

The possible diamictite origin of the "lower" gravels accounts for the presence of well rounded chert pebbles, the allochthonous pebble constituents in, and the clayey matrix of the "lower" gravels. Three initial cycles of gravel deposition can be identified, namely the "lower", "upper" and "Rooisloot" gravel deposits. After deposition of the "Rooisloot" gravel, erosion took place which led to the presence of manganese-rich diamondiferous gravel and surface rubble that flank the gravel runs.

Although kimberlite occurrences near Lichtenburg have as yet not been described in the literature, the kimberlitic garnet found in Pienaar's Pothole, the amount of boart and cleavage chips of diamond present in the gravel, the lack of abrasion on diamond crystal edges and the fact that the "upper" gravels are richer in diamonds than the "lower" gravels point to the presence of kimberlite intrusions in the vicinity of the gravels.

Although the gravity method is very time consuming and thus expensive it proved to be extremely successful in this investigation. Due to the substantial (1gm/cm^3) difference in density between gravels or weathered dolomite and solid dolomite, leached zones in the dolomite can be identified in which gravel deposits may be present. The presence of diamondiferous gravel has to be proved with drilling. With the gravity method the existence of sinkholes (potholes) filled with virgin diamondiferous gravel has been proved and these sinkholes usually occur under a red soil cover.

The computer program devised for the interpretation of gravity data is also believed to be much more efficient than earlier programs of the same kind.

Although the magnetic method is not suitable to distinguish between areas underlain by gravels and leached dolomite it proved very valuable in locating the position of dykes. Drilling for gravel could thus be undertaken on the flanks of weathered dykes where conditions are very favourable for the formation of sinkholes that can be gravel-bearing.

REFERENCES

- ALLSOPP, H.L. and BARRETT, D.R. (1975). Rb-Sr Age determinations on South African kimberlite pipes, p. 605-617. In L.H. Ahrens J.B. Dawson, A.R. Duncan and A.J. Erlank, Editors, *Physics and Chemistry of the Earth*, 9, Permagon Press, New York, 940 pp.
- AWASTHI, A.K. (1970). Skewness as an environmental indicator in the Solani River System, Rooikee (India). *Sed. Geol.*, 4, 177-183.
- BANERJEE, B. and DAS GUPTA, S.P. (1977). Gravitational attraction of a rectangular parallelepiped. *Geophys.*, 42, 1053-1055.
- BARNETT, C.T. (1976). Theoretical modelling of the magnetic and gravitational fields of an arbitrarily shaped three-dimensional body. *Geophys.*, 41, 1353-1364.
- BHATTACHARYYA, B.K. (1978). Computer modelling in gravity and magnetic interpretation, *Geophys.*, 43, 912-929.
- BEETZ, P.F.W. (1930). Processes of concentration in alluvial and allied diamond placers of South-West, South, Central and East Africa. *Rep. Int. Congr. Min. 6th*, Liege (1930), 49-68.
- BLATT, H., MIDDELTON, G. and MURRAY, R. (1972). *Origin of sedimentary rocks*. Prentice-Hall, Inc. New Jersey. 634pp.
- BÖGLI, A. (1960). "Kalklösung und Karrenbildung" *Z. Geomorph. Suppl.*, 2, 4-21.
- BOTT, M.P.H. (1960). The use of rapid digital computing methods for direct gravity interpretation of sedimentary basins. *Geophys. J.*, 3, 63-65.
- CORDELL, L. and HENDERSON, R.G. (1968). Iterative three-dimensional solution of gravity anomaly data using a digital computer. *Geophys.*, 33, 596-601.

- DAL CHIN, R. (1968). "Pebble Clusters" : their origin and utilisation in the study of palaeocurrents. *Sed. Geol.*, 2, 233-241.
- DANES, Z.F. (1960). On a successive approximation method for interpreting gravity anomalies. *Geophys.*, 25, 1215-1228.
- DARRACOTT, B.W. (1973). Preliminary results from gravity and magnetic surveys of the diamondiferous deposits of the Lichtenburg-Bakerville area. *Unpubl. Rep. geol. Surv. S. Afr.*
- DAVIS, J.C. (1973). *Statistics and data analysis in geology.* John Wiley and Sons, Inc., New York, 550pp.
- DAVIS, G. and PREVOST, X.M. (1978). The geology and mineralogical resources of an area around Lichtenburg. *Unpubl. Rep. geol. Surv. S. Afr.*
- DAWSON, J.B. (1971). Advances in kimberlite geology. *Earth Sci. Rev.*, 7, 187-214.
- DE WIT, M.C.J. (1978). Geophysical investigation and geological interpretation of part of the diamondiferous gravels on the Grasfontein farm (356 JP), west of Bakerville, Lichtenburg District. *Unpubl. Rep. geol. Surv. S. Afr.*
- DOROFYEVA, I.I. (1963). Origin of various types of diamond placer deposits on stream divides. *Int. Geol. Rev.* (1965), 37, 724-728.
- DRAPER, D. (1972). On the occurrence of diamonds associated with the chert beds of the Dolomite Series in the districts of Ventersdorp and Lichtenburg. *Trans. geol. Soc. S. Afr.*, XXX, 57-67.
- DU TOIT, A.L. (1933). Crustal warping as a factor in the geographical evolution of South Africa. *S. Afr. geogr. J.*, 16, 3-20.
- (1935). *The diamondiferous alluvials. Explan. Sheet 53 (Bakerville).* Geol. Surv. S. Afr., 65pp.

- DU TOIT, A.L. (1951). *The diamondiferous gravels of Lichtenburg*.
Geol. Surv. S. Afr. Memoir No. 44, 35pp.
- ENSLIN, J.F., KLEYWEGT, R.J., BEUKES, J.H.T. and GORDON-WELSH, J.F. (1976).
Artificial recharge of dolomitic ground-water compartments in the
Far West Rand goldfields of South Africa. *Intern. Assoc. of
Hydrol. Sciences*, Publ. 121, 495-506.
- ERVIN, C.P. (1977). Theory of the Bouguer anomaly. *Geophys.*, 42, 1458.
- FOLK, R.L. (1968). *Petrology of sedimentary rocks*. The University of
Texas. Geology. 370k, 383l, 383M, 140pp.
- FRICK, C. (1976). Diamante - *Delfstowwe van die Republiek van Suid-Afrika*.
Staatsdrukker, Pretoria, 462pp.
- HARGER, H.S. (1928). *Proc. geol. Soc. S. Afr.*, XXX, XXXIV-XLV.
- HEDBERG, H.D. (1926). The effect of gravitational compaction on the structure
of sedimentary rocks. *A.A.P.G. Bull.*, 10, 1035-1072.
- HEILAND, C.A. (1940). *Geophysical exploration*. Prentice-Hall, Inc., New
York, 1013pp.
- JENNINGS, J.E. (1965). Building on dolomites in the Transvaal. Kanthack
memorial lecture. *Trans. S.A. Inst. of Civ. Engineers*, 8, 41-62.
- KAMMEYER, S.C. and FRICK, C. (1978(a)). Report on possible kimberlite ilmenite and
garnet from palaeoriver gravels near Bakerville
—————(1978(b)). Ondersoek van twee granaat en drie ilmeniet
monsters van Lichtenburg. *Unpubl. Rep. geol. Surv. S. Afr.*
- KOULOMZINE, T.H., LAMONTAGNE, Y. and NADEAU, A. (1970). New methods for
the direct interpretation of magnetic anomalies caused by inclined
dykes of infinite length. *Geophys.*, 35, 812-830.

- KLEYWEGT, R.J. and ENSLIN, J. (1973). The application of the gravity method to the problem of ground settlement and sinkhole formation in dolomite on the Far West Rand, South Africa. *Symp. of IAEG on sinkholes and subsidence and engineering geological problems.*
- KLEYWEGT, R.J. and STETTLER, E.H. (1979). A new approach to three-dimensional gravity modelling by computer. *Unpubl. Rep. geol. Surv. S. Afr.*
- KRUMBEIN, W.C. (1934). Size frequency distributions of sediments. *J. Sedim. Petrol.*, 4, 65-77.
- KU, C.C. (1977). A direct computation of gravity and magnetic anomalies caused by 2- and 3-dimensional bodies of arbitrary shape and arbitrary magnetic polarisation by equivalent-point method and a simplified cubic spline. *Geophys.*, 42, 610-622.
- MAHER, M.J. (1979(a)). The establishment of a gravity base station in the Old Land Bank Building. *Unpubl. Rep. geol. Surv. S. Afr.*
- (1979(b)). The transformation of X and Y co-ordinates to longitude and latitude by digital computer. *Unpubl. Rep. geol. Surv. S. Afr.*
- MARKER, M.E. (1973). Karst landform analysis as evidence for climatic change in the Transvaal. *S.A. geogr. J.*, 5A, 152-162.
- MARTINI, I.P. (1977). Gravelly flood deposits of Irvine Creek, Ontario, Canada. *Sed.*, 24, 603-622.
- MARTINI, J. and KAVALLIERIS, I. (1976). The karst of the Transvaal (SA) *Int. J. speleo.*, 8, 229-251.
- MAYER, J.J. (1973). Morphotectonic development of the Harts River Valley in relation to the Griqualand-Transvaal axis and the Vaal and Moloporiver. *Trans. geol. Soc. S.A.* 73, 183-194.

- McKEE, E.D. and WEIR, G.W. (1953). Terminology for stratification and cross-stratification in sedimentary rocks. *Bull. geol. Soc. Am.*, 64, 381-389.
- McMANUS, (1963). A criticism of certain usage of the "phi" notation. *J. Sedim. Petrol.*, 33, 670-674.
- MARQUARDT, D.W. (1963). An algorithm for least-squares estimation of non-linear parameters. *J. Soc. ind. appl. Math.*, 17, 431-441.
- MORGAN, H.A. and FAESSLER, G.W. (1972). A two- and three-dimensional gravity dot chart. *Geophys., Prospect.*, 20, 363-374.
- MUFTI, I.E. (1975). Iterative gravity modelling by using cubical blocks *Geophys., Prospect.*, 23, 163-198.
- MUFTI, I.R. and WANG, R. (1975). Comments on "Rapid determination of cubes" gravity field. *Geophys., Prospect.*, 23, 199-202.
- NETTLETON, L.L. (1976). *Gravity and magnetics in oil prospecting.* McGraw-Hill, New York, 464pp.
- PALMER, E. (1978). A geophysical study of the Grootfontein dolomitic groundwater compartment in the Rooigrond area. *Unpubl. Rep. geol. Surv. S. Afr.*
- PETTIJOHN, F.J. (1957). *Sedimentary rocks.* Second Edition. Harper and Row Pub, New York. 718pp.
- POWELL, M.J.D. (1965). A method for minimising a sum of squares of non-linear functions without calculating derivatives. *Comput. J.*, 7, 303-307.
- REFORD, M.S. (1964). Magnetic anomalies over thin sheets. *Geophys.*, 24, 532-536.
- (1978). Magnetic anomalies over the edge, dyke and thin sheet. *Lecture presented at SAGA in May 1978.*

- RETIEF, E.A. (1961). The diamondiferous gravels in the Lichtenburg and Ventersdorp area. *Unpubl. Rep. geol. Surv. S. Afr.*
- RICHARDS, D.J. (1978). Magnetic surveys : notes for Geological Survey Colloquium. *Unpubl. Rep. geol. Surv. S. Afr.*
- (1979). Possible kimberlite occurrences from aeromagnetic data between Alexander Bay and Port Nolloth. *Unpubl. Rep. geol. Surv. S. Afr.*
- ROBINSON, D. (1978). The characteristics of natural diamond and their interpretation. *Minerals Sci. Engng*, 10, 55-72.
- RHODINE, J.D. and JOHNSON, A.M. (1976). The ability of debris, heavily freighted with coarse clastic materials to flow, on gentle slopes. *Sed.*, 23, 213-234.
- SNYMAN, C.P. (1973). Possible classification parameters of South African kimberlites. *Trans. geol. Soc. S.A.*, 77, 35-91.
- SPARKS, B.W. (1972). *Geomorphology*. Second Edition. Long Man Group Ltd., London, 480pp.
- STRATTEN, T.S. (1977). The origin of the gravels in the alluvial diamond deposits of the South-Western Transvaal. *Abstracts, Geocongress (1977)*.
- SWEETING, M.M. (1972). *Karst Landforms*. McMillan Press Ltd, New York, 510pp.
- TALWANI, M. and HEIRTZLER, J.R. (1964). Computation of magnetic anomalies caused by two-dimensional structures of any shape. *Computers in the mineral industry*, G.A. Parks, Stanford University.

- TALWANI, M. and EWING, M. (1960). Rapid computation of gravitational attraction of three-dimensional bodies of arbitrary shape. *Geophys.*, 25, 203-225.
- TELFORD, W.M., GELDART, L.P., SHERIFF, R.E., and KEYS, D.A. (1976). *Applied Geophysics*. Cambridge University Press, London, 860pp.
- VON GOTTBURG, B. (1970). The occurrence of Dwyka rocks and glacial topography in the South-Western Transvaal. *Trans. geol. Soc. S.A.*, 73, 99-106.
- VAN GENDEREN, J.L. (1977). Nomograms for morphometric gravel analysis *Sedim. Geol.*, 17, 285-294.
- VAN VUUREN, C., COLE, D. and STETTLER, E. (1979). The Lichtenburg diamond bearing gravels. Some observations. *Unpubl. Rep. geol. Surv. S. Afr.*
- WILLIAMS, P.F. and RUST, B.R. (1969). The sedimentology of a braided river. *J. Sedim. Petrol.*, 39, 649-679.

A P P E N D I X 1

DENSITIES OF THE ROCKS AND GRAVELS IN THE AREA

The source of gravity anomalies and the significant parameter in gravity exploration are the local variation in density. The success with which the gravity method can be applied depends on the density contrast between host rock and the material prospected for. Thus for the interpretation of residual gravity anomalies a reasonable estimate of the bulk density of the rock material under consideration is essential.

On Ruigtelaagte 353 JP fresh chert-rich and chert-poor dolomite, weathered dolomite, red manganese-rich soil, gravel from fossil rivers, kaolinitic clay and weathered dyke material are encountered.

The density of gravel, clay, soil and weathered dolomite.

Factors that normally influence the density of sediments are porosity, the presence of pore fluids, age, previous history and depth below surface (Telfort et al, 1976).

Ideally undisturbed samples are required to determine the bulk density of the gravel in situ. Efforts to cut out a sample from virgin gravel without disturbing its state of consolidation only had very limited success.

Thus a sturdy container made of galvanised sheet iron and with an exact volume of 8 200 cc (determined with a buret and measuring cylinder of 1 000 ml) was used to determine densities. The volume of the container was checked periodically as the sediments were lightly compacted in the container.

The water-table is about 29 m below the surface but no correction was applied to the density determinations of the gravels occurring below the present water-table since it is doubtful if the increase in density due to the water saturation will play an important role in gravity modelling. The results of the density determinations are shown in Table A. These densities are subject to errors since the gravel has no formal stratification and considerable variations in the size of the pebbles and in the ratio of pebbles to matrix are present.

An increase in density with depth has also to be considered (Hedberg, 1926) and an increase of 10 per cent in the density of the gravels is proposed to account for the abovementioned errors. A density of 1,85 gm/cc was therefore used for the gravels.

The density contrast between the gravels and the residual cherty products of leached dolomite is very small (Table A) and it is therefore impossible to distinguish between gravels, clay and weathered dolomitic material on the basis of residual gravity anomalies alone. Drilling was therefore used to outline the different sediments.

No satisfactory density estimate of the dolomite could be made. The methods of Nettleton and Parasins (Telford et al, 1976) were applied over a hill in the northern portion of the experimental area, but the values obtained were too low due to the influence of bordering gravity lows.

Due to the presence of quartz veins and chert layers in the dolomite density determinations on small samples do not provide satisfactory values. The density of dolomitic bedrock is thus assumed to be 2,85 gm/cc, the same as that of dolomitic bedrock in the Carletonville area (Kleywegt and

TABLE A : The densities of gravel and weathered dolomitic chert in the Ruigtelaagte Area

Locality	Description	Density gm/cm ³
The Welverdiend-Grasfontein run (Y27/X4,5)	Gravel with soil matrix	1,79
The Welverdiend-Grasfontein run (Y14/X4)	Gravel with soil matrix	1,79
The Welverdiend-Grasfontein run (Y35/X4)	Gravel with clay matrix	1,70
Pienaar's Pothole (Y20/X14)	Gravel with soil matrix	1,82
Pienaar's Pothole (Y21,5/X13)	Gravel with clay matrix	1,75
Southern part of the Ruigtelaagte area (Y7/X23)	Clay	1,68
Southern part of the Ruigtelaagte area (Y7/X23)	Gravel with soil matrix	1,72
Southern part of the Ruigtelaagte area (Y7/X23)	Gravel with clay matrix	1,76
(Y8/X22)	Weathered cherty dolomite	1,72
(Y19/X6)	Weathered cherty dolomite	1,71
(Y14/X4)	Weathered cherty dolomite	1,77
(Y17/X17)	Weathered cherty dolomite	1,75

Enslin, 1973). A density contrast of 1 gm/cc was thus used for the interpretation of residual gravity anomalies.

The density of the weathered dyke material was not determined since it played no role in the gravity modelling.

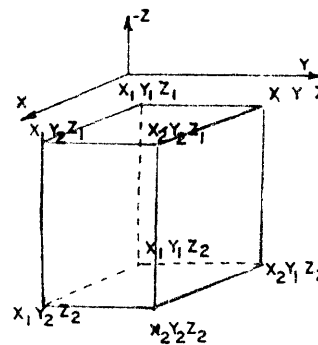
A P P E N D I X 2

MATHEMATICAL BASIS FOR THE GRAVITY FORMULA OVER A RECTANGULAR
PARALLELEPIPED

The vertical component of the gravitational attraction at the origin of a right rectangular parallelepiped bounded by planes

$$x = x_1 \quad x = x_2 \quad y = y_1 \quad y = y_2 \quad z = z_1 \quad z = z_2 \text{ is}$$

$$g_z(0,0,0) = g_z$$



$$= -\gamma \rho \int_{x_1}^{x_2} \int_{y_1}^{y_2} \int_{z_1}^{z_2} \frac{z \, dx \, dy \, dz}{(x^2 + y^2 + z^2)^{3/2}} \Big|_2 \quad \text{where } \gamma = \text{universal gravitational constant}$$

$$\rho = \text{density contrast}$$

neglecting the sign

$$= \rho \gamma \int_{x_1}^{x_2} \int_{y_1}^{y_2} \left\{ \frac{1}{\sqrt{x^2 + y^2 + z^2}} \Big|_{z_1}^{z_2} \right\} dx \, dy$$

$$= \rho \gamma \int_{x_1}^{x_2} \int_{y_1}^{y_2} \left\{ \frac{1}{\sqrt{x^2 + y^2 + z_2^2}} - \frac{1}{\sqrt{x^2 + y^2 + z_1^2}} \right\} dx \, dy$$

$$\begin{aligned}
&= \gamma \rho \int_{x_1}^{x_2} \left\{ \ln(y + \sqrt{x^2 + y^2 + z_2^2}) \Big|_{y_1}^{y_2} - \ln(y + \sqrt{x^2 + y^2 + z_1^2}) \Big|_{y_1}^{y_2} \right\} dx \\
&= \gamma \rho \int_{x_1}^{x_2} \ln(y_2 + \sqrt{x^2 + y_2^2 + z_2^2}) - \ln(y_1 + \sqrt{x^2 + y_1^2 + z_2^2}) - \ln(y_2 + \sqrt{x^2 + y_2^2 + z_2^2}) \\
&\quad + \ln(y_1 + \sqrt{x^2 + y_1^2 + z_1^2}) dx
\end{aligned}$$

Let us evaluate the $\int \ln(y_2 + \sqrt{x^2 + y^2 + z^2}) dx$. Bearing in mind that

$\int f(x) \cdot g'(x) = f(x) \cdot g(x) - \int g(x) \cdot f'(x)$ where $f'(x)$ indicates the derivative of $f(x)$ and $\ln(y + \sqrt{x^2 + y^2 + z^2}) = f(x)$ then

$$\begin{aligned}
\int \ln(y + \sqrt{x^2 + y^2 + z^2}) dx &= x \ln(y + \sqrt{x^2 + y^2 + z^2}) - \int \frac{x \cdot \frac{1}{2}(x^2 + y^2 + z^2)^{-\frac{1}{2}} \cdot 2x}{y + \sqrt{x^2 + y^2 + z^2}} \\
&= x \ln(y + \sqrt{x^2 + y^2 + z^2}) - \int \frac{x^2}{(y + \sqrt{x^2 + y^2 + z^2}) \sqrt{x^2 + y^2 + z^2}} dx \\
&= x \ln(y + \sqrt{x^2 + y^2 + z^2}) - \int \frac{x^2}{(y + \sqrt{x^2 + y^2 + z^2}) (\sqrt{x^2 + y^2 + z^2})} \cdot \frac{(\sqrt{x^2 + y^2 + z^2} - y) dx}{(\sqrt{x^2 + y^2 + z^2} - y)} \\
&= x \ln(y + \sqrt{x^2 + y^2 + z^2}) - \int \frac{x^2 \sqrt{x^2 + y^2 + z^2} - y}{(x^2 + z^2) (\sqrt{x^2 + y^2 + z^2})} dx \\
&= x \ln(y + \sqrt{x^2 + y^2 + z^2}) - \int \frac{x^2 (\sqrt{x^2 + y^2 + z^2}) dx}{(x^2 + z^2) (\sqrt{x^2 + y^2 + z^2})} + y \int \frac{x^2 dx}{(x^2 + z^2) \sqrt{x^2 + y^2 + z^2}}
\end{aligned}$$

$$\begin{aligned}
&= x \ln(y + \sqrt{x^2 + y^2 + z^2}) - \int \frac{x^2 dx}{(x^2 + z^2)} + y \int \frac{dx}{\sqrt{x^2 + y^2 + z^2}} - z^2 y \int \frac{dx}{(x^2 + z^2) \sqrt{x^2 + y^2 + z^2}} \\
&= x \ln(y + \sqrt{x^2 + y^2 + z^2}) + y \ln(x + \sqrt{x^2 + y^2 + z^2}) - \int \frac{x^2 dx}{x^2 + z^2} \\
&\quad - z^2 y \int \frac{dx}{(x^2 + z^2) \sqrt{x^2 + y^2 + z^2}}
\end{aligned}$$

When the limits of y are introduced $\int \frac{x^2 dx}{x^2 + z^2}$ will eventually become zero.

To evaluate $z^2 y \int \frac{dx}{(x^2 + z^2) \sqrt{x^2 + y^2 + z^2}}$

the following substitution is performed

$$x = (y^2 + z^2)^{\frac{1}{2}} \tan \theta$$

$$dx = (y^2 + z^2)^{\frac{1}{2}} \sec^2 \theta d\theta$$

substitute:

$$\begin{aligned}
&= z^2 y \int \frac{(y^2 + z^2)^{\frac{1}{2}} \sec^2 \theta d\theta}{[(y^2 + z^2) \tan^2 \theta + z^2] [(y^2 + z^2) \tan^2 \theta + y^2 + z^2]^{\frac{1}{2}}} \\
&= z^2 y \int \frac{(y^2 + z^2)^{\frac{1}{2}} \sec^2 \theta d\theta}{[y^2 \tan^2 \theta + z^2 \tan^2 \theta + z^2] [y^2 \tan^2 \theta + z^2 \tan^2 \theta + y^2 + z^2]^{\frac{1}{2}}} \\
&= z^2 y \int \frac{(y^2 + z^2)^{\frac{1}{2}} \sec^2 \theta d\theta}{[y^2 \tan^2 \theta + z^2 \sec^2 \theta] [y^2 \sec^2 \theta + z^2 \sec^2 \theta]^{\frac{1}{2}}}
\end{aligned}$$

$$\begin{aligned}
&= z^2 y \int \frac{[(y^2+z^2)^{\frac{1}{2}} \sec^2 \theta] [y^2 \sec^2 \theta + z^2 \sec^2 \theta]^{\frac{1}{2}} d\theta}{[y^2 \tan^2 \theta + z^2 \sec^2 \theta] [y^2 \sec^2 \theta + z^2 \sec^2 \theta]} \\
&= z^2 y \int \frac{[(y^2+z^2)^{\frac{1}{2}} \sec^2 \theta] [y^2 \sec^2 \theta + z^2 \sec^2 \theta]^{\frac{1}{2}} d\theta}{y^4 \tan^2 \theta \sec^2 \theta + y^2 z^2 \tan^2 \theta \sec^2 \theta + z^2 y^2 \sec^2 \theta + z^4 \sec^2 \theta} \\
&= z^2 y \int \frac{(y^2+z^2)^{\frac{1}{2}} [y^2 \sec^2 \theta + z^2 \sec^2 \theta]^{\frac{1}{2}} d\theta}{(y^2+z^2) [y^2 \tan^2 \theta + z^2 \sec^2 \theta]} \\
&= z^2 y \int \frac{\left(\frac{y^2}{\cos^2 \theta} + \frac{z^2}{\cos^2 \theta}\right)^{\frac{1}{2}} d\theta}{\sqrt{y^2+z^2} \left[\frac{y^2 \sin^2 \theta}{\cos^2 \theta} + \frac{z^2}{\cos^2 \theta}\right]} \\
&= z^2 y \int \frac{\frac{(y^2+z^2)^{\frac{1}{2}}}{\cos^2 \theta} d\theta}{\sqrt{y^2+z^2} \left[\frac{y^2 \sin^2 \theta + z^2}{\cos^2 \theta}\right]} \\
&= z^2 y \int \frac{\sqrt{y^2+z^2} \cos^2 \theta d\theta}{\sqrt{y^2+z^2} \cos \theta (y^2 \sin^2 \theta + z^2)} \\
&= z^2 y \int \frac{\cos^2 \theta d\theta}{y^2 \sin^2 \theta + z^2}
\end{aligned}$$

This integral cannot be solved in its present form thus the following substitution is made

$$\begin{aligned}
y \sin \theta &= \tau \\
d\tau &= y \cos \theta d\theta \\
d\theta &= \frac{d\tau}{y \cos \theta}
\end{aligned}$$

Substitute:

$$= z^2 y \int \frac{\cos \theta d\tau}{y \cos \theta (\tau^2 + z^2)}$$

$$= z^2 \int \frac{d\tau}{\tau^2 + z^2} = z \tan^{-1} \frac{\tau}{z}$$

Substitute backwards:

$$= z^2 \tan^{-1} \frac{y \sin \theta}{z}$$

but

$$\tan^2 \theta = \frac{x^2}{y^2 + z^2}$$

$$\sec^2 \theta = \frac{x^2}{y^2 + z^2} + 1$$

$$= \frac{x^2 + y^2 + z^2}{y^2 + z^2}$$

$$\cos^2 \theta = \frac{y^2 + z^2}{z^2 + y^2 + z^2}$$

thus

$$z \tan^{-1} \frac{y \sin \theta}{z} = z \tan^{-1} y \frac{\sqrt{1 - \cos^2 \theta}}{z}$$

$$= z \tan^{-1} y \frac{\sqrt{1 - \frac{y^2 + z^2}{z^2 + y^2 + z^2}}}{z}$$

$$= z \tan^{-1} y \sqrt{\frac{x^2}{x^2+y^2+z^2}}$$

$$= z \tan^{-1} \frac{yx}{z\sqrt{x^2+y^2+z^2}}$$

The whole solution is

$$g_z = \gamma \rho x \ln(y + \sqrt{x^2+y^2+z^2}) + y \ln(x + \sqrt{x^2+y^2+z^2})$$

$$- z \tan^{-1} \frac{xy}{z\sqrt{x^2+y^2+z^2}} \quad \begin{array}{c} x_2 \\ / \\ x_1 \end{array} \quad \begin{array}{c} y_2 \\ / \\ y_1 \end{array} \quad \begin{array}{c} z_2 \\ / \\ z_1 \end{array}$$

When the integration limits are introduced then

$$g_z = \gamma \rho x_2 \ln(y_2 + \sqrt{x_2^2+y_2^2+z_2^2}) + y_2 \ln(x_2 + \sqrt{x_2^2+y_2^2+z_2^2}) - z_2 \tan^{-1} \frac{y_2 x_2}{z_2 \sqrt{x_2^2+y_2^2+z_2^2}}$$

$$- x_1 \ln(y_2 + \sqrt{x_1^2+y_2^2+z_2^2}) - y_2 \ln(x_1 + \sqrt{x_1^2+y_2^2+z_2^2}) + z_2 \tan^{-1} \frac{x_1 y_2}{z_2 \sqrt{x_1^2+y_2^2+z_2^2}}$$

$$- x_2 \ln(y_1 + \sqrt{x_2^2+y_1^2+z_2^2}) - y_1 \ln(x_2 + \sqrt{x_2^2+y_1^2+z_2^2}) + z_2 \tan^{-1} \frac{x_2 y_1}{z_2 \sqrt{x_2^2+y_1^2+z_2^2}}$$

$$+ x_1 \ln(y_1 + \sqrt{x_1^2+y_1^2+z_2^2}) + y_1 \ln(x_1 + \sqrt{x_1^2+y_1^2+z_2^2}) - z_2 \tan^{-1} \frac{x_1 y_1}{z_2 \sqrt{x_1^2+y_1^2+z_2^2}}$$

$$- x_2 \ln(y_2 + \sqrt{x_2^2 + y_2^2 + z_1^2}) - y_2 \ln(x_2 + \sqrt{x_2^2 + y_2^2 + z_1^2}) + z_1 \tan^{-1} \frac{x_2 y_2}{z_1 \sqrt{x_2^2 + y_2^2 + z_1^2}}$$

$$+ x_1 \ln(y_2 + \sqrt{x_1^2 + y_2^2 + z_1^2}) + y_2 \ln(x_1 + \sqrt{x_1^2 + y_2^2 + z_1^2}) - z_1 \tan^{-1} \frac{x_1 y_2}{z_1 \sqrt{x_1^2 + y_2^2 + z_1^2}}$$

$$+ x_2 \ln(y_1 + \sqrt{x_2^2 + y_1^2 + z_1^2}) + y_1 \ln(x_2 + \sqrt{x_2^2 + y_1^2 + z_1^2}) - \bar{z}_1 \tan^{-1} \frac{x_2 y_1}{z_1 \sqrt{x_2^2 + y_1^2 + z_1^2}}$$

$$- x_1 \ln(y_1 + \sqrt{x_1^2 + y_1^2 + z_1^2}) - y_1 \ln(x_1 + \sqrt{x_1^2 + y_1^2 + z_1^2}) + \bar{z}_1 \tan^{-1} \frac{x_1 y_1}{z_1 \sqrt{x_1^2 + y_1^2 + z_1^2}}$$

A P P E N D I X 3

APPLICATION, DISCUSSION AND PRINTOUT OF THE ITERATIVE THREE-DIMENSIONAL GRAVITY INTERPRETATION PROGRAM

A complete program printout and flow diagram are presented at the end of this appendix. This program which actually represents a program package can calculate the following:

- (a) the thickness of any outcropping body from the residual gravity values;
- (b) the thickness of any body where the upper or lower depth of the body is specified or where the body is required to be lens-shaped;
- (c) the thickness of a dipping sheet or dyke-like body;
- (d) the theoretical gravity field if the thickness of the layers or body is specified. A different program exists for this application.

Program Logic

The program is written in Fortran IV language and starts off by reading the density contrast (DNSTYC), the station spacing grid (SPACEX), the number of rows (N), the number of columns (M) and the number of iterations (L).

The first data card would look as follows:

```
1.0 0.0 5.0 1.5 1.5 1.5 1.5 2
```

This is followed by the residual gravity values in NXM MATRIX FORM. Up to 10 values can be printed on a card and the computer reads the MATRIX row-wise. The FORMAT for the rows are (10F8.2):

The residual gravity values are then transformed into thicknesses with the Bouguer slab formula:

$$\text{Thickness} = g \text{ observed} / 2\pi\rho G$$

where G = gravitational constant and ρ = density contrast and
 g = residual gravity values.

These thicknesses are stored in MATRIX B.

The formula for a rectangular parallelepiped as presented in Appendix 2 is now used to calculate the exact gravitational attraction of every rectangular parallelepiped with width = SPACEX and thickness B(i,j). These calculations are performed by SUBROUTINE GRV. The gravitational attraction over the centres of the parallelepipeds and also the gravitational influences of neighbouring parallelepipeds are summed and stored in MATRIX C. These summations are performed by SUBROUTINE GRVEK.

The differences between the observed and calculated gravity values are calculated and stored in MATRIX D and converted to thicknesses by again using the Bouguer slab formula.

Increasing or decreasing thicknesses are added to or subtracted from the existing thicknesses in MATRIX B and the increasing or decreasing gravity values are added to or subtracted from the gravity values in MATRIX C. Subsequently the difference between the calculated and observed gravity values is again calculated and adjusted another two times.

The program then clears MATRIX C and calculates the exact gravity field corresponding to the thicknesses that are stored in MATRIX B.

The whole process is then repeated and the number of repetitions depends on the user's whim. This iteration process is governed by L, and the author rarely experienced a case where L had to be greater than 2. When L=2 it means that the program iterates six times because for every increase of L in steps of one the iterative process that involves the cylinder adjustment takes place three times.

To change the number of cylinder iterations go to Step 20.

20 CONTINUE

K = K+1

IF (K.LT.3) GO TO 16

A1 = A1 + 1

if e.g. 4 cylinder iterations are desired then change to:

IF (K.LT.4) GO TO 16 etc.

It must be remembered that increasing the iterative process increases the cost of running the program. When the whole iterative process is completed the program prints out the interpreted thicknesses and the final differences between the calculated and observed gravity values that have been stored in MATRIX D.

Adjustment of the Program for Different Calculations

For calculations 1 to 3 mentioned at the beginning of this appendix all adjustments are made in SUBROUTINE GRV. It must thus be remembered that

when entering this program in a library, SUBROUTINE GRV must be kept out.

1. When the anomalous body is outcropping.

GO to the beginning of SUBROUTINE GRV

$$X3 = -X/2 - X0$$

$$X4 = X/2 - X0$$

$$Y3 = -X/2$$

$$Y4 = X/2$$

$$Z3 = .001$$

$$Z4 = Z3 + Z2$$

where:

Z2 is the thickness of the parallelepiped, Z3 is the upper limit and Z4 is the lower limit of the parallelepiped.

2(a) When the anomalous body is at a constant depth (a) beneath the surface interchange $Z3 = .001$ with $Z3 = a$

2(b) When the lower limit of the anomalous body is known interchange

$$Z3 = .001$$

$$Z4 = Z3 + Z2 \text{ with:}$$

$$Z4 = a$$

$$Z3 = Z4 - Z2$$

$$\text{IF (Z3.LE.0) Z3 = .001}$$

2(c) When a lens-shaped body is required:

The average depth = a to the middle of the lens must be specified

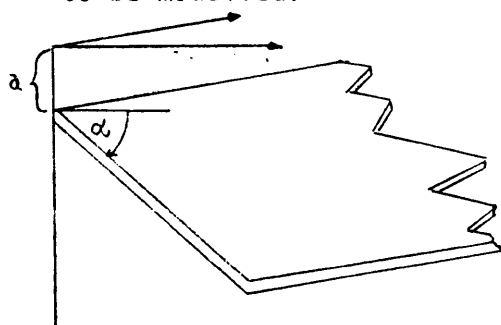
$$Z3 = a$$

$$Z4 = Z3 + 0,5*Z2$$

$$Z3 = Z3 - 0,5*Z2$$

$$\text{IF (Z3.LE.0) Z3 = .001}$$

3. When a dyke-like body or a dipping sheet with one inclination has to be modelled.



```
SUBROUTINE GRV (GRV,X,DNSTYC,Z2 X0,Z3,j)
```

```
ANGLE =  $\alpha$ 
```

```
X3 = -X/2-X0
```

```
X4 = X/2-X0
```

```
Y3 = -X/2
```

```
Y4 = .X/2
```

```
SPACEX = a
```

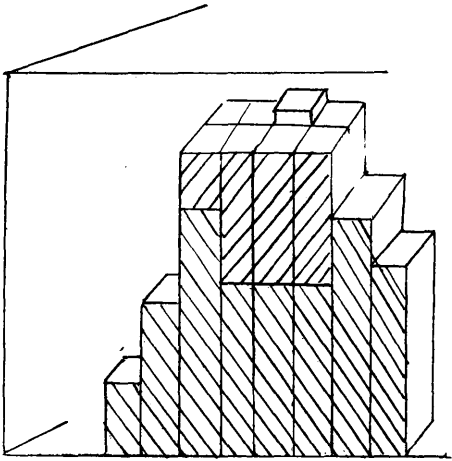
```
Z3 = a + (j) * SPECEX * TAN (ANGLE)
```


```
Z4 = Z3 + Z2
```


Where a = depth to the top of the sheet.

4. To calculate theoretical gravity fields for synthetic models an entirely different program was worked out although some of the subroutines from the previous program were used.

Any number of layers with positive or negative density contrasts can be used. The thickness and density contrast of each parallelepiped are specified for each layer, e.g.



 First layer with density contrast a

 Second layer with density contrast b

```

C THREE-DIMENSIONAL GRAVITY MODELLING.
C THE POLCHER STAR FORMULA IS USED TO CALCULATE THE STARTER MODEL.
C THE GRAVITY EFFECT OF THE STARTER MODEL IS CALCULATED WITH THE EXACT
C FORMULA FOR A RECTANGULAR PARALLELEPIPED.
C ADJUSTMENTS TO THE STARTER MODEL ARE CARRIED OUT WITH CYLINDERS USING
C SOLID ANGLES.
C AFTER EVERY K ADJUSTMENTS THE GRAVITY EFFECT OF THE MODEL IS CALCU
C LATED WITH THE EXACT FORMULA AND COMPARED WITH THE OBSERVED VALUES.
C K=NUMBER OF ITERATIONS WITH CYLINDER FORMULA
C MATRIXA=OBSERVED GRAVITY VALUES IN NXM MATRIX FORM
C MATRIXB=THICKNESS OF STARTER MODEL + ADJUSTMENTS IN METERS
C MATRIXC=GRAVITY VALUES FOR STARTER MODEL + ADJUSTMENTS
C MATRIXD=DIFFERENCE BETWEEN OBSERVED AND MODEL GRAVITY EFFECTS
C SPACEX= GRID SPACING IN METERS
C DNSTYC= DENSITY CONTRAST
C N=AMOUNT OF COLUMNS
C M=AMOUNT OF ROWS
C READ DENSITY CONTRAST,SPACEX,SIZE OF MATRIX,NUMBER OF ITERATIONS.
      DIMENSION A(10,14),B(10,14),C(10,14),D(10,14)
      READ(6,1000) DNSTYC,SPACEX,N,M,N2,M2,L
      WRITE(6,1000) DNSTYC,SPACEX,N,M,N2,M2,L
C READ OBSERVED GRAVITY VALUES
      CALL READM(A,N,M,N2,M2)
      WRITE(6,4)
      4 FORMAT('I',PCX,'INLET RESIDUAL GRAVITY VALUES')
      CALL PRINTM(A,N,M,N2,M2)
C CALCULATE STARTER MODEL
      DO 5 I=1,N
      DO 5 J=1,M
      B(I,J)=A(I,J)/(2*3.1415*0.00667*DNSTYC)
      5 CONTINUE
C CALCULATE GRAVITY EFFECT OF STARTER MODEL
      A1=C
      10 DO 15 I=1,N
      DO 15 J=1,M
      Z2=P(I,J)
      IF (Z2 .EQ. 0) GO TO 15
      XC=C
      CALL GRV(GRVA,SPACEX,DNSTYC,Z2,X0)
      XC=SPACEX
      CALL GRV(GRVB,SPACEX,DNSTYC,Z2,X0)
      XC=SQRT((SPACEX**2)*2)
      CALL GRV(GRVC,SPACEX,DNSTYC,Z2,X0)
      XC=2*SPACEX
      CALL GRV(GRVD,SPACEX,DNSTYC,Z2,X0)
      XC=SQRT((SPACEX*2)**2+(SPACEX)**2)
      CALL GRV(GRVE,SPACEX,DNSTYC,Z2,X0)
      XC=SQRT((SPACEX*2)**2+(SPACEX*2)**2)
      CALL GRV(GRVF,SPACEX,DNSTYC,Z2,X0)
      XC=3*SPACEX
      CALL GRV(GRVG,SPACEX,DNSTYC,Z2,X0)
      XC=SQRT((2*SPACEX)**2+(SPACEX)**2)
      CALL GRV(GRVH,SPACEX,DNSTYC,Z2,X0)
      XC=SQRT((2*SPACEX)**2+(2*SPACEX)**2)
      CALL GRV(GRVI,SPACEX,DNSTYC,Z2,X0)
      XC=4*SPACEX
      CALL GRV(GRVJ,SPACEX,DNSTYC,Z2,X0)
      XC=SQRT((4*SPACEX)**2+(2*SPACEX)**2)

```



```

CALL GRV(GRVK,SPACEX,DASTYC,ZZ,XO)
XC=5*SPACEX
CALL GRV(GRVL,SPACEX,DASTYC,ZZ,XO)
CALL GRVFK(GRVA,GRVP,GRVC,GRVE,GRVH,GRVG,GRVJ,GRVI,GRVJ,
1GRVK,GRVL,N,M,I,J,C)
15 CONTINUE
IF (A1 .GE. 1) GO TO 30
K=C
16 DO 20 I=1,N
DO 20 J=1,M
IF (C(I,J) .LT. C) C(I,J)=C
D(I,J)=(A(I,J)-C(I,J))/(2*3.1415*O)5673DASTYC)
PLKLTH=R(I,J)
R(I,J)=R(I,J)+D(I,J)
IF (R(I,J) .IF. C) GO TO 20
STHICK=R(I,J)
XC=C
CALL SLNDER(GRVA,STHICK,XO,DASTYC,SPACEX,PLKLTH)
XC=SPACEX
CALL SLNDER(GRVP,STHICK,XO,DASTYC,SPACEX,PLKLTH)
XC=SQRT((SPACEX**2)*2)
CALL SLNDER(GRVC,STHICK,XO,DASTYC,SPACEX,PLKLTH)
XC=2*SPACEX
CALL SLNDER(GRVE,STHICK,XO,DASTYC,SPACEX,PLKLTH)
XC=SQRT((SPACEX**2)*2+(SPACEX)**2)
CALL SLNDER(GRVH,STHICK,XO,DASTYC,SPACEX,PLKLTH)
XC=SQRT((SPACEX**2)*2+(SPACEX**2)**2)
CALL SLNDER(GRVJ,STHICK,XO,DASTYC,SPACEX,PLKLTH)
XC=3*SPACEX
CALL SLNDER(GRVI,STHICK,XO,DASTYC,SPACEX,PLKLTH)
XC=4*SPACEX
CALL SLNDER(GRVJ,STHICK,XO,DASTYC,SPACEX,PLKLTH)
XC=SQRT((4*SPACEX)**2+(2*SPACEX)**2)
CALL SLNDER(GRVK,STHICK,XO,DASTYC,SPACEX,PLKLTH)
XC=5*SPACEX
CALL SLNDER(GRVL,STHICK,XO,DASTYC,SPACEX,PLKLTH)
CALL GRVFK(GRVA,GRVP,GRVC,GRVE,GRVH,GRVG,GRVJ,GRVI,GRVJ,
1GRVK,GRVL,N,M,I,J,C)
20 CONTINUE
K=K+1
IF (K .LT. 3) GO TO 16
A1=A1+1
DO 25 I=1,N
DO 25 J=1,M
25 C(I,J)=C.C
GO TO 10
30 DO 35 I=1,N
DO 35 J=1,M
35 D(I,J)=A(I,J)-C(I,J)
WRITE(6,36)
36 FORMAT('1',2(X,'THICKNESS OF BODY'))
40 CALL PRINTM(P,N,M,N2,N2)
WRITE(6,41)
41 FORMAT('1',10X,'DIFFERENCE BETWEEN CALCULATED AND OBSERVED GRAVITY
VALUES')
45 CALL PRINTM(D,N,M,N2,N2)
1000 FORMAT(F6.2,F4.0,4(3,I2)
STOP
END

```

```

SUBROUTINE READM(A,N,M,M1,M1)
DIMENSION A(M1,M1)
DO 100 I=1,N
READ (5,1001) (A(I,J),J=1,M)
100 CONTINUE
RETURN
1001 FORMAT (10F8.2)
END

```

```

SUBROUTINE PRINTM(A,N,M,M1,M1)
DIMENSION A(M1,M1)
DO 100 IP=1,M,LC
IF=IP+S
IF (IF-M) 2,2,1
1 IF=M
2 WRITE (6,2000) (I,I=IP,IF)
DO 101 J=1,M
WRITE (6,2001) J,(A(J,K),K=IP,IF)
101 CONTINUE
100 CONTINUE
RETURN
2000 FORMAT (1H0,1X,10I12)
2001 FORMAT (1H0,15,10F12.4)
END

```

```

SUBROUTINE COM(GCVA,X,CASLYC,Z2,Y2)
X2=-X/2-XC
Y4=X/2-YC
Y3=-X/2
Y4=X/2
Z2=.001
Z4=Z2+Z3
S222=SQRT(X4**2+Y4**2+Z4**2)
S122=SQRT(X2**2+Y4**2+Z4**2)
S212=SQRT(X4**2+Y3**2+Z4**2)
S112=SQRT(X2**2+Y3**2+Z4**2)
S221=SQRT(X4**2+Y4**2+Z3**2)
S121=SQRT(X2**2+Y4**2+Z3**2)
S211=SQRT(X4**2+Y3**2+Z3**2)
S111=SQRT(X2**2+Y3**2+Z3**2)
A=X4*ALOG((S222+Y4)/(S222-Y4))+Y4*ALOG((S222+X4)/(S222-X4))
1-2*Z4*ATAN((X4*Y4)/(Z4*S222))
B=-X2*ALOG((S122+Y4)/(S122-Y4))-Y4*ALOG((S122+X2)/(S122-X2))
2+2*Z4*ATAN((X2*Y4)/(Z4*S122))
C=-X4*ALOG((S212+Y3)/(S212-Y3))-Y3*ALOG((S212+X4)/(S212-X4))
3+2*Z4*ATAN((X4*Y3)/(Z4*S212))
D=X2*ALOG((S112+Y3)/(S112-Y3))+Y3*ALOG((S112+X2)/(S112-X2))
4-2*Z4*ATAN((X2*Y3)/(Z4*S112))
E=-X4*ALOG((S221+Y4)/(S221-Y4))-Y4*ALOG((S221+X4)/(S221-X4))
5+2*Z3*ATAN((X4*Y4)/(Z3*S221))
F=X2*ALOG((S121+Y4)/(S121-Y4))+Y4*ALOG((S121+X2)/(S121-X2))
6-2*Z3*ATAN((X2*Y4)/(Z3*S121))
G=X4*ALOG((S211+Y3)/(S211-Y3))+Y3*ALOG((X4+S211)/(S211-X4))
7-2*Z3*ATAN((X4*Y3)/(Z3*S211))
H=-X2*ALOG((S111+Y3)/(S111-Y3))-Y3*ALOG((S111+X2)/(S111-X2))
8+2*Z3*ATAN((X2*Y3)/(Z3*S111))
C=A+B+C+D+E+F+G+H
GCVA=(-.00007*G*CASLYC)/2
RETURN
END

```

```

SUBROUTINE SINDR(GRV,STHICK,X0,DNSTYC,SPACEX,A)
IF (STHICK .LT. 0) GO TO 15
IF (X0 .NE. 0) GO TO 5
GRV=.04192*DNSTYC*(STHICK+SQRT(A**2+(SPACEX/2)**2))
1-SQRT((A+STHICK)**2+(SPACEX/2)**2))
GO TO 30
5 P=(A+STHICK/2)/(SQRT((A+STHICK/2)**2+X0**2))
SOLIDA=(P**2.1416*(SPACEX/2)**2)/
1((A+STHICK/2)**2+X0**2)
10 GRV=.00667*SOLIDA*DNSTYC*STHICK
GO TO 30
15 IF (X0 .NE. 0) GO TO 20
STHICK=-STHICK
GRV=-.04192*DNSTYC*(STHICK+SQRT(A**2+(SPACEX/2)**2))
1-SQRT((A+STHICK)**2+(SPACEX/2)**2))
STHICK=-STHICK
GO TO 30
20 STHICK=-STHICK
P=(A+STHICK/2)/(SQRT((A+STHICK/2)**2+X0**2))
SOLIDA=(P**2.1416*(SPACEX/2)**2)/
1((A-STHICK/2)**2+X0**2)
GRV=-.00667*SOLIDA*DNSTYC*STHICK
STHICK=-STHICK
30 CONTINUE
RETURN
END

```

```

SUBROUTINE GRVFK(GRVA,GRVB,GRVC,GRVD,GRVE,GRVF,GRVG,GRVH,GRVI,
IGRVJ,GRVK,GRVL,N,M,I,J,C)
DIMENSION C(N,M)
C(I,J)=C(I,J)+GRVA
IF ((I-1) .LT. 1) GO TO 2
C((I-1),J)=C((I-1),J)+GRVB
2 IF ((I+1) .GT. N) GO TO 3
C((I+1),J)=C((I+1),J)+GRVB
2 IF ((J-1) .LT. 1) GO TO 4
C(I,(J-1))=C(I,(J-1))+GRVB
4 IF ((J+1) .GT. M) GO TO 5
C(I,(J+1))=C(I,(J+1))+GRVB
5 IF ((I-1) .LT. 1 .OR. (J-1) .LT. 1) GO TO 6
C((I-1),(J-1))=C((I-1),(J-1))+GRVC
6 IF ((I-1) .LT. 1 .OR. (J+1) .GT. M) GO TO 7
C((I-1),(J+1))=C((I-1),(J+1))+GRVC
7 IF ((I+1) .GT. N .OR. (J-1) .LT. 1) GO TO 8
C((I+1),(J-1))=C((I+1),(J-1))+GRVC
8 IF ((I+1) .GT. N .OR. (J+1) .GT. M) GO TO 9
C((I+1),(J+1))=C((I+1),(J+1))+GRVC
9 IF ((J-2) .LT. 1) GO TO 10
C(I,(J-2))=C(I,(J-2))+GRVD
10 IF ((J+2) .GT. M) GO TO 11
C(I,(J+2))=C(I,(J+2))+GRVD
11 IF ((I-2) .LT. 1) GO TO 12
C((I-2),J)=C((I-2),J)+GRVD
12 IF ((I+2) .GT. N) GO TO 13
C((I+2),J)=C((I+2),J)+GRVD
13 IF ((I-2) .LT. 1 .OR. (J+1) .GT. M) GO TO 14
C((I-2),(J+1))=C((I-2),(J+1))+GRVE
14 IF ((I-1) .LT. 1 .OR. (J+2) .GT. M) GO TO 15
C((I-1),(J+2))=C((I-1),(J+2))+GRVE
15 IF ((I+1) .GT. N .OR. (J+2) .GT. M) GO TO 16

```

```

      C((I+1),(J+2))=C((I+1),(J+2))+C*V*F
16 IF ((I+2).GT.N.CR.(J+1).GT.M) GO TO 17
      C((I+2),(J+1))=C((I+2),(J+1))+C*V*F
17 IF ((I-2).LT.1.CR.(J-1).LT.1) GO TO 18
      C((I-2),(J-1))=C((I-2),(J-1))+C*V*F
18 IF ((I-1).LT.1.CR.(J-2).LT.1) GO TO 19
      C((I-1),(J-2))=C((I-1),(J-2))+C*V*F
19 IF ((I+1).GT.N.CR.(J-2).LT.1) GO TO 20
      C((I+1),(J-2))=C((I+1),(J-2))+C*V*F
20 IF ((I+2).GT.N.CR.(J-1).LT.1) GO TO 21
      C((I+2),(J-1))=C((I+2),(J-1))+C*V*F
21 IF ((I-2).LT.1.CR.(J+2).GT.M) GO TO 22
      C((I-2),(J+2))=C((I-2),(J+2))+C*V*F
22 IF ((I+2).GT.N.CR.(J-2).LT.1) GO TO 23
      C((I+2),(J-2))=C((I+2),(J-2))+C*V*F
23 IF ((I-2).LT.1.CR.(J-2).LT.1) GO TO 24
      C((I-2),(J-2))=C((I-2),(J-2))+C*V*F
24 IF ((I+2).GT.N.CR.(J+2).GT.M) GO TO 25
      C((I+2),(J+2))=C((I+2),(J+2))+C*V*F
25 IF ((I+3).GT.N) GO TO 26
      C((I+3),J)=C((I+3),J)+C*V*G
26 IF ((I-3).LT.1) GO TO 27
      C((I-3),J)=C((I-3),J)+C*V*G
27 IF ((J+3).GT.M) GO TO 28
      C(I,(J+3))=C(I,(J+3))+C*V*G
28 IF ((J-3).LT.1) GO TO 29
      C(I,(J-3))=C(I,(J-3))+C*V*G
29 IF ((I+3).GT.N.CR.(J+1).GT.M) GO TO 34
      C((I+3),(J+1))=C((I+3),(J+1))+C*V*F
34 IF ((I+3).GT.N.CR.(J-1).LT.1) GO TO 35
      C((I+3),(J-1))=C((I+3),(J-1))+C*V*F
35 IF ((I-3).LT.1.CR.(J+1).GT.M) GO TO 36
      C((I-3),(J+1))=C((I-3),(J+1))+C*V*F
36 IF ((I-3).LT.1.CR.(J-1).LT.1) GO TO 37
      C((I-3),(J-1))=C((I-3),(J-1))+C*V*F
37 IF ((I+1).GT.N.CR.(J+3).GT.M) GO TO 38
      C((I+1),(J+3))=C((I+1),(J+3))+C*V*F
38 IF ((I+1).GT.N.CR.(J-3).LT.1) GO TO 39
      C((I+1),(J-3))=C((I+1),(J-3))+C*V*F
39 IF ((I-1).LT.1.CR.(J+3).GT.M) GO TO 40
      C((I-1),(J+3))=C((I-1),(J+3))+C*V*F
40 IF ((I-1).LT.1.CR.(J-3).LT.1) GO TO 41
      C((I-1),(J-3))=C((I-1),(J-3))+C*V*F
41 IF ((I+3).GT.N.CR.(J+2).GT.M) GO TO 42
      C((I+3),(J+2))=C((I+3),(J+2))+C*V*I
42 IF ((I+3).GT.N.CR.(J-2).LT.1) GO TO 43
      C((I+3),(J-2))=C((I+3),(J-2))+C*V*I
43 IF ((I-3).LT.1.CR.(J+2).GT.M) GO TO 44
      C((I-3),(J+2))=C((I-3),(J+2))+C*V*I
44 IF ((I-3).LT.1.CR.(J-2).LT.1) GO TO 45
      C((I-3),(J-2))=C((I-3),(J-2))+C*V*I
      C((I+2),(J+3))=C((I+2),(J+3))+C*V*I
45 IF ((I+2).GT.N.CR.(J+3).GT.M) GO TO 46
46 IF ((I+2).GT.N.CR.(J-3).LT.1) GO TO 47
      C((I+2),(J-3))=C((I+2),(J-3))+C*V*I
47 IF ((I-2).LT.1.CR.(J+3).GT.M) GO TO 48
      C((I-2),(J+3))=C((I-2),(J+3))+C*V*I
48 IF ((I-2).LT.1.CR.(J-3).LT.1) GO TO 49
      C((I-2),(J-3))=C((I-2),(J-3))+C*V*I
49 IF ((I+4).GT.N) GO TO 50
      C((I+4),J)=C((I+4),J)+C*V*J
50 IF ((I-4).LT.1) GO TO 51
      C((I-4),J)=C((I-4),J)+C*V*J
51 IF ((J+4).GT.M) GO TO 52

```

```

      C(I,(J+4))=C(I,(J+4))+CFVJ
52 IF ((J-4) .LT. 1) GO TO 53
      C(I,(J-4))=C(I,(J-4))+CFVJ
53 IF ((I+4) .GT. N .OR. (J+1) .GT. M) GO TO 54
      C((I+4),(J+1))=C((I+4),(J+1))+CFVJ
54 IF ((I+4) .GT. N .OR. (J-1) .LT. 1) GO TO 56
      C((I+4),(J-1))=C((I+4),(J-1))+CFVJ
56 IF ((I-4) .LT. 1 .OR. (J+1) .GT. M) GO TO 57
      C((I-4),(J+1))=C((I-4),(J+1))+CFVJ
57 IF ((I-4) .LT. 1 .OR. (J-1) .LT. 1) GO TO 58
      C((I-4),(J-1))=C((I-4),(J-1))+CFVJ
58 IF ((I+1) .GT. N .OR. (J+4) .GT. M) GO TO 59
      C((I+1),(J+4))=C((I+1),(J+4))+CFVJ
59 IF ((I+1) .GT. N .OR. (J-4) .LT. 1) GO TO 60
      C((I+1),(J-4))=C((I+1),(J-4))+CFVJ
60 IF ((I-1) .LT. 1 .OR. (J+4) .GT. M) GO TO 61
      C((I-1),(J+4))=C((I-1),(J+4))+CFVJ
61 IF ((I-1) .LT. 1 .OR. (J-4) .LT. 1) GO TO 62
      C((I-1),(J-4))=C((I-1),(J-4))+CFVJ
62 IF ((I+3) .GT. N .OR. (J+3) .GT. M) GO TO 63
      C((I+3),(J+3))=C((I+3),(J+3))+CFVJ
63 IF ((I+3) .GT. N .OR. (J-3) .LT. 1) GO TO 64
      C((I+3),(J-3))=C((I+3),(J-3))+CFVJ
64 IF ((I-3) .LT. 1 .OR. (J+3) .GT. M) GO TO 65
      C((I-3),(J+3))=C((I-3),(J+3))+CFVJ
65 IF ((I-3) .LT. 1 .OR. (J-3) .LT. 1) GO TO 66
      C((I-3),(J-3))=C((I-3),(J-3))+CFVJ
66 IF ((I+4) .GT. N .OR. (J+2) .GT. M) GO TO 67
      C((I+4),(J+2))=C((I+4),(J+2))+CFVK
67 IF ((I+4) .GT. N .OR. (J-2) .LT. 1) GO TO 68
      C((I+4),(J-2))=C((I+4),(J-2))+CFVK
68 IF ((I-4) .LT. 1 .OR. (J+2) .GT. M) GO TO 69
      C((I-4),(J+2))=C((I-4),(J+2))+CFVK
69 IF ((I-4) .LT. 1 .OR. (J-2) .LT. 1) GO TO 70
      C((I-4),(J-2))=C((I-4),(J-2))+CFVK
70 IF ((I+2) .GT. N .OR. (J+4) .GT. M) GO TO 71
      C((I+2),(J+4))=C((I+2),(J+4))+CFVK
71 IF ((I+2) .GT. N .OR. (J-4) .LT. 1) GO TO 72
      C((I+2),(J-4))=C((I+2),(J-4))+CFVK
72 IF ((I-2) .LT. 1 .OR. (J+4) .GT. M) GO TO 73
      C((I-2),(J+4))=C((I-2),(J+4))+CFVK
73 IF ((I-2) .LT. 1 .OR. (J-4) .LT. 1) GO TO 74
      C((I-2),(J-4))=C((I-2),(J-4))+CFVK
74 IF ((I+5) .GT. N) GO TO 75
      C((I+5),J)=C((I+5),J)+CFVL
75 IF ((J+5) .GT. M) GO TO 76
      C(I,(J+5))=C(I,(J+5))+CFVL
76 IF ((J-5) .LT. 1) GO TO 77
      C(I,(J-5))=C(I,(J-5))+CFVL
77 IF ((I-5) .LT. 1) GO TO 78
      C((I-5),J)=C((I-5),J)+CFVL
78 IF ((I+4) .GT. N .OR. (J+3) .GT. M) GO TO 79
      C((I+4),(J+3))=C((I+4),(J+3))+CFVL
79 IF ((I+4) .GT. N .OR. (J-3) .LT. 1) GO TO 80
      C((I+4),(J-3))=C((I+4),(J-3))+CFVL
80 IF ((I-4) .LT. 1 .OR. (J+3) .GT. M) GO TO 81
      C((I-4),(J+3))=C((I-4),(J+3))+CFVL
81 IF ((I-4) .LT. 1 .OR. (J-3) .LT. 1) GO TO 82
      C((I-4),(J-3))=C((I-4),(J-3))+CFVL
82 CONTINUE
      RETURN
      END

```

```

C PROGRAM TO CALCULATE SYNTHETIC GRAVITY ANOMALIES
C MORE THAN ONE LAYER WITH POS. OR NEG. DENSITY CONTRAST CAN BE USED.
C THE THICKNESSES OF EACH PARALLELEPIPED FOR EACH LAYER ARE SPECIFIED
C AS INPUT
C READ NUMBER OF LAYERS
  DIMENSION A(5,5),P(5,5),C(5,5),D(5,5)
  READ(5,1000) LAYER
C READ PARAMETERS OF FIRST LAYER
  READ(5,2000) DNASTYC,SPACEX,N,M,N2,M2
  CALL READM(A,N,M,N2,M2)
  WRITE(6,3000)
  CALL PRINTM(A,N,M,N2,M2)
  CALL READM(P,N,M,N2,M2)
  WRITE(6,6000)
  WRITE(6,7000) DNASTYC
  WRITE(6,4000)
  CALL PRINTM(P,N,M,N2,M2)
  L=0
10 DO 15 I=1,M
  DO 15 J=1,M
    B(I,J)=A(I,J)+P(I,J)
    Z3=A(I,J)
    Z4=P(I,J)
    XC=0
    CALL GRV(GRVA,SPACEX,DNASTYC,Z3,Z4,XC)
    XC=SPACEX
    CALL GRV(GRVB,SPACEX,DNASTYC,Z3,Z4,XC)
    XC=SQRT((SPACEX**2)*2)
    CALL GRV(GRVC,SPACEX,DNASTYC,Z3,Z4,XC)
    XC=2*SPACEX
    CALL GRV(GRVD,SPACEX,DNASTYC,Z3,Z4,XC)
    XC=SQRT((SPACEX*2)**2+(SPACEX)**2)
    CALL GRV(GRVE,SPACEX,DNASTYC,Z3,Z4,XC)
    XC=SQRT((SPACEX*2)**2+(SPACEX*2)**2)
    CALL GRV(GRVF,SPACEX,DNASTYC,Z3,Z4,XC)
    XC=3*SPACEX
    CALL GRV(GRVG,SPACEX,DNASTYC,Z3,Z4,XC)
    XC=SQRT((3*SPACEX)**2+(SPACEX)**2)
    CALL GRV(GRVH,SPACEX,DNASTYC,Z3,Z4,XC)
    XC=SQRT((3*SPACEX)**2+(2*SPACEX)**2)
    CALL GRV(GRVI,SPACEX,DNASTYC,Z3,Z4,XC)
    XC=4*SPACEX
    CALL GRV(GRVJ,SPACEX,DNASTYC,Z3,Z4,XC)
    XC=SQRT((4*SPACEX)**2+(2*SPACEX)**2)
    CALL GRV(GRVK,SPACEX,DNASTYC,Z3,Z4,XC)
    XC=5*SPACEX
    CALL GRV(GRVL,SPACEX,DNASTYC,Z3,Z4,XC)
    CALL GRVK(GRVA,GRVB,GRVC,GRVD,GRVE,GRVF,GRVG,GRVH,GRVI,GRVJ,
    1GRVK,GRVL,N,M,I,J,C)
  15 CONTINUE
  L=L+1
  IF (L.EQ. LAYER) GO TO 50
C READ DENSITY OF FOLLOWING LAYER
20 READ(5,7000) DNASTYC
  WRITE(6,8000)
  WRITE(6,7000) DNASTYC
  CALL READM(P,N,M,N2,M2)
  WRITE(6,9000)

```

```

      CALL PRINTM(P,N,M,N2,M2)
      DO 40 I=1,N
      DO 40 J=1,M
      A(I,J)=D(I,J)
40    CONTINUE
      GO TO 10
      50 WRITE(6,('CCC'))
      100 CALL PRINTM(C,N,M,N2,M2)
1000  FORMAT(I2)
2000  FORMAT(F4.2,F6.0,4I3)
3000  FORMAT('11',4X,'DEPTH OF BODY TOP BELOW SURFACE')
4000  FORMAT('11',10X,'THICKNESS OF FIRST LAYER')
5000  FORMAT('11',10X,'THICKNESS OF FOLLOWING LAYER')
6000  FORMAT('11',10X,'RESIDUAL GRAVITY ANOMALY')
7000  FORMAT(F4.2)
8000  FORMAT('11',10X,'DENSITY CONTR. OF LAYER')
      STOP
      END

```

```

SUBROUTINE GRV(GRVA,X,DNSTYC,Z3,Z4,X0)
  X2=-X/2-X0
  X4=X/2-X0
  Y3=-Y/2
  Y4=Y/2
  S222=SQRT(X4**2+Y4**2+Z4**2)
  S122=SQRT(X2**2+Y4**2+Z4**2)
  S212=SQRT(X4**2+Y3**2+Z4**2)
  S112=SQRT(X2**2+Y3**2+Z4**2)
  S221=SQRT(X4**2+Y4**2+Z3**2)
  S121=SQRT(X2**2+Y4**2+Z3**2)
  S211=SQRT(X4**2+Y3**2+Z3**2)
  S111=SQRT(X2**2+Y3**2+Z3**2)
  A=X4*ALFC((S222+Y4)/(S222-Y4))+Y4*ALFC((S222+Y4)/(S222-X4))
  B=2*Z4*ATAN((X4*Y4)/(Z4*S222))
  C=-X2*ALFC((S122+Y4)/(S122-Y4))-Y4*ALFC((S122+Y3)/(S122-X2))
  D=2*Z4*ATAN((X2*Y4)/(Z4*S122))
  E=-X4*ALFC((S212+Y3)/(S212-Y3))-Y3*ALFC((S212+X4)/(S212-X4))
  F=2*Z4*ATAN((X4*Y3)/(Z4*S212))
  G=X3*ALFC((S112+Y3)/(S112-Y3))+Y3*ALFC((S112+X3)/(S112-X3))
  H=2*Z4*ATAN((X3*Y3)/(Z4*S112))
  I=-Y4*ALFC((S221+Y4)/(S221-Y4))-Y4*ALFC((S221+X4)/(S221-X4))
  J=2*Z3*ATAN((X4*Y4)/(Z3*S221))
  K=Y2*ALFC((S121+Y4)/(S121-Y4))+Y4*ALFC((S121+X3)/(S121-X3))
  L=-2*Z3*ATAN((X2*Y4)/(Z3*S121))
  M=X4*ALFC((S211+Y3)/(S211-Y3))+Y3*ALFC((X4+S211)/(S211-X4))
  N=2*Z3*ATAN((X4*Y3)/(Z3*S211))
  O=-X3*ALFC((S111+Y3)/(S111-Y3))-Y3*ALFC((S111+X3)/(S111-X3))
  P=2*Z3*ATAN((X3*Y3)/(Z3*S111))
  Q=A+P+C+D+E+F+G+H
  GRVA=(-.00067*Q*DNSTYC)/2
  RETURN
  END

```

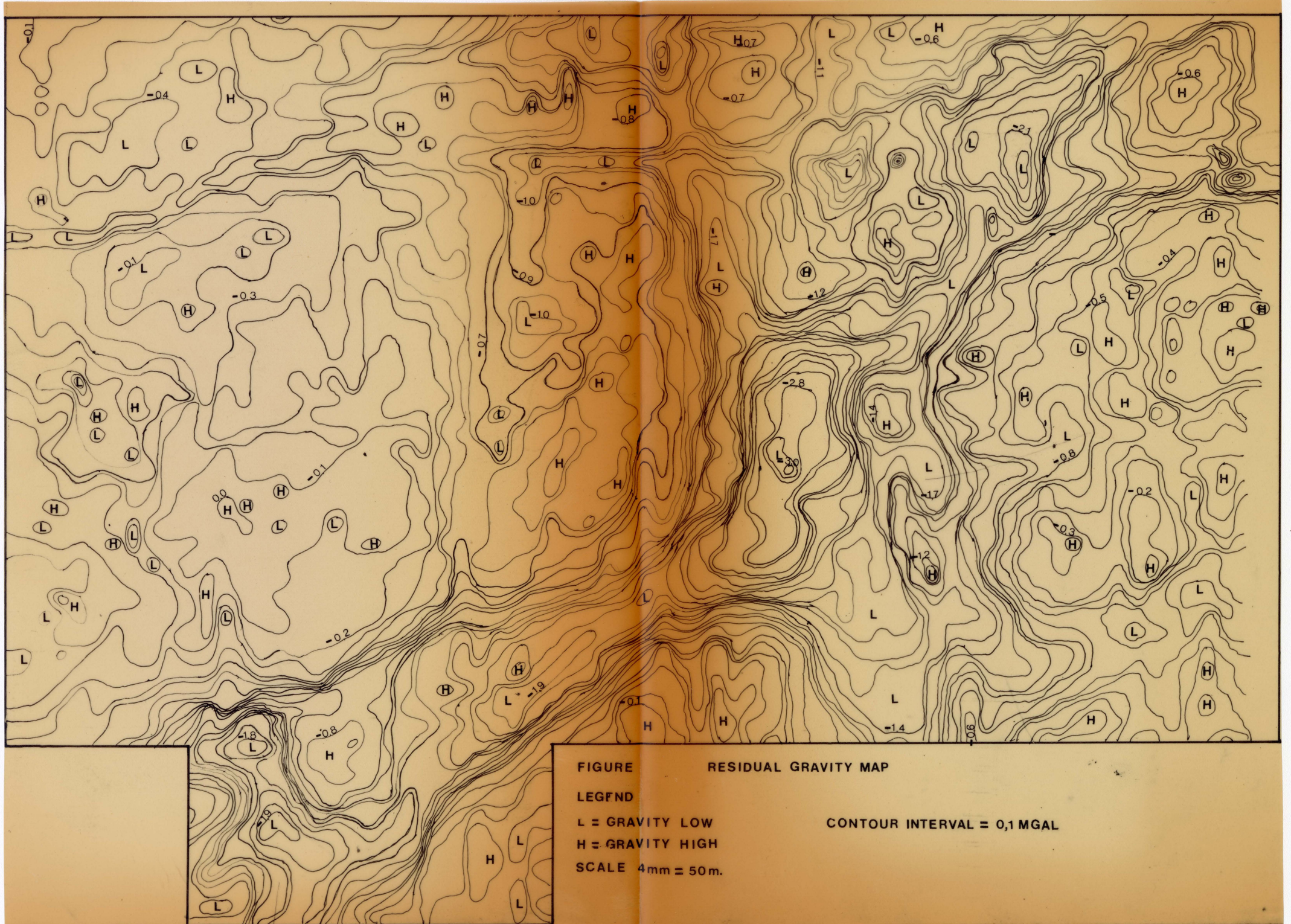



FIGURE RESIDUAL GRAVITY MAP

LEGEND

L = GRAVITY LOW

H = GRAVITY HIGH

SCALE 4mm = 50m.

CONTOUR INTERVAL = 0,1 MGAL

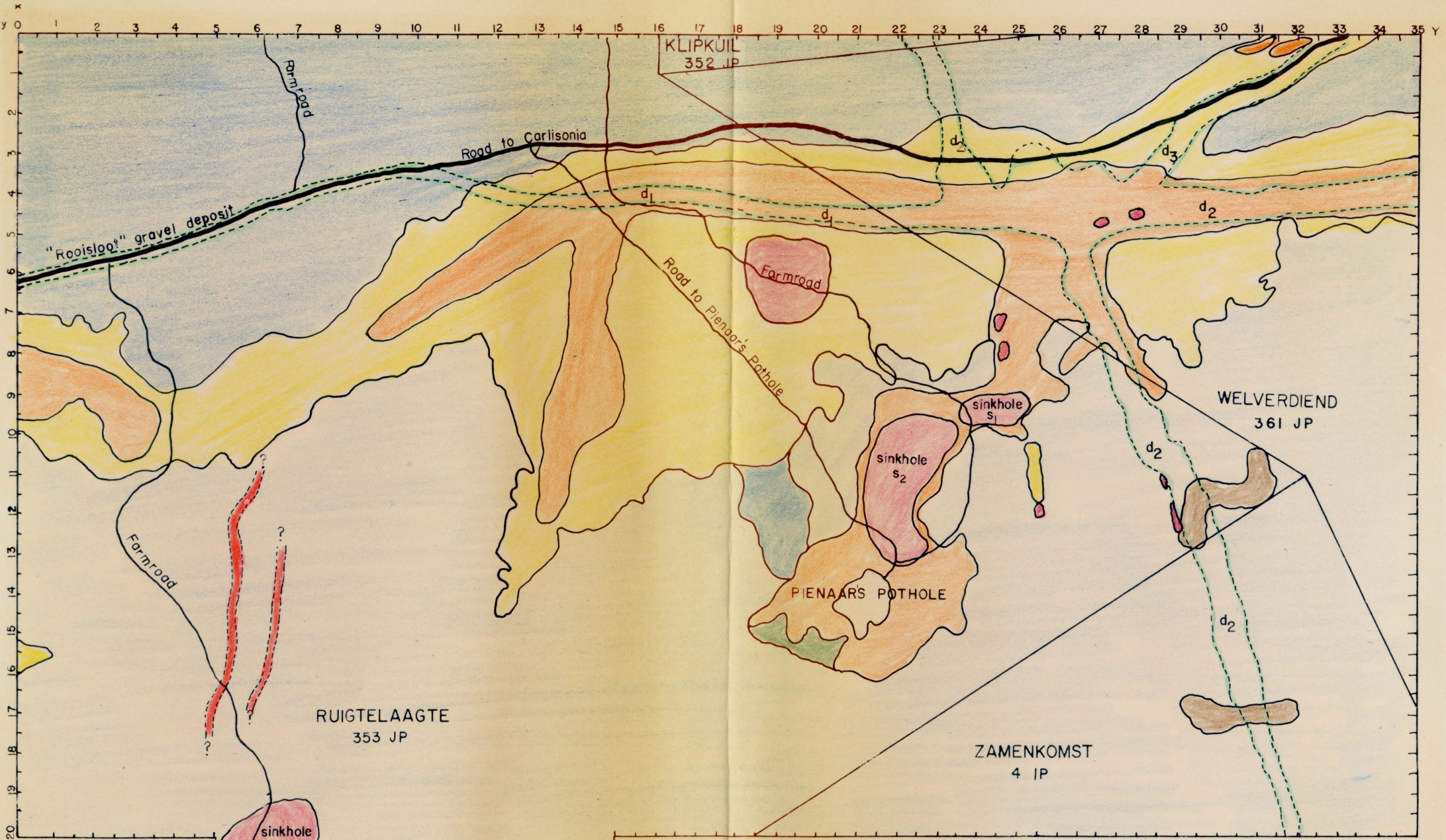


FIGURE 2 GEOLOGY OF THE RUIGTELAAGTE AREA

LEGEND

- | | | | |
|--|--|--|---------------------|
| | RED BROWN SOIL LAYER | | } DWYKA FORMATION ? |
| | DIAMONDIFEROUS GRAVELS (0 < thickness < 2m) | | |
| | DIAMONDIFEROUS GRAVELS (2m < thickness) | | |
| | NEWLY DISCOVERED VIRGIN GRAVEL DEPOSITS OCCURRING UNDER A RED BROWN SOIL COVER | | } MALMANI SUBGROUP |
| | | | |

scale: 1 cm = 40 m

FLOW-DIAGRAM OF THREE-DIMENSIONAL
ITERATIVE GRAVITY INTERPRETATION
PROGRAM

